

# **FINAL SAFETY ANALYSIS REPORT**

for the

**HOLTEC INTERNATIONAL STORAGE AND TRANSFER  
OPERATION REINFORCED MODULE CASK SYSTEM  
(HI-STORM 100 CASK SYSTEM)**

**NRC DOCKET NO. 72-1014**

**HOLTEC REPORT HI-2002444, VOLUME II of II**

Prepared by



**FINAL SAFETY ANALYSIS REPORT**

**for the**

**HOLTEC INTERNATIONAL**

**STORAGE, AND TRANSFER**

**OPERATION REINFORCED MODULE**

**CASK SYSTEM**

**(HI-STORM 100 CASK SYSTEM)**

**DOCKET 72-1014**

**VOLUME II OF II**

## CHAPTER 4<sup>†</sup> THERMAL EVALUATION

The HI-STORM System is designed for long-term storage of spent nuclear fuel (SNF) in a vertical orientation. An array of HI-STORM Systems laid out in a rectilinear pattern will be stored on a concrete ISFSI pad in an open environment. In this section, compliance of the HI-STORM thermal performance to 10CFR72 requirements for outdoor storage at an ISFSI is established. Safe thermal performance during on-site loading, unloading and transfer operations utilizing the HI-TRAC transfer cask is also demonstrated. The analysis considers passive rejection of decay heat from the stored SNF assemblies to the environment under the most severe design basis ambient conditions. Effects of incident solar radiation (insolation) and partial radiation blockage due to the presence of neighboring casks at an ISFSI site are included in the analyses. Finally, the thermal margins of safety for long-term storage of both moderate burnup (up to 45,000 MWD/MTU) and high burnup spent nuclear fuel (greater than 45,000 MWD/MTU) in the HI-STORM 100 System are quantified.

The guidelines presented in NUREG-1536 [4.4.10] include eight specific acceptance criteria that should be fulfilled by the cask thermal design. These eight criteria are summarized here as follows:

1. The fuel cladding temperature at the beginning of dry cask storage should generally be below the anticipated damage-threshold temperatures for normal conditions and a minimum of 20 years of cask storage.
2. The fuel cladding temperature should generally be maintained below 570°C (1058°F) for accident, off-normal, and fuel transfer conditions.
3. The maximum internal pressure of the cask should remain within its design pressures for normal (1% rod rupture), off-normal (10% rod rupture), and accident (100% rod rupture) conditions.
4. The cask and fuel materials should be maintained within their minimum and maximum temperature criteria for normal, off-normal, and accident conditions.
5. For fuel assemblies proposed for storage, the cask system should ensure a very low probability of cladding breach during long-term storage.

---

<sup>†</sup> This chapter has been prepared in the format and section organization set forth in Regulatory Guide 3.61. However, the material content of this chapter also fulfills the requirements of NUREG-1536. Pagination and numbering of sections, figures, and tables are consistent with the convention set down in Chapter 1, Section 1.0, herein. Finally, all terms-of-art used in this chapter are consistent with the terminology of the glossary (Table 1.0.1) and component nomenclature of the Bill-of-Materials (Section 1.5).

6. Fuel cladding damage resulting from creep cavitation should be limited to 15% of the original cladding cross sectional area.
7. The cask system should be passively cooled.
8. The thermal performance of the cask should be within the allowable design criteria specified in FSAR Chapters 2 and 3 for normal, off-normal, and accident conditions.

As demonstrated in this chapter (see Subsections 4.4.6 and 4.5.6), the HI-STORM System is designed to comply with all eight criteria listed above. All thermal analyses to evaluate normal conditions of storage in a HI-STORM storage module are described in Section 4.4. All thermal analyses to evaluate normal handling and on-site transfer in a HI-TRAC transfer cask are described in Section 4.5. All analyses for off-normal conditions are described in Section 11.1. All analyses for accident conditions are described in Section 11.2. Sections 4.1 through 4.3 describe thermal analyses and input data that are common to all conditions. This FSAR chapter is in full compliance with NUREG-1536 requirements, subject to the exceptions and clarifications discussed in Chapter 1, Table 1.0.3.

- This revision to the HI-STORM Safety Analysis Report, the first since the HI-STORM 100 System was issued a Part 72 Certificate of Compliance, incorporates several features into the thermal analysis to respond to the changing needs of the U.S. nuclear power generation industry. The most significant changes are:
  - Post-core decay time (PCDT) limitations on high burnup fuel (burnup > 45,000 MWD/MTU) have been computed. The allowable cladding temperatures for high burnup PWR and BWR fuel, required to establish PCDT limits, are computed using a methodology consistent with ISG-11.
  - Both uniform and regionalized storage are permitted, the latter being particularly valuable in mitigating the dose emitted by the MPC by restricting "cold and old" SNF in the locations surrounding the core region of the basket (where the "hot and new" fuel is stored).
  - The effect of convective heat transfer in the MPC, originally included in the analysis but subsequently neglected to enable the NRC to make a more considered assessment of gravity-driven convective heat transfer in honeycomb basket equipped MPCs, is now reintroduced.
  - In the absence of the credit for convective (thermosiphon) effect, the previous analysis relied on the conduction heat transfer through the clearance between the basket and the MPC enclosure vessel. The conduction heat flow path was provided by the Aluminum Heat Conduction Elements (AHCE). The AHCE hardware is retained in the MPC and credit for AHCE heat dissipation is eliminated in the

thermal analyses to maintain a solid margin of conservatism in the computed results. In a similar spirit of conservatism, the heat transfer in narrow cavities (the Rayleigh effect), approved by the SFPO in the previous analysis, is neglected in this revision.

Aside from the above-mentioned changes, this revision of this chapter is essentially identical to its predecessor.

#### 4.1 DISCUSSION

A sectional view of the HI-STORM dry storage system has been presented earlier (see Figure 1.2.1). The system consists of a sealed MPC situated inside a vertical ventilated storage overpack. Air inlet and outlet ducts that allow for air cooling of the stored MPC are located at the bottom and top, respectively, of the cylindrical overpack. The SNF assemblies reside inside the MPC, which is sealed with a welded lid to form the confinement boundary. The MPC contains an all-alloy honeycomb basket structure with square-shaped compartments of appropriate dimensions to allow insertion of the fuel assemblies prior to welding of the MPC lid and closure ring. Each box panel, with the exception of exterior panels on the MPC-68 and MPC-32, is equipped with a Boral (thermal neutron absorber) panel sandwiched between an alloy steel sheathing plate and the box panel, along the entire length of the active fuel region. The MPC is backfilled with helium up to the design-basis initial fill level (Table 1.2.2). This provides a stable, inert environment for long-term storage of the SNF. Heat is rejected from the SNF in the HI-STORM System to the environment by passive heat transport mechanisms only.

The helium backfill gas is an integral part of the MPC thermal design. The helium fills all the spaces between solid components and provides an improved conduction medium (compared to air) for dissipating decay heat in the MPC. Additionally, helium in the spaces between the fuel basket and the MPC shell is heated differentially and, therefore, subject to the "Rayleigh" effect which is discussed in detail later. For added conservatism, the increase in the heat transfer rate due to the Rayleigh effect contribution is neglected in this revision of the FSAR. To ensure that the helium gas is retained and is not diluted by lower conductivity air, the MPC confinement boundary is designed and fabricated to comply with the provisions of the ASME B&PV Code Section III, Subsection NB (to the maximum extent practical), as an all-seal-welded pressure vessel with redundant closures. It is demonstrated in Section 11.1.3 that the failure of one field-welded pressure boundary seal will not result in a breach of the pressure boundary. The helium gas is therefore retained and undiluted, and may be credited in the thermal analyses.

An important thermal design criterion imposed on the HI-STORM System is to limit the maximum fuel cladding temperature to within design basis limits (Table 4.3.7) for long-term storage of design basis SNF assemblies. An equally important design criterion is to minimize temperature gradients in the MPC so as to minimize thermal stresses. In order to meet these design objectives, the MPC baskets are designed to possess certain distinctive characteristics, which are summarized in the following.

The MPC design minimizes resistance to heat transfer within the basket and basket periphery regions. This is ensured by an uninterrupted panel-to-panel connectivity realized in the all-welded honeycomb basket structure. The MPC design incorporates top and bottom plenums with interconnected downcomer paths. The top plenum is formed by the gap between the bottom of the MPC lid and the top of the honeycomb fuel basket, and by elongated semicircular holes in each basket cell wall. The bottom plenum is formed by large elongated semicircular holes at the base of all cell walls. The MPC basket is designed to eliminate structural discontinuities (i.e., gaps) which introduce large thermal resistances to heat flow. Consequently, temperature gradients are minimized in the design, which results in lower thermal stresses within the basket. Low thermal stresses are also ensured by an MPC design that permits unrestrained axial and radial growth of the basket. The possibility of stresses due to restraint on basket periphery thermal growth is eliminated by providing adequate basket-to-canister shell gaps to allow for basket thermal growth during heat-up to design basis temperatures.

It is heuristically apparent from the geometry of the MPC that the basket metal, the fuel assemblies, and the contained helium mass will be at their peak temperatures at or near the longitudinal axis of the MPC. The temperatures will attenuate with increasing radial distance from this axis, reaching their lowest values at the outer surface of the MPC shell. Conduction along the metal walls and radiant heat exchange from the fuel assemblies to the MPC metal mass would therefore result in substantial differences in the bulk temperatures of helium columns in different fuel storage cells. Since two fluid columns at different temperatures in communicative contact cannot remain in static equilibrium, the non-isotropic temperature field in the MPC internal space due to conduction and radiation heat transfer mechanisms guarantee the incipience of the third mode of heat transfer: natural convection.

The preceding paragraph introduced the internal helium thermosiphon feature engineered into the MPC design. It is recognized that the backfill helium pressure, in combination with low pressure drop circulation passages in the MPC design, induces a thermosiphon upflow through the multi-cellular basket structure to aid in removing the decay heat from the stored fuel assemblies. The decay heat absorbed by the helium during upflow through the basket is rejected to the MPC shell during the subsequent downflow of helium in the peripheral downcomers. This helium thermosiphon heat extraction process significantly reduces the burden on the MPC metal basket structure for heat transport by conduction, thereby minimizing internal basket temperature gradients and resulting thermal stresses.

The helium columns traverse the vertical storage cavity spaces, redistributing heat within the MPC. Elongated holes in the bottom of the cell walls, liberal flow space and elongated holes at the top, and wide-open downcomers along the outer periphery of the basket ensure a smooth helium flow regime. The most conspicuous beneficial effect of the helium thermosiphon circulation, as discussed above, is the mitigation of internal thermal stresses in the MPC. Another beneficial effect is reduction of the peak fuel cladding temperatures of the fuel assemblies located in the interior of the basket. In the original HI-STORM licensing

analyses, no credit for the thermosiphon action was taken. To partially compensate for the reduction in the computed heat rejection capability due to the complete neglect of the global thermosiphon action within the MPC, heat conduction elements made of aluminum were interposed in the large peripheral spaces between the MPC shell and the fuel basket. These heat conduction elements, shown in the MPC Drawings in Section 1.5, are engineered such that they can be installed in the peripheral spaces to create a nonstructural thermal connection between the basket and the MPC shell. In their installed condition, the heat conduction elements will contact the MPC shell and the basket walls. MPC manufacturing procedures have been established to ensure that the thermal design objectives for the conduction elements set forth in this document are realized in the actual hardware. The presence of heat conduction elements in the canister design has been conservatively neglected in the thermal models of the HI-STORM 100 System in this revision of the Safety Analysis Report.

Four distinct MPC basket geometries are evaluated for thermal performance in the HI-STORM System. For intact PWR fuel storage, the MPC-24, MPC-24E, and MPC-32 designs are available. Four locations are designated for storing damaged PWR fuel in the MPC-24E design. A 68-cell MPC design (MPC-68, MPC-68F, and MPC-68FF) is available for storing BWR fuel (intact or damaged (including fuel debris)). All of the four basic MPC geometries (MPC-32, MPC-24, MPC-24E and MPC-68) are described in Chapter 1 wherein their design drawings can also be found.

The design maximum decay heat loads for storage of intact zircaloy clad fuel in the four MPCs are listed in Tables 4.4.20, 4.4.21, 4.4.28, and 4.4.29. Storage of intact stainless steel is evaluated in Subsection 4.3.2. . . Storage of zircaloy clad fuel with stainless steel clad fuel in an MPC is permitted. In this scenario, the zircaloy clad fuel is conservatively stipulated to meet the lower decay heat limits for stainless steel clad fuel. Storage of damaged, zircaloy clad fuel is evaluated in Subsection 4.4.1.1.4. . The axial heat distribution in each fuel assembly is assumed to follow the burnup profiles set forth by Table 2.1.11.

Thermal analysis of the HI-STORM System is based on including all three fundamental modes of heat transfer, namely conduction, natural convection and radiation. Different combinations of these modes are active in different parts of the system. These modes are properly identified and conservatively analyzed within each part of the MPC, the HI-STORM storage overpack and the HI-TRAC transfer cask, to enable bounding calculations of the temperature distribution within the HI-STORM System to be performed. In addition to storage within the HI-STORM overpack, loaded MPCs will also be located for short durations inside the transfer cask (HI-TRAC) designed for moving MPCs into and out of HI-STORM storage modules.

Heat is dissipated from the outer surface of the storage overpack and HI-TRAC to the environment by buoyancy induced airflow (natural convection) and thermal radiation. Heat transport through the cylindrical wall of the storage overpack and HI-TRAC is solely by conduction. While stored in a HI-STORM overpack, heat is rejected from the surface of the MPC via the parallel action of thermal radiation to the

inner shell of the overpack and convection to a buoyancy driven airflow in the annular space between the outer surface of the MPC and the inner shell of the overpack. This situation is similar to the familiar case of natural draft flow in furnace stacks. When placed into a HI-TRAC cask for transfer operations, heat is rejected from the surface of the MPC to the inner shell of the HI-TRAC by conduction and thermal radiation.

Within the MPC, heat is transferred between metal surfaces (e.g., between neighboring fuel rod surfaces) via a combination of conduction through a gaseous medium (helium) and thermal radiation. Heat is transferred between the fuel basket and the MPC shell by thermal radiation and conduction. The heat transfer between the fuel basket external surface and the MPC shell inner surface is further influenced by the "Rayleigh" effect. The heat transfer augmentation effect of this mechanism, as discussed earlier, is conservatively neglected.

As discussed later in this chapter, an array of conservative assumptions bias the results of the thermal analysis towards much reduced computed margins than would be obtained by a rigorous analysis of the problem. In particular, the thermal model employed in determining the MPC temperatures is consistent with the model presented in Rev. 9 of the HI-STAR FSAR submittal (Docket No. 72-1008).

As discussed in Chapter 2, the HI-STORM MPCs are identical to those utilized in the NRC-accepted HI-STAR System (Docket 71-1008 for storage). As such, many of the analysis methods utilized herein for performing thermal evaluations of the HI-STORM MPCs are identical to those already accepted for the HI-STAR System. Specifically, the analysis methods for evaluation of the following items are identical to those for the HI-STAR System:

- i. fuel assembly effective thermal conductivity
- ii. MPC fuel basket effective thermal conductivity
- iii. MPC fuel basket peripheral region effective thermal conductivity
- iv. aluminum heat conduction elements effective thermal conductivity
- v. MPC internal cavity free volume
- vi. MPC contents effective heat capacity and density
- vii. bounding fuel rod internal pressures and hoop stresses

In addition, thermal properties for all materials common to both the HI-STORM and HI-STAR systems are identical, including stainless and carbon steels, zircaloy, UO<sub>2</sub>, aluminum alloy 1100, Boral, Holtite-A, helium, air and paint.

The complete thermal analysis is performed using the industry standard ANSYS finite element modeling package [4.1.1] and the finite volume Computational Fluid Dynamics (CFD) code FLUENT [4.1.2]. ANSYS has been previously used and accepted by the NRC on numerous dockets [4.4.10,4.V.5.a]. The FLUENT CFD program is independently benchmarked and validated with a wide class of theoretical and experimental studies reported in the technical journals. Additionally, Holtec has confirmed the code's capability to reliably predict temperature fields in dry storage applications using independent full-scale test data from a loaded cask [4.1.3]. A series of Holtec topical reports, culminating in "Topical report on the HI-STAR/HI-STORM thermal model and its benchmarking with full-size cask test data", Holtec Report HI-992252, Rev. 1, document the comparison of the Holtec thermal model against the full-size cask test data [4.1.3]. In reference [4.1.3], the Holtec thermal model is shown to overpredict the measured fuel cladding temperature by a modest amount for every test set. In early 2000, PNL evaluated the thermal performance of HI-STORM 100 at discrete ambient temperatures using the COBRA-SFS Code. (Summary report communicated by T.E. Michener to J. Guttman (NRC staff) dated May 31, 2000 titled "TEMPEST Analysis of the Utah ISFSI Private Fuel Storage Facility and COBRA-SFS Analysis of the Holtec HI-STORM 100 Storage System"). The above-mentioned topical report has been updated to include a comparison of the Holtec thermal model results with the PNL solution. Once again, the Holtec thermal model is uniformly conservative, albeit by small margins. The benchmarking of the Holtec thermal model against the EPRI test data [4.1.3] and PNL COBRA-SFS study validate the suitability of the thermal model employed to evaluate the thermal performance of the HI-STORM 100 System in this document.

## 4.2 SUMMARY OF THERMAL PROPERTIES OF MATERIALS

Materials present in the MPCs include stainless steels (Alloy X), Boral neutron absorber, aluminum Alloy 1100 heat conduction elements, and helium. Materials present in the HI-STORM storage overpack include carbon steels and concrete. Materials present in the HI-TRAC transfer cask include carbon steels, lead, Holtite-A neutron shield, and demineralized water. In Table 4.2.1, a summary of references used to obtain cask material properties for performing all thermal analyses is presented.

Individual thermal conductivities of the alloys that comprise the Alloy X materials and the bounding Alloy X thermal conductivity are reported in Appendix 1.A of this report. Tables 4.2.2, 4.2.3 and 4.2.9 provide numerical thermal conductivity data of materials at several representative temperatures. Thermal conductivity data for Boral components (i.e., B<sub>2</sub>C core and aluminum cladding) is provided in Table 4.2.8. The temperature dependence of the thermal conductivities of helium and air is shown in Figure 4.2.1.

For the HI-STORM overpack, the thermal conductivity of concrete and the emissivity/absorptivity of painted surfaces are particularly important. Recognizing the considerable variations in reported values for these properties, we have selected values that are conservative with respect to both authoritative references and values used in analyses on previously licensed cask docket. Specific discussions of the conservatism of the selected values are included in the following paragraphs.

As specified in Table 4.2.1, the concrete thermal conductivity is taken from Marks' Standard Handbook for Mechanical Engineers, which is conservative compared to a variety of recognized concrete codes and references. Neville, in his book "Properties of Concrete" (4<sup>th</sup> Edition, 1996), gives concrete conductivity values as high as 2.1 Btu/(hr×ft×°F). For concrete with siliceous aggregates, the type to be used in HI-STORM overpacks, Neville reports conductivities of at least 1.2 Btu/(hr×ft×°F). Data from Loudon and Stacey, extracted from Neville, reports conductivities of 0.980 to 1.310 Btu/(hr×ft×°F) for normal weight concrete protected from the weather. ACI-207.1R provides thermal conductivity values for seventeen structures (mostly dams) at temperatures from 50-150°F. Every thermal conductivity value reported in ACI-207.1R is greater than the 1.05 Btu/(hr×ft×°F) value used in the HI-STORM thermal analyses.

Additionally, the NRC has previously approved analyses that use higher conductivity values than those applied in the HI-STORM thermal analysis. For example, thermal calculations for the NRC approved Vectra NUHOMS cask system (June 1996, Rev. 4A) used thermal conductivities as high as 1.17 Btu/(hr×ft×°F) at 100°F. Based on these considerations, the concrete thermal conductivity value stipulated for HI-STORM thermal analyses is considered to be conservative.

Holtite-A is a composite material consisting of approximately 37 wt% epoxy polymer, 1% B<sub>4</sub>C and 62% Aluminum trihydrate. Thermal conductivity of the polymeric component is low because polymers are generally characterized by a low conductivity (0.05 to 0.2 Btu/ft-hr-°F). Addition of fillers in substantial amounts raises the mixture conductivity up to a factor of ten. Thermal conductivity of epoxy filled resins with

Alumina is reported in the technical literature† as approximately 0.5 Btu/ft-hr-°F and higher. In the HI-STORM FSAR, a conservatively postulated conductivity of 0.3 Btu/ft-hr-°F is used in the thermal models for the neutron shield region (in the HI-TRAC transfer cask). As the thermal inertia of the neutron shield is not credited in the analyses, the density and heat capacity properties are not reported herein.

Surface emissivity data for key materials of construction are provided in Table 4.2.4. The emissivity properties of painted external surfaces are generally excellent. Kern [4.2.5] reports an emissivity range of 0.8 to 0.98 for a wide variety of paints. In the HI-STORM thermal analysis, an emissivity of 0.85<sup>††</sup> is applied to painted surfaces. A conservative solar absorptivity coefficient of 1.0 is applied to all exposed overpack surfaces.

In Table 4.2.5, the heat capacity and density of the different overpack materials are presented. These properties are used in performing transient (i.e., hypothetical fire accident condition) analyses. The temperature dependence of the viscosities of helium and air are provided in Table 4.2.6 and plotted in Figure 4.2.2.

The heat transfer coefficient for exposed surfaces is calculated by accounting for both natural convection and thermal radiation heat transfer. The natural convection coefficient depends upon the product of Grashof (Gr) and Prandtl (Pr) numbers. Following the approach developed by Jakob and Hawkins [4.2.9], the product  $Gr \cdot Pr$  is expressed as  $L^3 \Delta T Z$ , where L is height of the overpack,  $\Delta T$  is overpack surface temperature differential and Z is a parameter based on air properties, which are known functions of temperature, evaluated at the average film temperature. The temperature dependence of Z is provided in Table 4.2.7.

---

† "Principles of Polymer Systems", F. Rodriguez, Hemisphere Publishing Company (Chapter 10).  
†† This is conservative with respect to prior cask industry practice, which has historically utilized higher emissivities. For example, a higher emissivity for painted surfaces ( $\epsilon = 0.95$ ) is used in the previously licensed TN-32 cask TSAR (Docket 72-1021).

Table 4.2.1

SUMMARY OF HI-STORM SYSTEM MATERIALS  
THERMAL PROPERTY REFERENCES

| Material   | Emissivity          | Conductivity              | Density             | Heat Capacity       |
|--|---------------------|---------------------------|---------------------|---------------------|
| Helium   | N/A                 | Handbook<br>[4.2.2]       | Ideal Gas Law       | Handbook<br>[4.2.2] |
| Air  | N/A                 | Handbook<br>[4.2.2]       | Ideal Gas Law       | Handbook<br>[4.2.2] |
| Zircaloy   | EPRI<br>[4.2.3]     | NUREG<br>[4.2.6], [4.2.7] | Rust [4.2.4]        | Rust [4.2.4]        |
| UO <sub>2</sub>  | Not Used            | NUREG<br>[4.2.6], [4.2.7] | Rust [4.2.4]        | Rust [4.2.4]        |
| Stainless Steel  | Kern [4.2.5]        | ASME [4.2.8]              | Marks' [4.2.1]      | Marks' [4.2.1]      |
| Carbon Steel   | Kern [4.2.5]        | ASME [4.2.8]              | Marks' [4.2.1]      | Marks' [4.2.1]      |
| Boral <sup>†</sup>   | Not Used            | Test Data                 | Test Data           | Test Data           |
| Holtite-A <sup>††</sup>  | Not Used            | Lower Bound<br>Value Used | Not Used            | Not Used            |
| Concrete   | Not Used            | Marks' [4.2.1]            | Marks' [4.2.1]      | Handbook<br>[4.2.2] |
| Lead   | Not Used            | Handbook<br>[4.2.2]       | Handbook<br>[4.2.2] | Handbook<br>[4.2.2] |
| Water  | Not Used            | ASME [4.2.10]             | ASME [4.2.10]       | ASME [4.2.10]       |
| Aluminum Alloy<br>1100 (Optional<br>Heat Conduction<br>Elements) | Handbook<br>[4.2.2] | ASME [4.2.8]              | ASME [4.2.8]        | ASME [4.2.8]        |

† AAR Structures Boral thermophysical test data.

†† From neutron shield manufacturer's data [1.2.11].

Table 4.2.2

SUMMARY OF HI-STORM SYSTEM MATERIALS  
THERMAL CONDUCTIVITY DATA

| Material               | @ 200°F<br>(Btu/ft-hr-°F) | @ 450°F<br>(Btu/ft-hr-°F) | @ 700°F<br>(Btu/ft-hr-°F) |
|------------------------|---------------------------|---------------------------|---------------------------|
| Helium                 | 0.0976                    | 0.1289                    | 0.1575                    |
| Air <sup>†</sup>       | 0.0173                    | 0.0225                    | 0.0272                    |
| Alloy X                | 8.4                       | 9.8                       | 11.0                      |
| Carbon Steel           | 24.4                      | 23.9                      | 22.4                      |
| Concrete <sup>††</sup> | 1.05                      | 1.05                      | 1.05                      |
| Lead                   | 19.4                      | 17.9                      | 16.9                      |
| Water                  | 0.392                     | 0.368                     | N/A                       |

† At lower temperatures, Air conductivity is between 0.0139 Btu/ft-hr-°F (at 32°F) and 0.0176 Btu/ft-hr-°F at 212°F.

†† Assumed constant for the entire range of temperatures.

Table 4.2.3

SUMMARY OF FUEL ELEMENT COMPONENTS  
THERMAL CONDUCTIVITY DATA

| Zircaloy Cladding |                                | Fuel (UO <sub>2</sub> ) |                                |
|-------------------|--------------------------------|-------------------------|--------------------------------|
| Temperature (°F)  | Conductivity<br>(Btu/ft-hr-°F) | Temperature (°F)        | Conductivity<br>(Btu/ft-hr-°F) |
| 392               | 8.28 <sup>†</sup>              | 100                     | 3.48                           |
| 572               | 8.76                           | 448                     | 3.48                           |
| 752               | 9.60                           | 570                     | 3.24                           |
| 932               | 10.44                          | 793                     | 2.28 <sup>†</sup>              |

---

<sup>†</sup> Lowest values of conductivity used in the thermal analyses for conservatism.

Table 4.2.4

SUMMARY OF MATERIALS SURFACE EMISSIVITY DATA

| Material             | Emissivity |
|----------------------|------------|
| Zircaloy             | 0.80       |
| Painted surfaces     | 0.85       |
| Stainless steel      | 0.36       |
| Carbon Steel         | 0.66       |
| Sandblasted Aluminum | 0.40       |

Note: The emissivity of a metal surface is a function of the surface finish. In general, oxidation of a metal surface increases the emissivity. As stated in Marks' Standard Handbook for Mechanical Engineers: "Unless extraordinary pains are taken to prevent oxidation, however, a metallic surface may exhibit several times the emittance or absorptance of a polished specimen." This general statement is substantiated with a review of tabulated emissivity data from several standard references. These comparisons show that oxidized metal surfaces do indeed have higher emissivities than clean surfaces.

Table 4.2.5

## DENSITY AND HEAT CAPACITY PROPERTIES SUMMARY

| Material  | Density (lbm/ft <sup>3</sup> ) | Heat Capacity (Btu/lbm-°F) |
|---|--------------------------------|----------------------------|
| Helium  | (Ideal Gas Law)                | 1.24                       |
| Zircaloy  | 409                            | 0.0728                     |
| Fuel (UO <sub>2</sub> )                                       | 684                            | 0.056                      |
| Carbon steel  | 489                            | 0.1                        |
| Stainless steel   | 501                            | 0.12                       |
| Boral   | 154.7                          | 0.13                       |
| Concrete  | 142 <sup>†</sup>               | 0.156                      |
| Lead  | 710                            | 0.031                      |
| Water   | 62.4                           | 0.999                      |
| Aluminum Alloy 1100<br>(Optional Heat Conduction<br>Elements) | 169.9                          | 0.23                       |

<sup>†</sup> A minimum allowable density for concrete is specified as 146 lb/ft<sup>3</sup> (HI-STORM Overpack Serial Numbers 1 through 7) and 155 lb/ft<sup>3</sup> (HI-STORM Overpack Serial Number 8 onward) in Appendix 1.D. For conservatism in transient heatup calculations, a lower value is specified here.

Table 4.2.6

GASES VISCOSITY<sup>†</sup> VARIATION WITH TEMPERATURE

| Temperature<br>(°F) | Helium Viscosity<br>(Micropoise) <sup>††</sup> | Temperature<br>(°F) | Air Viscosity<br>(Micropoise) |
|---------------------|--|---------------------|-------------------------------|
| 167.4               | 220.5  | 32.0                | 172.0                         |
| 200.3               | 228.2  | 70.5                | 182.4                         |
| 297.4               | 250.6  | 260.3               | 229.4                         |
| 346.9               | 261.8  | -                   | -                             |
| 463.0               | 288.7  | -                   | -                             |
| 537.8               | 299.8  | -                   | -                             |
| 737.6               | 338.8  | -                   | -                             |

---

† Obtained from Rohsenow and Hartnett [4.2.2].

†† This data is also provided in graphical form in Figure 4.2.2.

Table 4.2.7

VARIATION OF NATURAL CONVECTION PROPERTIES  
PARAMETER "Z" FOR AIR WITH TEMPERATURE

| Temperature (°F) | Z (ft <sup>3</sup> °F <sup>1</sup> ) |
|------------------|--------------------------------------|
| 40               | 2.1×10 <sup>6</sup>                  |
| 140              | 9.0×10 <sup>5</sup>                  |
| 240              | 4.6×10 <sup>5</sup>                  |
| 340              | 2.6×10 <sup>5</sup>                  |
| 440              | 1.5×10 <sup>5</sup>                  |

---

† Obtained from Jakob and Hawkins [4.2.9].

Table 4.2.8

BORAL COMPONENT MATERIALS<sup>†</sup>  
THERMAL CONDUCTIVITY DATA

| Temperature (°F) | B <sub>4</sub> C Core Conductivity<br>(Btu/ft-hr-°F) | Aluminum Cladding<br>Conductivity (Btu/ft-hr-°F) |
|------------------|--|--|
| 212              | 48.09  | 100.00   |
| 392              | 48.03  | 104.51   |
| 572              | 47.28  | 108.04   |
| 752              | 46.35  | 109.43   |

---

<sup>†</sup> Both B<sub>4</sub>C and aluminum cladding thermal conductivity values are obtained from AAR Structures Boral thermophysical test data.

Table 4.2.9

HEAT CONDUCTION ELEMENTS (ALUMINUM ALLOY 1100)  
THERMAL CONDUCTIVITY DATA

| Temperature (°F) | Conductivity (Btu/ft-hr-°F) |
|------------------|-----------------------------|
| 100              | 131.8                       |
| 200              | 128.5                       |
| 300              | 126.2                       |
| 400              | 124.5                       |

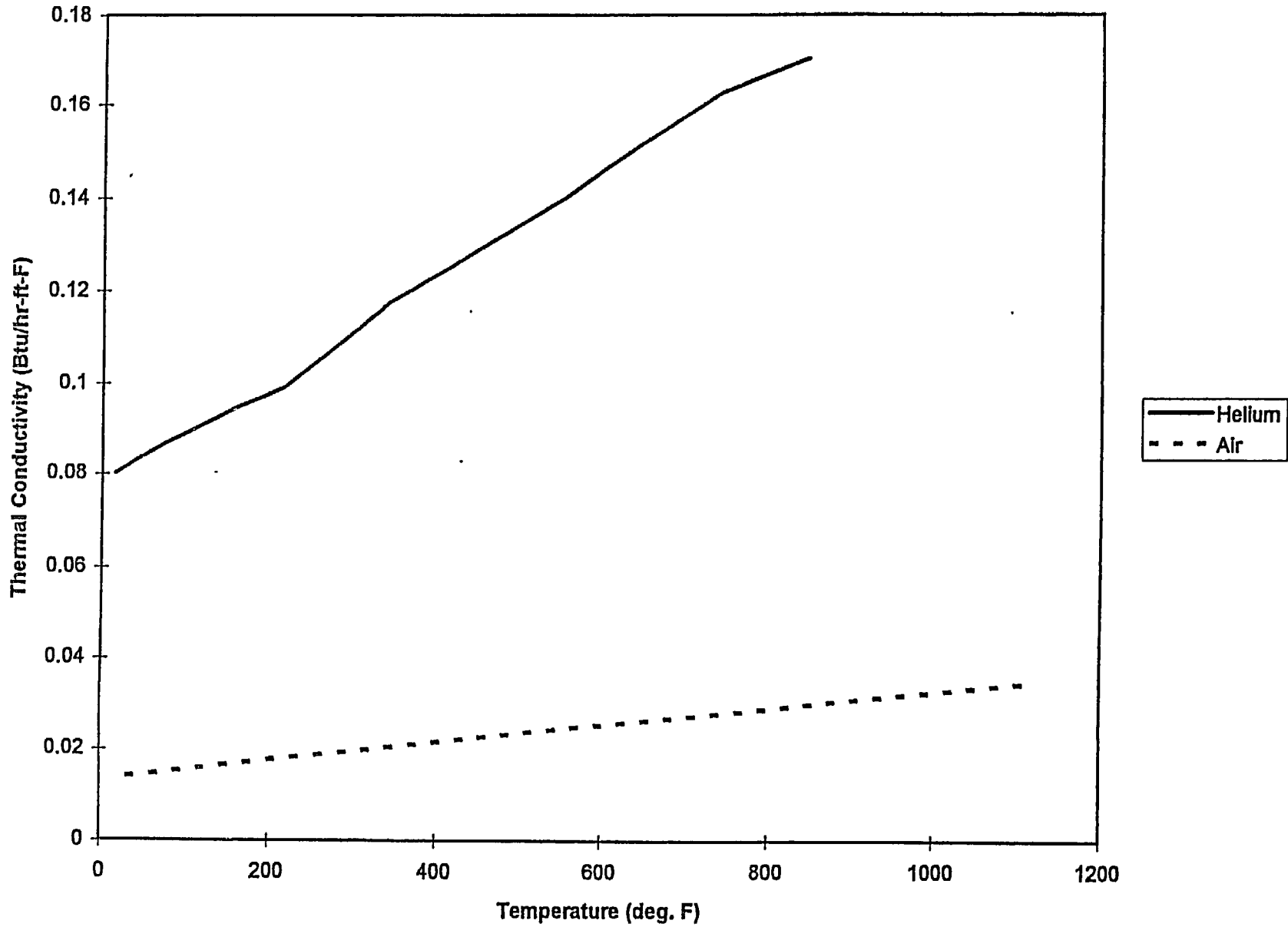


FIGURE 4.2.1: THERMAL CONDUCTIVITY OF HELIUM AND AIR VS. TEMPERATURE

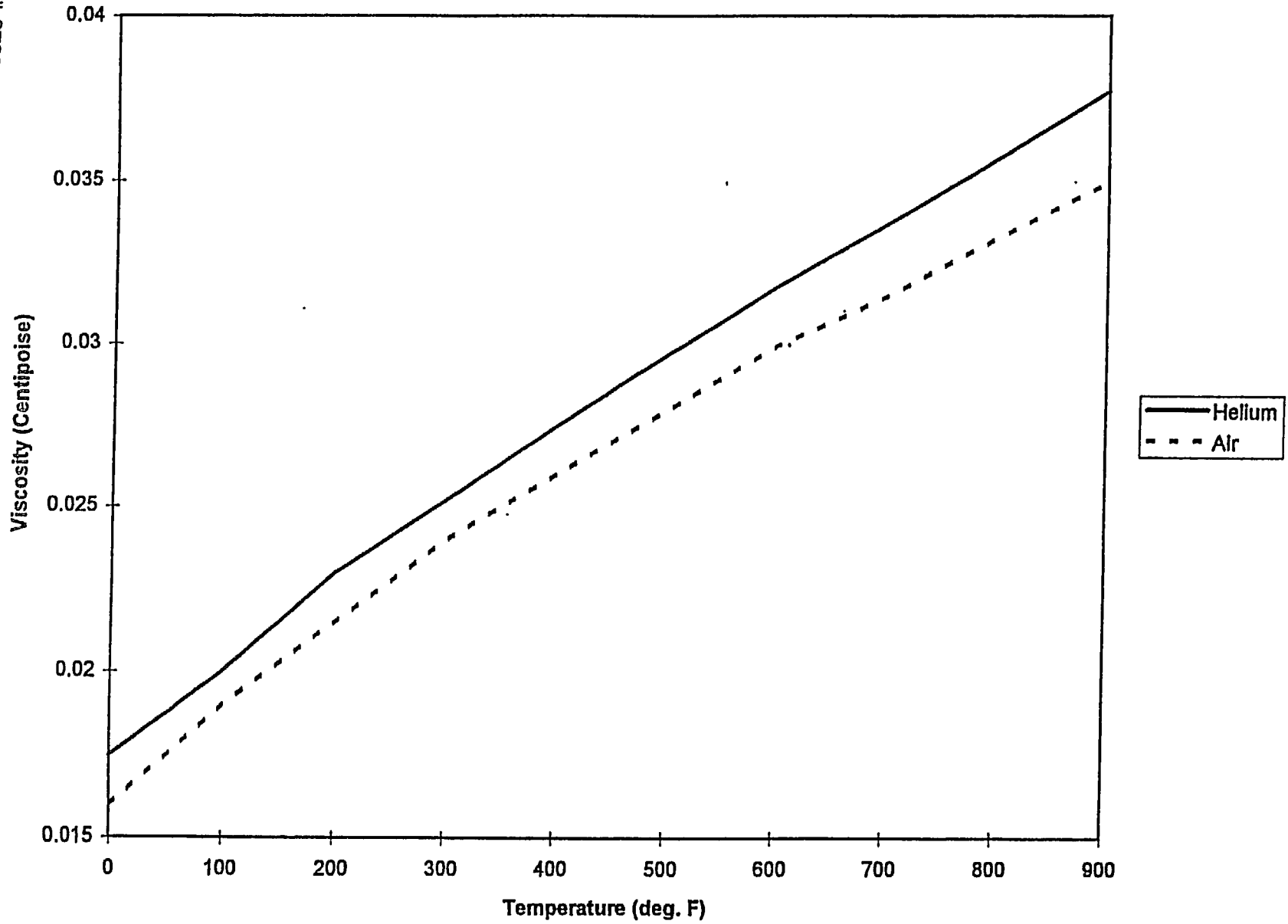


FIGURE 4.2.2: VISCOSITY OF HELIUM AND AIR VS. TEMPERATURE

### 4.3 SPECIFICATIONS FOR COMPONENTS

HI-STORM System materials and components designated as "Important to Safety" (i.e., required to be maintained within their safe operating temperature ranges to ensure their intended function) which warrant special attention are summarized in Table 4.3.1. The neutron shielding ability of Holtite-A neutron shield material used in the HI-TRAC onsite transfer overpack is ensured by demonstrating that the material exposure temperatures are maintained below the maximum allowable limit. Long-term integrity of SNF is ensured by the HI-STORM System thermal performance that demonstrates that fuel cladding temperatures are maintained below design basis limits. Boral used in MPC baskets for criticality control (a composite material composed of B<sub>4</sub>C and aluminum) is stable up to 1000°F for short-term and 850°F for long-term dry storage<sup>†</sup>. However, for conservatism, a significantly lower maximum temperature limit is imposed. The overpack concrete, the primary function of which is shielding, will maintain its structural, thermal and shielding properties provided that American Concrete Institute (ACI) temperature limits are not exceeded.

Compliance to 10CFR72 requires, in part, identification and evaluation of short-term off-normal and severe hypothetical accident conditions. The inherent mechanical stability characteristics of cask materials and components ensure that no significant functional degradation is possible due to exposure to short-term temperature excursions outside the normal long-term temperature limits. For evaluation of HI-STORM System thermal performance under off-normal or hypothetical accident conditions, material temperature limits for short-duration events are provided in Table 4.3.1.

#### 4.3.1 Evaluation of Moderate Burnup Zircaloy Clad Fuel

Demonstration of fuel cladding integrity against the potential for degradation and gross rupture throughout the entire dry cask storage period is mandated by the Code of Federal Regulations (Part 72, Section 72.122(h)). The specific criteria required to establish fuel cladding integrity, set forth in NUREG-1536 (4.0,IV,5&6) are:

- i. For each fuel type proposed for storage, the dry cask storage system should ensure a very low probability of cladding breach during long-term storage.
- ii. Fuel cladding damage resulting from creep cavitation should be limited to 15% of the original cladding cross sectional area during dry storage.

Consistent with the NUREG-1536 criteria, the HI-STORM System is designed to preclude gross fuel cladding failures during the entire duration of storage. A method for establishing the peak cladding temperature limits in accordance with the diffusion-controlled cavity growth (DCCG) methodology was proposed by the Lawrence Livermore National Laboratory [4.3.5]. Recent NRC guidelines<sup>††</sup>, applicable

---

<sup>†</sup> AAR Advanced Structures Boral thermophysical test data.

<sup>††</sup> Interim Staff Guidance-11, "Storage of Spent Fuel Having Burnups in Excess of 45,000 MWD/MtU", USNRC.

for high burnup fuel (greater than 45,000 MWD/MTU), require that alternate methods be adopted for computing peak cladding temperature limits (see Appendix 4.A). For the FSAR request for approval for fuel burnups up to 45,000 MWD/MTU, the PNL-6189 [4.3.1] creep rupture criteria has been conservatively adopted in accord with the latest NRC guidelines so as to develop more restrictive permissible peak fuel cladding temperatures for the HI-STORM System. A discussion of the DCCG and PNL criteria for establishing allowable cladding temperatures is provided in the balance of the section.

#### 4.3.1.1 Cladding Temperature Limits (DCCG Criteria)

For SNF of a given age (decay time), the permissible peak cladding temperature is a direct function of the cladding hoop stress, which in turn depends on the radius-to-thickness ratio of the fuel rod and its internal pressure. The rod internal pressure  $P_i$  is a function of the maximum initial fill pressures (Tables 4.3.2 and 4.3.5) and fuel burnup dependent fission gas release. The free rod volumes in the third column of Tables 4.3.2 and 4.3.5 are defined as free rod volumes in each fuel rod available for pressurization with fill gas. The free rod volume is the cumulative sum of the open top plenum space, the pellet-to-cladding annular space and the inter-pellet junction space. As a lower bound value of the free rod volume is conservative for cladding stress at operating temperatures, only the nominal gas plenum space is shown. The plenum length for miscellaneous BWR fuel assemblies is set to 12 inches. The radius-to-thickness ratio  $r$  is determined based on rod nominal dimension values (Tables 4.3.3 and 4.3.6), with consideration of maximum cladding thickness loss due to in-reactor oxidation, as reported by PNL [4.3.4].

The data presented in Tables 4.3.2 and 4.3.5 are combined with theoretical bounding fuel rod internal gas pressures from published technical sources [4.3.1 and 4.3.6], to absolutely ensure that bounding clad hoop stress values are used in the determination of gross cladding integrity. These bounding pressures are so large that they approach physical upper bounds for some fuel assemblies, as the corresponding hoop stresses approach the yield stress of zircaloy (approximately 172 MPa at 750°F [4.3.7]). The theoretical bounding rod internal pressure for PWR assemblies is compared, in Figure 4.3.1, to the published test data for assemblies from two different plants. From this figure, the large conservatism in the theoretical bounding pressure is evident.

These theoretical bounding pressures, from two sources, are provided below for PWR and BWR fuel:

PWR: 2416 psia [4.3.1], 16 MPa (2320 psia) [4.3.6]

BWR: 1094 psia [4.3.1], 70 atm (1029 psia) [4.3.6]

The coincident gas plenum temperatures reported in the PNL report [4.3.1] are 387°C for PWR assemblies and 311°C for BWR assemblies at reactor operating conditions. It can be seen in Figures 4.4.16 and 4.4.17 that the temperature distribution of gas in the fuel rods, a great bulk of which is located in the top gas plenum, is well below the in-core condition gas temperatures reported above (PWR fuel) and for the most part in the BWR fuel. In the interest of conservatism, no credit is taken for the substantially lower gas plenum temperatures that prevail during dry storage. Furthermore, the greater of the literature

pressure data listed above is adopted for performing peak clad temperature limit calculations. The values utilized for  $P_i$  are 2416 psia for PWR<sup>†</sup> assemblies and 1094 psia for BWR assemblies.

By utilizing  $P_i$  and  $r^*$ , the cladding stress for various PWR fuel types is calculated from Lame's formula and summarized in Table 4.3.3. For certain outlier fuel types (PWR), the stress calculations are provided in Table 4.3.9. An inspection of cladding stress data summarized in Tables 4.3.9 and 4.3.3 indicates 152.7 MPa as the theoretical bounding value of cladding stress ( $\sigma_{max}$ ) for the PWR SNF. Corresponding fill gas data and calculations of cladding stress for the various BWR SNF types are summarized in Tables 4.3.5 and 4.3.6, respectively. An inspection of the cladding stress data in Table 4.3.6 indicates that the theoretical bounding value of the cladding hoop stress for the BWR SNF is 72.7 MPa. The theoretical bounding values of  $\sigma_{max}$  for the array of PWR and BWR SNF types are thus 152.7 MPa and 72.7 MPa, respectively.

In this manner, the maximum conceivable values of cladding hoop stress are calculated for use in subsequent DCCG method calculations. As an additional conservatism, the peak fuel rod cladding hoop stresses are conservatively held constant throughout the dry storage period. In practice, the rod cladding hoop stresses are the maximum when the casks are initially loaded and monotonically decrease with the time-decreasing heat load and temperature. The Ideal Gas Law governs the decrease in pressure with decreasing temperature.

As stated earlier, the value of  $\sigma_{max}$  is required to establish the peak cladding temperature limit using the DCCG method. The DCCG model-based zircaloy cladding temperature limit computation, in accordance with the LLNL procedure [4.3.5], requires a solution to the following equation expressed in terms of the area fraction of de-cohesion (A):

$$\int_{A_i}^{A_f} \frac{dA}{f(A)} = \int_{t_0}^{t_0+t_s} G(t) dt$$

where:

- $A_i$  = initial area fraction of de-cohesion
- $A_f$  = end of storage life area fraction of de-cohesion (limited to 0.15)
- $t_0$  = age of fuel prior to dry cask storage (years)
- $t_s$  = dry cask storage period (40 years)
- $f(A)$  = area fraction of de-cohesion function
- $G(t)$  = damage function

The term on the left-hand side of this equation represents the area fraction of de-cohesion that occurs over the dry storage period. The term on the right-hand side represents the cumulative damage over the same period. The area fraction of de-cohesion function and the damage function,  $f(A)$  and  $G(t)$  respectively, are:

<sup>†</sup> Certain outlier fuels (Table 4.3.9) are stipulated to be below a postulated limiting rod pressure.

$$f(A) = \frac{[1 - (\frac{A_i}{A})^{1/2}](1 - A)}{A^{1/2} [\frac{1}{2} \ln \frac{1}{A} - \frac{3}{4} + A(1 - \frac{A}{4})]}$$

$$G(t) = \frac{32}{3\pi^{1/2}} \frac{F_B^{3/2}(\alpha)}{F_V(\alpha)} \frac{\Omega \delta \sigma_{\infty}(t)}{K \lambda^3} \frac{D_{GB}[T(t)]}{T(t)}$$

where:

$$F_B(\alpha) = \pi \sin^2(\alpha)$$

$$F_V(\alpha) = \frac{2\pi}{3} (2 - 3 \cos \alpha + \cos^3 \alpha)$$

$$T(t) = \text{time-dependent peak cladding temperature}$$

$$K = \text{Boltzmann constant } (1.38053 \times 10^{-23} \text{ J/K})$$

A discussion on the balance of parameters in the damage function  $G(t)$  is provided below.

#### Cladding Hoop Stress ( $\sigma_{\infty}(t)$ )

The cladding hoop stress is principally dependent upon the specific fuel rod dimensions, initial fill rod pressure, time-dependent storage temperature, and fuel burnup dependent fission gas release from the fuel pellets into the rod plenum space. The peak fuel rod pressure for various analyzed PWR and BWR fuel types at the start of the dry storage period are summarized in Tables 4.3.3 and 4.3.6. The highest peak rod stress among the various PWR and BWR fuel types, previously defined as  $\sigma_{max}$  are conservatively applied as constant (time-independent) cladding hoop stresses in the DCCG model-based damage function.

#### Grain Boundary Cavity Dihedral Angle ( $\alpha$ )

The LLNL report [4.3.5] has determined the dihedral angle ( $\alpha$ ) for pure metals to be  $75^\circ$ . To account for possible non-ideal conditions, a conservatively lower  $\alpha$  equal to  $60^\circ$  is applied to the DCCG model.

#### Zirconium Atomic Volume ( $\Omega$ )

The zirconium atomic volume estimated from several literature sources as documented in the LLNL report [4.3.5] is in the range of  $2.31 \times 10^{-29} \text{ m}^3$  to  $3.37 \times 10^{-29} \text{ m}^3$ . In the interest of conservatism, the maximum estimated atomic volume equal to  $3.37 \times 10^{-29} \text{ m}^3$  is used for the analysis.

### Grain Boundary Thickness ( $\delta$ )

The LLNL report [4.3.5] has recommended a grain boundary thickness of three Burgers vectors to be adequate for the analysis. Thus,  $\delta = 3 (3.23 \times 10^{-10}) = 9.69 \times 10^{-10}$  m is used in the analysis.

### Average Cavity Spacing ( $\lambda$ )

The type of nucleation mechanism and the density of nucleation sites control cavity spacing. The LLNL report [4.3.5] references an experimental study that found that the cavity spacing is in the range of  $10 \times 10^{-6}$  to  $20 \times 10^{-6}$  m. In the interest of conservatism, the minimum reported cavity spacing equal to  $10 \times 10^{-6}$  m is used in the analysis.

### Grain Boundary Diffusion Rate ( $D_{GB}$ )

Two grain boundary diffusion rate correlations for zirconium are reported in the LLNL report [4.3.5]. The two correlations provide diffusion rate estimates that are approximately two orders of magnitude apart from each other. Consequently, the more conservative correlation that provides a higher estimate of the grain boundary diffusion rate is used in the analysis. This more conservative correlation, yielding units of  $m^2/sec$ , is:

$$D_{GB} = 5.9 \times 10^{-6} \exp [-131,000/RT]$$

where R is the universal gas constant in J/mol $\times$ K units.

### Time-Dependent Peak Cladding Temperature (T(t))

The peak cladding temperature during long-term storage is principally dependent upon the thermal heat load from the stored fuel assemblies, which is imposed on the cask. It is well established that the rate of radioactive decay in a fuel assembly exponentially attenuates with the age of fuel. Consequently, the peak cladding temperature during long-term storage will also attenuate rapidly as a direct consequence of the heat load reduction with time, which is modeled using the data provided in USNRC Regulatory Guide 3.54 [4.3.3]. To confirm the applicability of the Reg. Guide 3.54 data, comparisons with the ORIGEN-S source term calculation results discussed in Chapter 5 of this FSAR were performed. Figures 4.3.2 and 4.3.3 present graphical comparisons of the decay heat versus decay time profiles from the Reg. Guide data with the profiles from the ORIGEN-S calculations. For the design-basis maximum decay heat load (which is approached with 5-year old fuel), the Reg. Guide data agrees favorably with the ORIGEN-S calculation results. The Reg. Guide data is, in fact, slightly conservative with respect to the ORIGEN-S calculations.

It should be noted that the area fraction of de-cohesion function  $f(A)$  approaches zero in the limit as  $A \rightarrow A_i$ . Consequently, the mathematical singularity in the integral  $\int_{A_i}^A \frac{dA}{f(A)}$  is numerically accommodated by using an alternate form given below:

$$\int_{A_i}^A \frac{dA}{f(A)} = \text{Limit } \varepsilon \rightarrow 0 \int_{A_i+\varepsilon}^{A_f} \frac{A^{1/2} \left[ \frac{1}{2} \ln \frac{1}{A} - \frac{3}{4} + A \left( 1 - \frac{A}{4} \right) \right] dA}{\left[ 1 - \left( \frac{A_i}{A} \right)^{1/2} \right] (1-A)}$$

The allowable area fraction of de-cohesion using  $A_i = 0.05$ ,  $\varepsilon = 0.0001$ , and  $A_f = 0.15$  is determined to be equal to 0.15211.

This is consistent with an alternate form of the DCCG model reported in the PNL study [4.3.1, Appendix D] as reproduced below:

$$A_f = \int_0^{t_f} G(t) dt \leq 0.15$$

The cumulative damage  $G(t)$  can be evaluated as a function of the initial fuel cladding temperature and corresponding cladding stress, which are the two primary constituents of the damage function. The initial cladding hoop stress at a bounding storage temperature has already been determined. All other parameters in the  $G(t)$  function (except for the initial peak cladding temperature limit  $T_o$ ) have been defined as discussed previously in this section. The cumulative cladding damage experienced during the 40-year dry cask storage period is determined by integrating the  $G(t)$  function. The initial peak cladding temperature limit parameter  $T_o$  is iteratively adjusted to limit the cumulative damage to 15% as required by the NUREG-1536 Criterion (ii) discussed earlier in this section. The initial peak cladding temperature limits for the bounding PWR and BWR fuel assemblies are provided in Table 4.3.7.

#### 4.3.1.2 Permissible Cladding Temperatures (PNL Method)

In this subsection, the permissible peak clad temperature limits for the HI-STORM System are computed using the so-called "generic CSFM temperature limits" data provided in a PNL report [4.3.1]. The generic CSFM temperature limits, known to be more conservative than the previously discussed DCCG method, define the maximum permissible initial storage temperature ( $T_p$ ) of cladding as a function of initial cladding stress ( $\sigma_{max}$ ) and fuel age ( $\tau_f$ ) at the start of dry storage. The stress developed in cladding is a function of rod diameter-to-thickness ratio ( $d_c$ ) and the internal rod gas pressure ( $P_o$ ) which prevails during dry storage conditions. In the previous subsection, the W-14x14 and GE-7x7 fuel types were identified to have the highest  $d_c$  in the class of PWR† and BWR fuels, respectively. The cladding thickness data in Tables 4.3.3

† Certain outlier fuels are excluded from this class as the cladding stress is bounded by the design basis W 14x14 fuel (Table 4.3.9).

and 4.3.6 is the corroded wall thickness after including maximum oxidation loss during reactor operation. The  $d_c$  for bounding PWR and BWR SNF is 18.3 and 19.3, respectively.

The cladding stress in a fuel rod is principally dependent upon the rod internal pressure  $P_o$  which is postulated to reasonably bound rod pressures of SNF during dry storage. PNL [4.3.2] and EPRI [4.3.4] provide in-core irradiation rod pressures information which are theoretical upper bounds. For reference, they are provided herein in Subsection 4.3.1.1. Other robust sources† which authoritatively deal with this matter report peak rod pressures of 1600 psia (PWR) and 900 psia (BWR) during in-core irradiation. The conservatism in the in-core irradiation rod pressures for bounding rods pressure during dry cask storage is illustrated in Figure 4.3.1. From published test data on rods pressure measured from two different plants, the projected rods pressure in dry storage is significantly lower than the in-core irradiation pressure (~1350 psia for PWR). For computing permissible cladding temperatures for SNF storage in the HI-STORM System, a conservatively postulated  $P_o$  of 2000 psia (PWR) and 1000 psia (BWR) are employed in this work.

The dry storage rod pressure  $P_o$  for PWR and BWR types is postulated as 2000 psia and 1000 psia, respectively. Having obtained  $P_o$ , the cladding stress ( $\sigma_{max}$ ) is readily obtained by the product of  $P_o$  and  $d_c$  and dividing the result by 2 (Lame's formula). The cladding stress computed in this manner is 18,300 psi (126.1 MPa) and 9,650 psia (66.5 MPa) for PWR and BWR fuel, respectively. From the generic CSFM temperature limits table in the PNL report [4.3.1, page 3-19] and  $\sigma_{max}$ , the permissible peak clad temperature limit ( $T_p$ ) as a function of  $\tau_f$  is readily obtained. The  $T_p$  vs.  $\tau_f$  results for PWR and BWR fuel are presented in Table 4.3.7. The peak clad temperature limits (DCCG criteria) and permissible cladding temperature limits (PNL criteria) data are graphically depicted in Figure 4.3.4. The more restrictive results (PNL criteria) are applied to the HI-STORM System. In Table 4.3.8, permissible (PNL criteria) temperatures for an outlier fuel type (Dresden-1 thin clad) are evaluated at a conservatively bounding stress (94.1 MPa, Table 4.3.6). These temperatures are applicable to Low Heat Emitting (LHE) fuel evaluated in Subsection 4.4.1.1.13.

#### 4.3.2 Evaluation of Stainless Steel Clad Fuel

Approximately 2,200 PWR and BWR fuel assemblies stored in the United States were manufactured with stainless steel cladding. All stainless steel cladding materials are of the austenitic genre with the ASTM alloy compositions being principally type 304 and 348H. For long-term storage conditions, a recent EPRI/PNL study [4.3.4] recommends a 430°C (806°F) peak stainless steel cladding temperature limit. This temperature limit is substantially higher than the peak fuel cladding temperatures calculated for the HI-STORM System with design-basis maximum decay heat loads and zircaloy clad fuel (see Tables 4.4.9 and 4.4.10).

---

† NRC SER for HI-STORM System (Docket 72-1014)

It is recognized that the peak cladding temperature of stainless fuel will differ from zircaloy clad fuel principally due to the following differences:

- i. Differences in decay heat levels
- ii. Differences in cladding emissivity
- iii. Differences in cladding conductivity
- iv. Differences in fuel rod array dimensions

The net planar thermal resistance of the equivalent homogenized axisymmetric MPC basket containing stainless steel clad fuel is greater than that with zircaloy clad fuel. The higher resistance arises principally from the significantly lower emissivity of the stainless steel cladding. This factor is, however, offset by significantly lower design-basis heat loads prescribed for a HI-STORM System containing stainless steel clad fuel. A 20% (MPC-68, MPC-24, and MPC-24E) and 25% (MPC-32) or greater reduction in the design basis heat duty for stainless steel fuel (i.e., 20%-25% lower than zircaloy clad fuel) bounds the nominal percentage decrease in MPC basket effective thermal conductivity<sup>†</sup> (stainless steel fueled baskets are between 9% (MPC-68) to 25% (MPC-32) less conducting, as shown in Table 4.4.3). The design basis maximum allowable decay heat for MPCs fueled with stainless steel clad fuel are conservatively set to be 20% lower than zircaloy-fueled basket maximum heat load for MPC-24, MPC-24E, and MPC-68 (25% lower for MPC-32). Therefore, it is concluded that the peak cladding temperature for stainless steel clad fuel will be bounded by zircaloy clad fuel results. Consequently, in view of the conservative heat loads prescribed for stainless steel clad fuel, a separate thermal analysis to demonstrate the adequacy of stainless steel cladding integrity for storage in the HI-STORM System is not necessary.

#### 4.3.3 Short-Term Cladding Temperature Limit

For short-term durations, relatively high fuel cladding temperature limits have been historically accepted. For example, the Safety Analysis Report of the STC transport cask (Docket No. 71-9235), recently certified by the USNRC, permits 1200°F (approximately 649°C) as the maximum value of the peak cladding temperature,  $T_{max}$  for transport of SNF with up to 45,000 MWD/MTU burnup. NUREG-1536 and PNL test data [4.3.2], limiting themselves to medium burnup levels (28,800 MWD/MTU), endorse a somewhat lower  $T_{max}$  ( $T_{max} = 570^{\circ}\text{C}$  or 1058°F). Based on the published industry test data, guidance in the literature, and analytical reasoning, we herein prescribe 570°C as the admissible value of  $T_{max}$  for SNF, with accumulated burnups up to 45,000 MWD/MTU, in the HI-STORM System.

A Brookhaven report written for EPRI [4.3.6] asserts that fuel cladding rupture becomes "virtually absent at stresses below about 200 MPa". It can be readily deduced that the peak cladding stress for the limiting condition of 570°C cladding temperature will be below 200 MPa for the SNF burnup levels considered in this FSAR. Recalling that  $\sigma_{max} = 152.7$  MPa (Table 4.3.3) at a 387°C average rod gas temperature, the

---

<sup>†</sup> The term "effective conductivity" of the fuel basket is defined in Section 4.4.1.

cladding circumferential stress  $\sigma_{\text{peak}}$  at 570°C is obtained by direct proportionality in absolute gas temperature:

$$\sigma_p = \sigma_{\text{max}} \times (570 + 273)/(387 + 273) = 195.0 \text{ MPa}$$

Therefore, a short-term fuel cladding temperature limit  $T_{\text{max}} = 570^\circ\text{C}$  is considered safe to preclude fuel cladding failure. For fuel claddings which have been exposed to higher levels of in-core irradiation, the irradiation process progressively hardens the cladding material, making high burnup fuel less susceptible to stress-induced creep and fracture at these stress levels (up to 200 MPa). A recent high burnup fuel cladding integrity study by German researchers<sup>†</sup> corroborates this physical reasoning. In the German study, fuel rods with up to 64,000 MWD/MTU burnup were tested at substantially higher stresses (~400 MPa and 600 MPa) without cladding failure.

The EPRI report [4.3.6] cites experiments on fourteen irradiated Turkey Point Unit 3 rods carried out by Einziger et al.<sup>††</sup> in 1982 which showed no breach in cladding even after as much as 7% strain was accumulated in elevated temperatures lasting for 740-1,000 hours. Einziger's test data corroborates our selection of  $T_{\text{max}} = 570^\circ\text{C}$  as the short duration limiting temperature.

---

<sup>†</sup> "Short-time Creep and Rupture Tests on High Burnup Fuel Rod Cladding", by W. Göll, E. Toscano and H. Spilker.

<sup>††</sup> "High Temperature Post Irradiation Materials Performance of Spent Pressurized Water Reactor Fuel Rods under Dry Storage Conditions," by R.E. Einziger, S.D. Atkin, D.E. Stallrecht, and V.S. Pasupathi, Nuclear Technology, 57:65-80 (1982)

Table 4.3.1

HI-STORM SYSTEM MATERIAL TEMPERATURE LIMITS

| Material                      | Normal Long-Term Temperature Limits [°F]          | Short-Term Temperature Limits [°F] |
|-------------------------------|---|------------------------------------|
| Zircaloy fuel cladding        | (Moderate <sup>†</sup> Burnup)<br>See Table 4.3.7 | 1058                               |
| Stainless steel fuel cladding | 806   | 1058                               |
| Boral <sup>††</sup>           | 800   | 950                                |
| Holtite-A <sup>†††</sup>      | 300   | 300                                |
| Concrete                      | 200   | 350                                |
| Water                         | 307 <sup>††††</sup>                               | N/A                                |

† High burnup fuel storage limits are established in Appendix 4.A.

†† Based on AAR Structures Boral thermophysical test data.

††† See Section 1.2.1.3.2.

†††† Saturation temperature at HI-TRAC water jacket design pressure.

Table 4.3.2

SUMMARY OF PWR ASSEMBLY RODS INITIAL GAS FILL DATA

| Assembly Type       | Rods Per Assembly | Free Rod Volume (in <sup>3</sup> ) | Fill Pressure (psig) at 70°F | Fill Gas Volume at STP <sup>†</sup> |                       |
|---------------------|-------------------|------------------------------------|------------------------------|-------------------------------------|-----------------------|
|                     |                   |                                    |                              | Per Rod (Liters)                    | Per Assembly (Liters) |
| W-14×14 Std.        | 179               | 0.67 <sup>††</sup>                 | 0-460                        | 0.845                               | 151.2                 |
| W-15×15 Std.        | 204               | 0.67 <sup>††</sup>                 | 0-475                        | 0.633                               | 129.1                 |
| W-17×17 Std.        | 264               | 0.59 <sup>††</sup>                 | 275-500                      | 0.666                               | 175.8                 |
| B&W-15×15 Mark B    | 208               | 1.308                              | 415                          | 0.582                               | 121.1                 |
| B&W-17×17 Mark C    | 264               | 0.819                              | 435                          | 0.381                               | 100.6                 |
| CE-14×14 Std.       | 164               | 1.693                              | 300-450                      | 0.814                               | 133.5                 |
| CE-16×16 Std.       | 220               | 1.411                              | 300-450                      | 0.678                               | 149.2                 |
| B&W-15x15 Mark B-11 | 208               | 1.260                              | 415                          | 0.560                               | 116.5                 |
| CE-14x14 (MP2)      | 176               | 1.728                              | 300-450                      | 0.831                               | 146.2                 |

<sup>†</sup> STP stands for standard temperature (0°C) and pressure (1 atmosphere).

<sup>††</sup> Bounding low values verified from Holtec's proprietary information database.

Table 4.3.3

## BOUNDING VALUES OF FUEL CLADDING STRESS FOR PWR SNF

|   | W-<br>14X14<br>Std. | W-<br>15X15<br>Std. | W-<br>17X17<br>Std. | B&W-<br>15X15<br>Mark B | B&W-<br>17X17<br>Mark C | CE-<br>14X14<br>Std. | CE-<br>16X16<br>Sys 80 | CE-14x14<br>(MP2) |
|---|---------------------|---------------------|---------------------|-------------------------|-------------------------|----------------------|------------------------|-------------------|
| Fresh Fuel Rods<br>O.D. (inch)                                      | 0.4220              | 0.422               | 0.374               | 0.430                   | 0.379                   | 0.440                | 0.382                  | 0.440             |
| End of Life<br>Oxidation<br>Thickness<br>(inch) <sup>†</sup>        | 0.0027              | 0.0027              | 0.0027              | 0.0027                  | 0.0027                  | 0.0027               | 0.0027                 | 0.0027            |
| End of Life Rods<br>O.D. (inch)                                     | 0.4166              | 0.4166              | 0.3686              | 0.4246                  | 0.3736                  | 0.4346               | 0.3766                 | 0.4346            |
| Rods I.D. (inch)  | 0.3734              | 0.373               | 0.329               | 0.377                   | 0.331                   | 0.384                | 0.332                  | 0.388             |
| Average Tube<br>Diameter (inch)                                     | 0.3950              | 0.3948              | 0.3488              | 0.4008                  | 0.3523                  | 0.4093               | 0.3493                 | 0.4113            |
| Wall Thickness<br>(inch)  | 0.0216              | 0.0218              | 0.0198              | 0.0238                  | 0.0213                  | 0.0253               | 0.0223                 | 0.0233            |
| Theoretical<br>Bounding Rod<br>Pressure (MPa<br>gage) <sup>††</sup> | 16.7                | 16.7                | 16.7                | 16.7                    | 16.7                    | 16.7                 | 16.7                   | 16.7              |
| Bounding<br>Cladding Stress<br>(MPa)                                | 152.7               | 151.2               | 147.1               | 140.6                   | 138.1                   | 135.0                | 130.8                  | 147.4             |

<sup>†</sup> PNL-4835 [4.3.2] reported maximum cladding thickness loss due to in-reactor oxidation.

<sup>††</sup> PNL-6189 [4.3.1] data.

Table 4.3.4

INTENTIONALLY DELETED.

Table 4.3.5  
SUMMARY OF BWR ASSEMBLY RODS INITIAL GAS FILL DATA

| Assembly Type          | Rods Per Assembly | Free Rod Volume (in <sup>3</sup> ) | Fill Pressure (psig) at 70°F | Fill Gas Volume at STP |                       |
|------------------------|-------------------|------------------------------------|------------------------------|------------------------|-----------------------|
|                        |                   |                                    |                              | Per Rod (liters)       | Per Assembly (liters) |
| GE-7x7 (1966)          | 49                | 2 073                              | 0-44.1 <sup>†</sup>          | 0.126                  | 6.17                  |
| GE-7x7 (1968)          | 49                | 2.073                              | 0-44.1                       | 0.126                  | 6.17                  |
| GE-7x7R                | 49                | 1.991                              | 0-44.1                       | 0.121                  | 5.93                  |
| GE-8x8                 | 60                | 1 504                              | 0-44.1                       | 0.0915                 | 5.49                  |
| GE-8x8R                | 62                | 1.433                              | 0-147 <sup>††</sup>          | 0.240                  | 14.88                 |
| Exxon-9x9              | 79                | 1.323                              | 58.8-88.2 <sup>†††</sup>     | 0.141                  | 11.1                  |
| 6x6 GE Dresden-1       | 36                | 2.304                              | 58.8-88.2                    | 0.245                  | 8.82                  |
| 6x6 Dresden-1 MOX      | 36                | 2.286                              | 58.8-88.2                    | 0.243                  | 8.75                  |
| 6x6 GE Humboldt Bay    | 36                | 2.346                              | 58.8-88.2                    | 0.250                  | 9.0                   |
| 7x7 GE Humboldt Bay    | 49                | 1 662                              | 58.8-88.2                    | 0.177                  | 8.67                  |
| 8x8 GE Dresden-1       | 64                | 1.235                              | 58.8-88.2                    | 0.131                  | 8.38                  |
| 8x8 SPC                | 63                | 1.615                              | 58.8-88.2                    | 0.172                  | 10.8                  |
| 9x9 SPC-2 water rods   | 79                | 1.248                              | 58.8-88.2                    | 0.133                  | 10.5                  |
| 9x9 SPC-1 water rod    | 80                | 1.248                              | 58.8-88.2                    | 0.133                  | 10.6                  |
| 9x9 GE11/GE13          | 74                | 1.389                              | 58.8-88.2                    | 0.150                  | 11.1                  |
| 9x9 Atrium 9B SPC      | 72                | 1.366                              | 58.8-88.2                    | 0.145                  | 10.4                  |
| 10x10 SVEA-96          | 96                | 1.022                              | 58.8-88.2                    | 0.109                  | 10.5                  |
| 10x10 GE12             | 92                | 1.167                              | 58.8-88.2                    | 0.124                  | 11.4                  |
| 6x6 Dresden-1          | 36                | 2.455                              | 58.8-88.2                    | 0.261                  | 9.4                   |
| 7x7 Oyster Creek       | 49                | 2.346                              | 58.8-88.2                    | 0.250                  | 12.2                  |
| 8x8 Oyster Creek       | 64                | 1.739                              | 58.8-88.2                    | 0.185                  | 11.8                  |
| 8x8 Quad† Westinghouse | 64                | 1.201                              | 58.8-88.2                    | 0.128                  | 8.2                   |
| 8x8 TVA Browns Ferry   | 61                | 1.686                              | 58.8-88.2                    | 0.179                  | 10.9                  |
| 9x9 SPC-5              | 76                | 1 249                              | 58.8-88.2                    | 0.133                  | 10.1                  |
| ANF 8x8                | 62                | 1 61                               | 58.8-88.2                    | 0.172                  | 10.7                  |
| ANF-9X (9x9)           | 72                | 1 249                              | 58.8-88.2                    | 0 133                  | 9 6                   |

<sup>†</sup> Conservatively bounding for GE-7x7 (1966), GE-7x7 (1968), GE-7x7R and GE-8x8 (ORNL/TM-9591/V1-R1).

<sup>††</sup> Conservatively bounding initial fill pressure. ORNL/TM-9591/V1-R1 reports GE-8x8R pre-pressurized to 3 atm.

<sup>†††</sup> BWR fuel rods internal pressurization between 4 to 6 atm (PNL-4835).

Table 4.3.6

BOUNDING VALUES OF FUEL CLADDING STRESS FOR BWR SNF

|   | GE-7x7<br>(1966) | GE-7x7<br>(1968) | GE-7x7R | GE-8x8 | GE-8x8R | Exxon-9x9 |
|---|------------------|------------------|---------|--------|---------|-----------|
| Fresh Fuel Rods O.D. (inch)                               | 0.563            | 0.570            | 0.563   | 0.493  | 0.483   | 0.42      |
| End of Life Oxidation Thickness (inch)                    | 0.0047           | 0.0047           | 0.0047  | 0.0047 | 0.0047  | 0.0047    |
| End of Life Rods O.D. (inch)                              | 0.5536           | 0.5606           | 0.5536  | 0.4836 | 0.4736  | 0.4106    |
| Rods I.D. (inch)  | 0.499            | 0.499            | 0.489   | 0.425  | 0.419   | 0.36      |
| Average Tube Diameter (inch)                              | 0.5263           | 0.5298           | 0.5213  | 0.4543 | 0.4463  | 0.3853    |
| Wall Thickness (inch)                                     | 0.0273           | 0.0308           | 0.0323  | 0.0293 | 0.0273  | 0.0253    |
| Theoretical Bounding Rod Pressure (MPa gage) <sup>†</sup> | 7.54             | 7.54             | 7.54    | 7.54   | 7.54    | 7.54      |
| Bounding Cladding Stress (MPa)                            | 72.7             | 64.8             | 60.8    | 58.5   | 61.6    | 57.4      |

<sup>†</sup> PNL-6189 [4.3.1] data.

Table 4.3.6 (continued)

BOUNDING VALUES OF FUEL CLADDING STRESS FOR BWR SNF

|   | 6x6 GE<br>Dresden-1 | 6x6 MOX<br>Dresden-1 | 6x6 GE<br>Humboldt<br>Bay | 7x7 GE<br>Humboldt<br>Bay | 8x8 GE<br>Dresden-1 | 8x8 SPC |
|---|---------------------|----------------------|---------------------------|---------------------------|---------------------|---------|
| Fresh Fuel<br>Rods O.D.<br>(inch)                                     | 0.5645              | 0.5625               | 0.563                     | 0.486                     | 0.412               | 0.484   |
| End of Life<br>Oxidation<br>Thickness<br>(inch)                       | 0.0047              | 0.0047               | 0.0047                    | 0.0047                    | 0.0047              | 0.0047  |
| End of Life<br>Rods O.D.<br>(inch)                                    | 0.5551              | 0.5531               | 0.5536                    | 0.4766                    | 0.4026              | 0.4746  |
| Rods I.D.<br>(inch)   | 0.4945              | 0.4925               | 0.499                     | 0.4204                    | 0.362               | 0.414   |
| Average<br>Tube<br>Diameter<br>(inch)                                 | 0.5248              | 0.5228               | 0.5263                    | 0.4485                    | 0.3813              | 0.4443  |
| Wall<br>Thickness<br>(inch)   | 0.0303              | 0.0303               | 0.0273                    | 0.0281                    | 0.0203              | 0.0303  |
| Theoretical<br>Bounding<br>Rod<br>Pressure<br>(MPa gage) <sup>†</sup> | 7.54                | 7.54                 | 7.54                      | 7.54                      | 7.54                | 7.54    |
| Bounding<br>Cladding<br>Stress (MPa)                                  | 65.3                | 65.0                 | 72.7                      | 60.1                      | 70.8                | 55.3    |

<sup>†</sup> PNL-6189 [4.3.1] data.

Table 4.3.6 (continued)

BOUNDING VALUES OF FUEL CLADDING STRESS FOR BWR SNF

|   | 9x9 SPC-2<br>water rods | 9x9 SPC-1<br>water rod | 9x9 GE-11/13 | 9x9 SPC<br>Atrium 9B | 10x10 SVEA -<br>96 | 10x10 GE12 |
|---|-------------------------|------------------------|--------------|----------------------|--------------------|------------|
| Fresh Fuel<br>Rods O.D.<br>(inch)                                     | 0.424                   | 0.423                  | 0.44         | 0.433                | 0.379              | 0.404      |
| End of Life<br>Oxidation<br>Thickness<br>(inch)                       | 0.0047                  | 0.0047                 | 0.0047       | 0.0047               | 0.0047             | 0.0047     |
| End of Life<br>Rods O.D.<br>(inch)                                    | 0.4146                  | 0.4136                 | 0.4306       | 0.4236               | 0.3696             | 0.3946     |
| Rods I.D.<br>(inch)   | 0.364                   | 0.364                  | 0.384        | 0.3808               | 0.3294             | 0.352      |
| Average<br>Tube<br>Diameter<br>(inch)                                 | 0.3893                  | 0.3888                 | 0.4073       | 0.4022               | 0.3495             | 0.3733     |
| Wall<br>Thickness<br>(inch)   | 0.0253                  | 0.0248                 | 0.0233       | 0.0214               | 0.0201             | 0.0213     |
| Theoretical<br>Bounding<br>Rod<br>Pressure<br>(MPa gage) <sup>†</sup> | 7.54                    | 7.54                   | 7.54         | 7.54                 | 7.54               | 7.54       |
| Bounding<br>Cladding<br>Stress (MPa)                                  | 58.0                    | 59.1                   | 65.9         | 70.9                 | 65.6               | 66.1       |

<sup>†</sup> PNL-6189 [4.3.1] data

Table 4.3.6 (continued)

## BOUNDING VALUES OF FUEL CLADDING STRESS FOR BWR SNF

|  | 6x6 Dresden-1 <sup>†</sup><br>Thin Clad | 7x7 Oyster Creek | 8x8 Oyster Creek | 8x8 Quad <sup>†</sup> |
|--|---|------------------|------------------|-----------------------|
| Fresh fuel Rods O.D.<br>(inch)                         | 0.5625                                  | 0.57             | 0.5015           | 0.4576                |
| End-of-Life<br>Oxidization Thin Clad<br>(inch)         | 0.0047                                  | 0.0047           | 0.0047           | 0.0047                |
| End-of-Life Rods<br>O.D. (inch)                        | 0.5531                                  | 0.5606           | 0.4921           | 0.4482                |
| Rods I.D. (inch)                                       | 0.5105                                  | 0.499            | 0.4295           | 0.3996                |
| Average Tube<br>Diameter (inch)                        | 0.5318                                  | 0.5298           | 0.4608           | 0.4239                |
| Wall Thickness<br>(inch)                               | 0.0213                                  | 0.0308           | 0.0313           | 0.0243                |
| Theoretical<br>Boundary Rod<br>Pressure (MPa<br>gauge) | 7.54                                    | 7.54             | 7.54             | 7.54                  |
| Bounding Cladding<br>Stress (MPa)                      | 94.1                                    | 64.5             | 55.5             | 65.8                  |

† Outlier fuel type evaluated in Table 4.3.8.

Table 4.3.6 (continued)

BOUNDING VALUES OF FUEL CLADDING STRESS FOR BWR SNF

|   | 8x8 TVA Browns Ferry | 9x9 SPC-5 | ANF 8x8 | ANF-9X (9x9) |
|---|----------------------|-----------|---------|--------------|
| O.D. Inch                               | 0.483                | 0.417     | 0.484   | 0.424        |
| End-of-Life Oxidation Thickness (inch)  | 0.0047               | 0.0047    | 0.0047  | 0.0047       |
| End-of-Life Rods O.D. (inch)            | 0.4736               | 0.4076    | 0.4746  | 0.4146       |
| Rods I.D. (inch)                        | 0.423                | 0.364     | 0.414   | 0.364        |
| Average Tube Diameter (inch)            | 0.4483               | 0.3858    | 0.4443  | 0.3893       |
| Wall Thickness (inch)                   | 0.0253               | 0.0218    | 0.0303  | 0.0253       |
| Theoretical Bounding Rod Pressure (MPa) | 7.54                 | 7.54      | 7.54    | 7.54         |
| Bounding Cladding Stress (MPa)          | 66.8                 | 66.7      | 55.3    | 58.0         |

Table 4.3.7

ZIRCALOY CLADDING TEMPERATURE LIMITS AND PERMISSIBLE TEMPERATURES

| Fuel Age (years) | PWR SNF (°C) [°F] |                       | BWR SNF (°C) [°F] |                       |
|------------------|-------------------|-----------------------|-------------------|-----------------------|
|                  | DCCG Limit        | Permissible PNL Limit | DCCG Limit        | Permissible PNL Limit |
| 5                | 419.4 [787]       | 366.0 [691]           | 440.2 [824]       | 393.2 [740]           |
| 6                | 416.7 [782]       | 358.0 [676]           | 436.2 [817]       | 377.9 [712]           |
| 7                | 397.0 [747]       | 335.0 [635]           | 416.4 [781]       | 353.7 [669]           |
| 10               | 379.4 [715]       | 329.6 [625]           | 398.9 [750]       | 347.9 [658]           |
| 15               | 370.2 [698]       | 323.2 [614]           | 390.2 [734]       | 341.1 [646]           |

Table 4.3.8

PERMISSIBLE TEMPERATURES FOR OUTLIER FUEL TYPES

| Fuel Age (Years) | 6x6 Dresden-1 Thin Clad (°C) [°F] (BWR) |       |
|------------------|---|-------|
| 5                | 383.7                                   | [723] |
| 6                | 370.9                                   | [700] |
| 7                | 347.7                                   | [658] |
| 10               | 342.1                                   | [648] |
| 15               | 334.9                                   | [635] |

Table 4.3.9

BOUNDING CLADDING STRESS FOR OUTLIER PWR FUEL

|  | B&W 15x15<br>Mark B-11 |
|--|------------------------|
| Fresh Fuel Rods O.D. (inch)            | 0.414                  |
| End of Life Oxidation Thickness (inch) | 0.0027                 |
| End of Life Rods O.D. (inch)           | 0.4086                 |
| Rods I.D. (inch)                       | 0.370                  |
| Average Rod Diameter (inch)            | 0.3893                 |
| Limiting Rod Pressure (MPa)            | 15 <sup>†</sup>        |
| Bounding Cladding Stress (MPa)         | 151.3                  |

<sup>†</sup> Rod pressure to be limited to 2175 psia at 387°C gas plenum temperature.

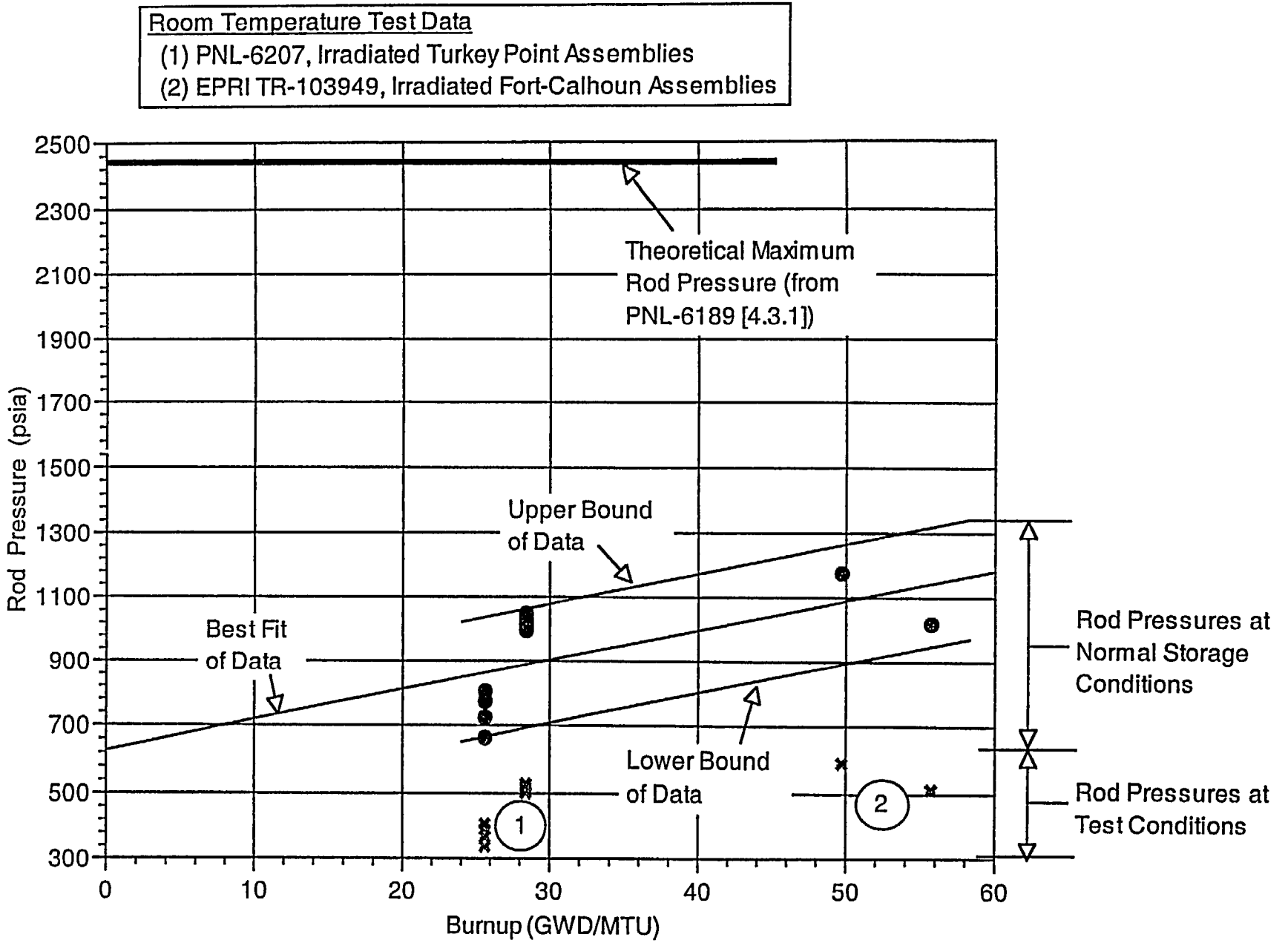


FIGURE 4.3.1; COMPARISON OF CALCULATED (BY EPRI AND PNL) AND THEORETICAL MAXIMUM FUEL ROD PRESSURES FOR PWR FUEL

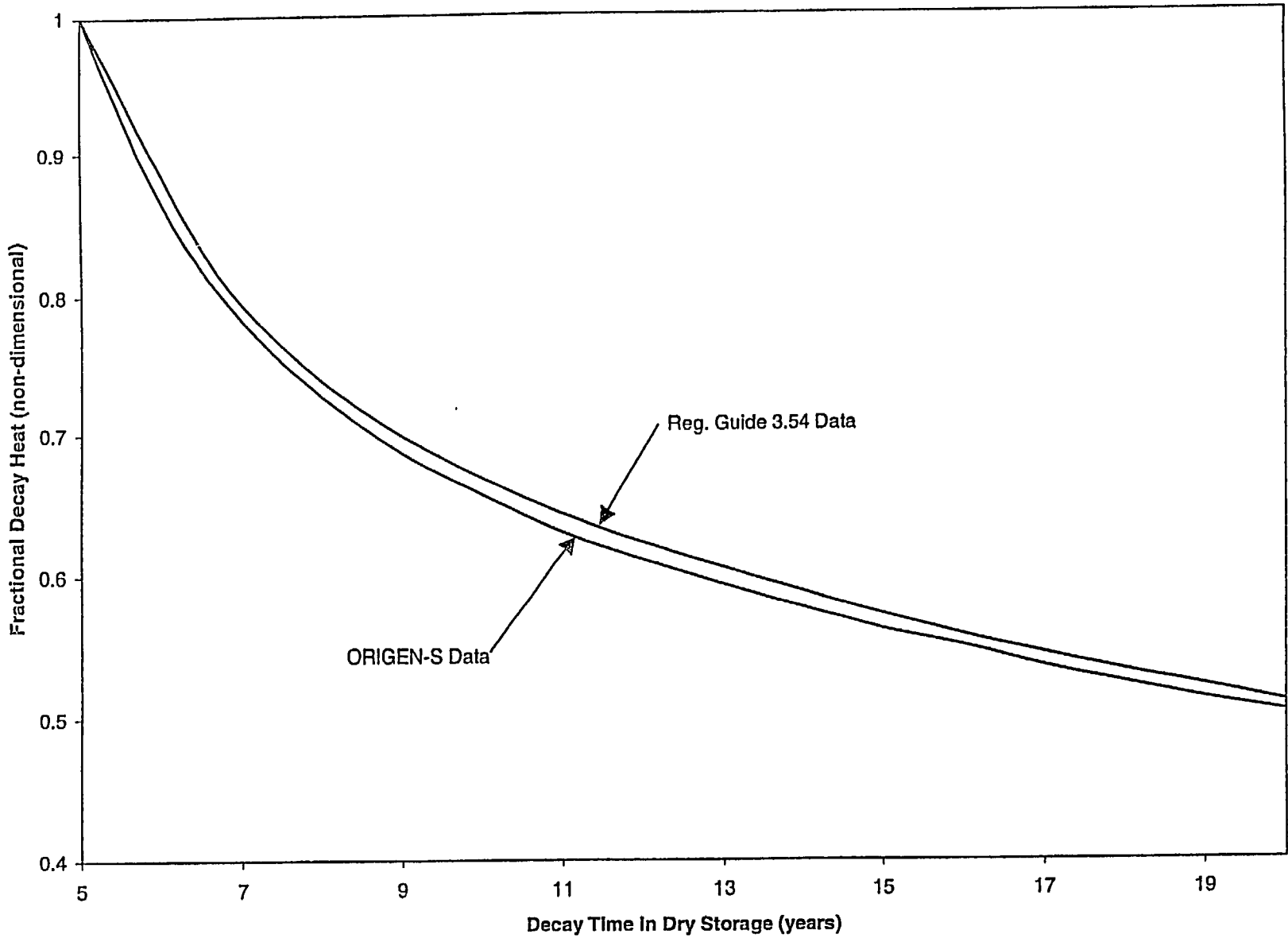


FIGURE 4.3.2; COMPARISON OF REG. GUIDE 3.54 DECAY HEAT DATA WITH ORIGEN-S FOR BWR FUEL

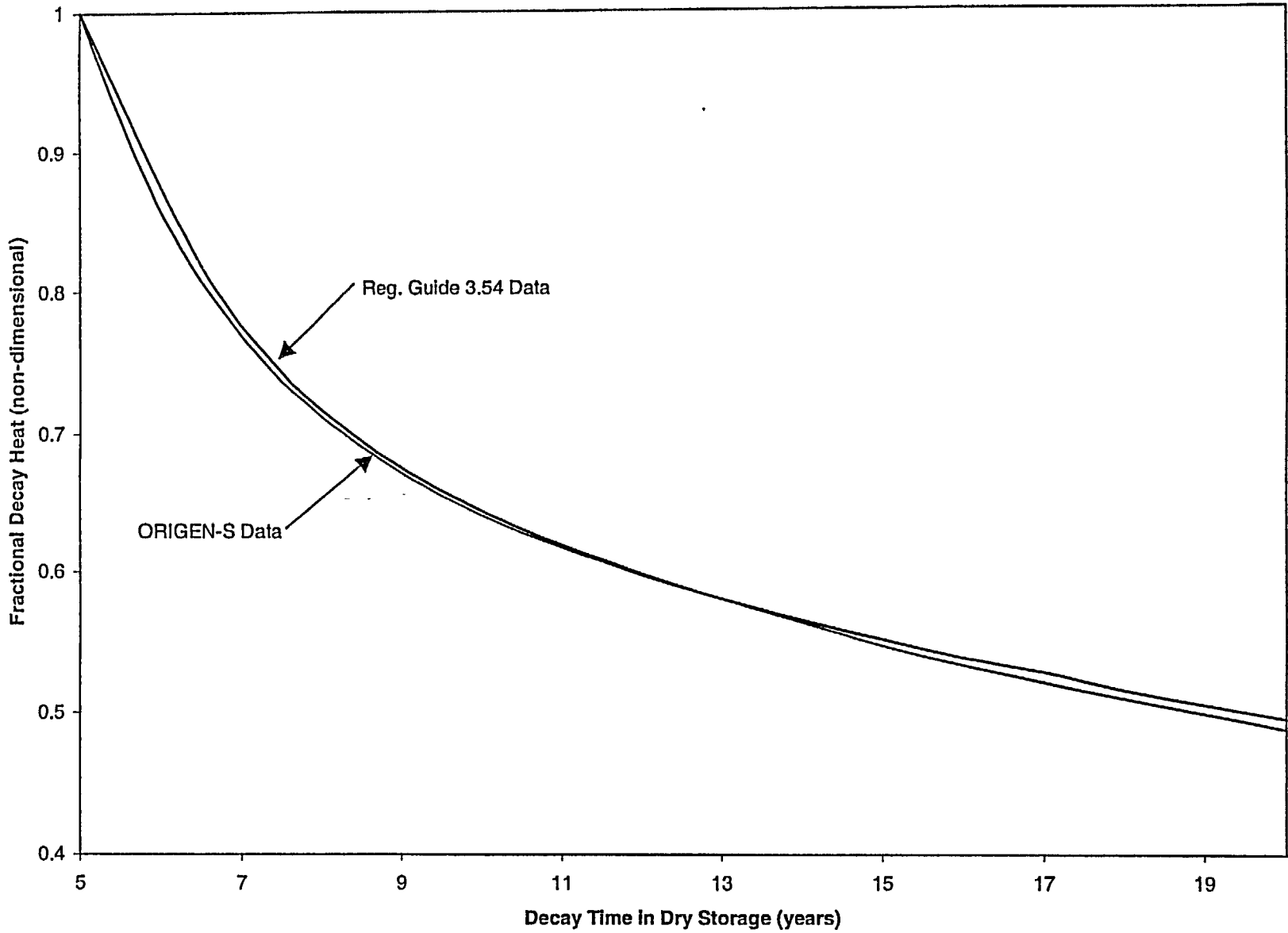


FIGURE 4.3.3; COMPARISON OF REG. GUIDE 3.54 DECAY HEAT DATA WITH ORIGEN-S FOR PWR FUEL

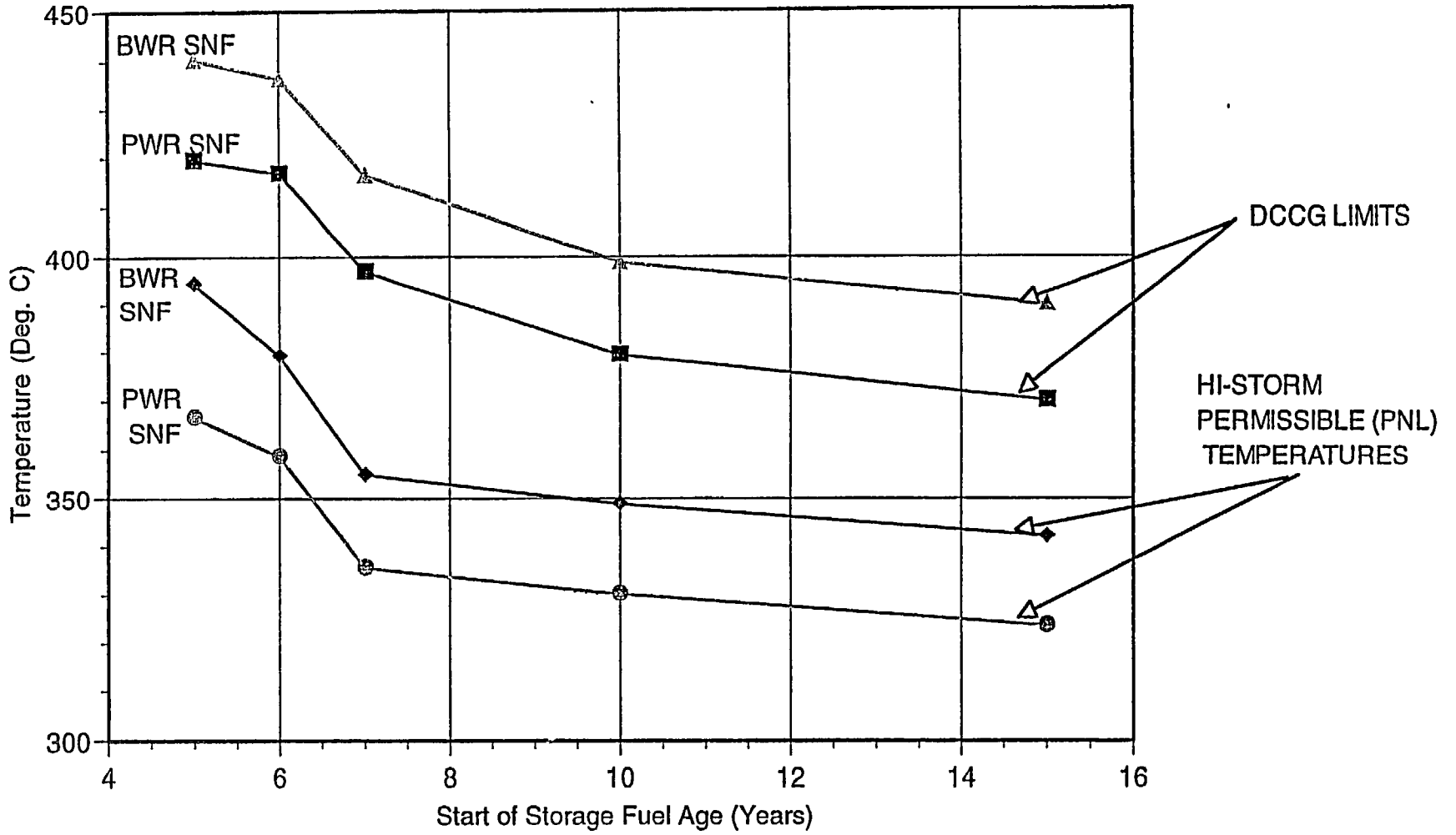


FIGURE 4.3.4: COMPARISON OF FUEL CLADDING TEMPERATURE LIMITS WITH HI-STORM PERMISSIBLE TEMPERATURES

## 4.4 THERMAL EVALUATION FOR NORMAL CONDITIONS OF STORAGE

Under long-term storage conditions, the HI-STORM System (i.e., HI-STORM overpack and MPC) thermal evaluation is performed with the MPC cavity backfilled with helium. Thermal analysis results for the long-term storage scenarios are obtained and reported in this section.

### 4.4.1 Thermal Model

The MPC basket design consists of four distinct geometries to hold 24 or 32 PWR, or 68 BWR fuel assemblies. The basket is a matrix of square compartments designed to hold the fuel assemblies in a vertical position. The basket is a honeycomb structure of alloy steel (Alloy X) plates with full-length edge-welded intersections to form an integral basket configuration. All individual cell walls, except outer periphery cell walls in the MPC-68 and MPC-32, are provided with Boral neutron absorber sandwiched between the box wall and a stainless steel sheathing plate over the full length of the active fuel region.

The design basis decay heat generation (per PWR or BWR assembly) for long-term normal storage is specified in Table 2.1.6. The decay heat is conservatively considered to be non-uniformly distributed over the active fuel length based on the design basis axial burnup distributions provided in Chapter 2 (Table 2.1.11).

Transport of heat from the interior of the MPC to its outer surface is accomplished by a combination of conduction through the MPC basket metal grid structure, and conduction and radiation heat transfer in the relatively small helium gaps between the fuel assemblies and basket cell walls. Heat dissipation across the gap between the MPC basket periphery and the MPC shell is by a combination of helium conduction, natural convection (by means of the "Rayleigh" effect)<sup>†</sup> radiation across the gap and conduction in the aluminum alloy 1100 heat conduction elements\*. MPC internal helium circulation is recognized in the thermal modeling analyses reported herein. Heat rejection from the outer surface of the MPC to the environment is primarily accomplished by convective heat transfer to a buoyancy driven airflow through the MPC-to-overpack annular gap. Inlet and outlet ducts in the overpack cylinder at its bottom and top, respectively, allow circulation of air through the annulus. A secondary heat rejection path from the outer surface of the MPC to the environment involves thermal radiation heat transfer across the annular gap, radial conduction through the overpack cylinder, and natural convection and thermal radiation from the outer surface of the overpack to the atmosphere.

<sup>†</sup> Neglected in the thermal analyses for conservatism.

\* Neglected in the thermal analyses for conservatism.

#### 4.4.1.1 Analytical Model - General Remarks

Transport of heat from the heat generation region (fuel assemblies) to the outside environment (ambient air or ground) is analyzed broadly in terms of three interdependent thermal models.

1. The first model considers transport of heat from the fuel assembly to the basket cell walls. This model recognizes the combined effects of conduction (through helium) and radiation, and is essentially a finite element technology based update of the classical Wootton & Epstein [4.4.1] (which considered radiative heat exchange between fuel rod surfaces) formulation.
2. The second model considers heat transport within an MPC cross section by conduction and radiation. The effective cross sectional thermal conductivity of the basket region, obtained from a combined fuel assembly/basket heat conduction-radiation model developed on ANSYS, is applied to an axisymmetric thermal model of the HI-STORM System on the FLUENT [4.1.2] code.
3. The third model deals with the transmission of heat from the MPC exterior surface to the external environment (heat sink). The upflowing air stream in the MPC/cask annulus extracts most of the heat from the external surface of the MPC, and a small amount of heat is radially deposited on the HI-STORM inner surface by conduction and radiation. Heat rejection from the outside cask surfaces to ambient air is considered by accounting for natural convection and radiative heat transfer mechanisms from the vertical (cylindrical shell) and top cover (flat) surfaces. The reduction in radiative heat exchange between cask outside vertical surfaces and ambient air, because of blockage from the neighboring casks arranged for normal storage at an ISFSI pad as described in Section 1.4, is recognized in the analysis. The overpack top plate is modeled as a heated surface in convective and radiative heat exchange with air and as a recipient of heat input through insolation. Insolation on the cask surfaces is based on 12-hour levels prescribed in 10CFR71, averaged over a 24-hour period, after accounting for partial blockage conditions on the sides of the overpack.

Subsections 4.4.1.1.1 through 4.4.1.1.9 contain a systematic description of the mathematical models devised to articulate the temperature field in the HI-STORM System. The description begins with the method to characterize the heat transfer behavior of the prismatic (square) opening referred to as the "fuel space" with a heat emitting fuel assembly situated in it. The methodology utilizes a finite element procedure to replace the heterogeneous SNF/fuel space region with an equivalent solid body having a well-defined temperature-dependent conductivity. In the following subsection, the method to replace the "composite" walls of the fuel basket cells with an equivalent "solid" wall is presented. Having created the mathematical equivalents for the SNF/fuel spaces and the fuel basket walls, the method to represent the MPC cylinder containing the fuel basket by an equivalent cylinder whose thermal conductivity is a function of the spatial location and coincident temperature is presented.

Following the approach of presenting descriptions starting from the inside and moving to the outer region of a cask, the next subsections present the mathematical model to simulate the overpack. Subsection 4.4.1.1.9 concludes the presentation with a description of how the different models for the specific regions within the HI-STORM System are assembled into the final FLUENT model.

#### 4.4.1.1.1 Overview of the Thermal Model

Thermal analysis of the HI-STORM System is performed by assuming that the system is subject to its maximum heat duty with each storage location occupied and with the heat generation rate in each stored fuel assembly equal to the design-basis maximum value. While the assumption of equal heat generation imputes a certain symmetry to the cask thermal problem, the thermal model must incorporate three attributes of the physical problem to perform a rigorous analysis of a fully loaded cask:

- i. While the rate of heat conduction through metals is a relatively weak function of temperature, radiation heat exchange is a nonlinear function of surface temperatures.
- ii. Heat generation in the MPC is axially non-uniform due to non-uniform axial burnup profiles in the fuel assemblies.
- iii. Inasmuch as the transfer of heat occurs from inside the basket region to the outside, the temperature field in the MPC is spatially distributed with the maximum values reached in the central core region.

It is clearly impractical to model every fuel rod in every stored fuel assembly explicitly. Instead, the cross section bounded by the inside of the storage cell, which surrounds the assemblage of fuel rods and the interstitial helium gas, is replaced with an "equivalent" square (solid) section characterized by an effective thermal conductivity. Figure 4.4.1 pictorially illustrates the homogenization concept. Further details of this procedure for determining the effective conductivity are presented in Subsection 4.4.1.1.2; it suffices to state here that the effective conductivity of the cell space will be a function of temperature because the radiation heat transfer (a major component of the heat transport between the fuel rods and the surrounding basket cell metal) is a strong function of the temperatures of the participating bodies. Therefore, in effect, every storage cell location will have a different value of effective conductivity (depending on the coincident temperature) in the homogenized model. The temperature-dependent fuel assembly region effective conductivity is determined by a finite volume procedure, as described in Subsection 4.4.1.1.2.

In the next step of homogenization, a planar section of MPC is considered. With each storage cell inside space replaced with an equivalent solid square, the MPC cross section consists of a metallic gridwork (basket cell walls with each square cell space containing a solid fuel cell square of effective thermal conductivity, which is a function of temperature) circumscribed by a circular ring (MPC shell). There are five distinct materials in this section, namely the homogenized fuel cell squares, the Alloy X structural materials in the MPC (including Boral sheathing), Boral, Alloy 1100 aluminum heat conduction elements, and helium gas. Each of the five constituent materials in this section has a different conductivity. It is emphasized that the conductivity of the homogenized fuel cells is a strong function of temperature.

In order to replace this thermally heterogeneous MPC section with an equivalent conduction-only region, resort to the finite element procedure is necessary. Because the rate of transport of heat within the MPC is influenced by radiation, which is a temperature-dependent effect, the equivalent conductivity of the MPC

region must also be computed as a function of temperature. Finally, it is recognized that the MPC section consists of two discrete regions, namely, the basket region and the peripheral region. The peripheral region is the space between the peripheral storage cells and the MPC shell. This space is essentially full of helium surrounded by Alloy X plates and optionally Alloy 1100 aluminum heat conduction elements. Accordingly, as illustrated in Figure 4.4.2 for MPC-68, the MPC cross section is replaced with two homogenized regions with temperature-dependent conductivities. In particular, the effective conductivity of the fuel cells is subsumed into the equivalent conductivity of the basket cross section. The finite element procedure used to accomplish this is described in Subsection 4.4.1.1.4. The ANSYS finite element code is the vehicle for all modeling efforts described in the foregoing.

In summary, appropriate finite-element models are used to replace the MPC cross section with an equivalent two-region homogeneous conduction lamina whose local conductivity is a known function of coincident absolute temperature. Thus, the MPC cylinder containing discrete fuel assemblies, helium, Boral and Alloy X, is replaced with a right circular cylinder whose material conductivity will vary with radial and axial position as a function of the coincident temperature. Finally, HI-STORM is simulated as a radially symmetric structure with a buoyancy-induced flow in the annular space surrounding the heat generating MPC cylinder.

The thermal analysis procedure described above makes frequent use of equivalent thermal properties to ease the geometric modeling of the cask components. These equivalent properties are rigorously calculated values based on detailed evaluations of actual cask system geometries. All these calculations are performed conservatively to ensure a bounding representation of the cask system. This process, commonly referred to as submodeling, yields accurate (not approximate) results. Given the detailed nature of the submodeling process, experimental validation of the individual submodels is not necessary.

Internal circulation of helium in the sealed MPC is modeled as flow in a porous media in the fueled region containing the SNF (including top and bottom plenums). The basket-to-MPC shell clearance space is modeled as a helium filled radial gap to include the downcomer flow in the thermal model. The downcomer region, as illustrated in Figure 4.4.2, consists of an azimuthally varying gap formed by the square-celled basket outline and the cylindrical MPC shell. At the locations of closest approach a differential expansion gap (a small clearance on the order of 1/10 of an inch) is engineered to allow free thermal expansion of the basket. At the widest locations, the gaps are on the order of the fuel cell opening (~6" (BWR) and ~9" (PWR) MPCs). It is heuristically evident that heat dissipation by conduction is maximum at the closest approach locations (low thermal resistance path) and that convective heat transfer is highest at the widest gap locations (large downcomer flow). In the FLUENT thermal model, a radial gap that is large compared to the basket-to-shell clearance and small compared to the cell opening is used. As a relatively large gap penalizes heat dissipation by conduction and a small gap throttles convective flow, the use of a single gap in the FLUENT model understates both conduction and convection heat transfer in the downcomer region. Heat dissipation by the inclusion of aluminum heat conduction elements, as stated earlier, is conservatively neglected in the HI-STORM thermal modeling.

The FLUENT thermal modeling methodology has been benchmarked with full-scale cask test data (EPRI TN-24P cask testing), as well as with PNNL's COBRA-SFS modeling of the HI-STORM System. The

benchmarking work has been documented in a Holtec topical report HI-992252 ("Topical Report on the HI-STAR/HI-STORM Thermal Model and Its Benchmarking with Full-Size Cask Test Data").

In this manner, a loaded MPC standing upright on the ISFSI pad in a HI-STORM overpack is replaced with a right circular cylinder with spatially varying temperature-dependent conductivity. Heat is generated within the basket space in this cylinder in the manner of the prescribed axial burnup distribution. In addition, heat is deposited from insolation on the external surface of the overpack. Under steady state conditions the total heat due to internal generation and insolation is dissipated from the outer cask surfaces by natural convection and thermal radiation to the ambient environment and from heating of upward flowing air in the annulus. Details of the elements of mathematical modeling are provided in the following.

#### 4.4.1.1.2 Fuel Region Effective Thermal Conductivity Calculation

Thermal properties of a large number of PWR and BWR fuel assembly configurations manufactured by the major fuel suppliers (i.e., Westinghouse, CE, B&W, and GE) have been evaluated for inclusion in the HI-STORM System thermal analysis. Bounding PWR and BWR fuel assembly configurations are determined using the simplified procedure described below. This is followed by the determination of temperature-dependent properties of the bounding PWR and BWR fuel assembly configurations to be used for cask thermal analysis using a finite volume (FLUENT) approach.

To determine which of the numerous PWR assembly types listed in Table 4.4.1 should be used in the thermal model for the PWR fuel baskets (MPC-24, MPC-24E, MPC-32), we must establish which assembly type has the maximum thermal resistance. The same determination must be made for the MPC-68, out of the menu of SNF types listed in Table 4.4.2. For this purpose, we utilize a simplified procedure that we describe below.

Each fuel assembly consists of a large array of fuel rods typically arranged on a square layout. Every fuel rod in this array is generating heat due to radioactive decay in the enclosed fuel pellets. There is a finite temperature difference required to transport heat from the innermost fuel rods to the storage cell walls. Heat transport within the fuel assembly is based on principles of conduction heat transfer combined with the highly conservative analytical model proposed by Wooton and Epstein [4.4.1]. The Wooton-Epstein model considers radiative heat exchange between individual fuel rod surfaces as a means to bound the hottest fuel rod cladding temperature.

Transport of heat energy within any cross section of a fuel assembly is due to a combination of radiative energy exchange and conduction through the helium gas that fills the interstices between the fuel rods in the array. With the assumption of uniform heat generation within any given horizontal cross section of a fuel assembly, the combined radiation and conduction heat transport effects result in the following heat flow equation:

$$Q = \sigma C_o F_e A [T_C^4 - T_B^4] + 13.5740 L K_{cs} [T_C - T_B]$$

where:

$$F_a = \text{Emissivity Factor} \\ = \frac{1}{\left(\frac{1}{\epsilon_C} + \frac{1}{\epsilon_B} - 1\right)}$$

$\epsilon_C, \epsilon_B$  = emissivities of fuel cladding, fuel basket (see Table 4.2.4)

$$C_o = \text{Assembly Geometry Factor} \\ = \frac{4N}{(N+1)^2} \text{ (when } N \text{ is odd)} \\ = \frac{4}{N+2} \text{ (when } N \text{ is even)}$$

$N$  = Number of rows or columns of rods arranged in a square array

$A$  = fuel assembly "box" heat transfer area =  $4 \times \text{width} \times \text{length}$

$L$  = fuel assembly length

$K_{cs}$  = fuel assembly constituent materials volume fraction weighted mixture conductivity

$T_C$  = hottest fuel cladding temperature ( $^{\circ}\text{R}$ )

$T_B$  = box temperature ( $^{\circ}\text{R}$ )

$Q$  = net radial heat transport from the assembly interior

$\sigma$  = Stefan-Boltzmann Constant ( $0.1714 \times 10^{-8} \text{ Btu/ft}^2 \cdot \text{hr} \cdot ^{\circ}\text{R}^4$ )

In the above heat flow equation, the first term is the Wooten-Epstein radiative heat flow contribution while the second term is the conduction heat transport contribution based on the classical solution to the temperature distribution problem inside a square shaped block with uniform heat generation [4.4.5]. The 13.574 factor in the conduction term of the equation is the shape factor for two-dimensional heat transfer in a square section. Planar fuel assembly heat transport by conduction occurs through a series of resistances formed by the interstitial helium, fill gas, fuel cladding and enclosed fuel. An effective planar mixture conductivity is determined by a volume fraction weighted sum of the individual constituent material resistances. For BWR assemblies, this formulation is applied to the region inside the fuel channel. A second conduction and radiation model is applied between the channel and the fuel basket gap. These two models are combined, in series, to yield a total effective conductivity.

The effective conductivity of the fuel for several representative PWR and BWR assemblies is presented in Tables 4.4.1 and 4.4.2. At higher temperatures (approximately 450 $^{\circ}\text{F}$  and above), the zircaloy clad fuel assemblies with the lowest effective thermal conductivities are the W-17 $\times$ 17 OFA (PWR) and the GE11-9 $\times$ 9 (BWR). A discussion of fuel assembly conductivities for some of the recent vintage 10 $\times$ 10 array and certain plant specific BWR fuel designs is presented near the end of this subsection. As noted in Table 4.4.2, the Dresden 1 (intact and damaged) fuel assemblies are excluded from consideration. The design basis decay heat load for Dresden-1 intact and damaged fuel (Table 2.1.7) is approximately 58% lower

than the MPC-68 design-basis maximum heat load (Table 2.1.6). Examining Table 4.4.2, the effective conductivity of the damaged Dresden-1 fuel assembly in a damaged fuel container is approximately 40% lower than the bounding (GE-11 9×9) fuel assembly. Consequently, the fuel cladding temperatures in the HI-STORM System with Dresden-1 intact or damaged fuel assemblies will be bounded by design basis fuel cladding temperatures. Based on this simplified analysis, the W-17×17 OFA PWR and GE11-9×9 BWR fuel assemblies are determined to be the bounding configurations for analysis of zircaloy clad fuel at design basis maximum heat loads. As discussed in Section 4.3.1, stainless clad fuel assemblies with significantly lower decay heat emission characteristics are not deemed to be bounding.

For the purpose of determining axial flow resistance for inclusion of MPC thermosiphon effect in the HI-STORM system modeling, equivalent porous media parameters for the W-17×17OFA and GE11-9×9 fuels are computed. Theoretically bounding expansion and contraction loss factors are applied at the grid spacer locations to conservatively maximize flow resistance. As an additional measure of conservatism, the grids are modeled by postulating that they are formed using thick metal sheets which have the effect of artificially throttling flow. Heat transfer enhancement by grid spacers turbulence is conservatively ignored in the analysis.

Having established the governing (most resistive) PWR and BWR SNF types, we use a finite-volume code to determine the effective conductivities in a conservative manner. Detailed conduction-radiation finite-volume models of the bounding PWR and BWR fuel assemblies developed on the FLUENT code are shown in Figures 4.4.3 and 4.4.4, respectively. The PWR model was originally developed on the ANSYS code, which enables individual rod-to-rod and rod-to-basket wall view factor calculations to be performed using the AUX12 processor. Limitations of radiation modeling techniques implemented in ANSYS do not permit taking advantage of quarter symmetry of the fuel assembly geometry. Unacceptably long CPU time and large workspace requirements necessary for performing gray body radiation calculations for a complete fuel assembly geometry on ANSYS prompted the development of an alternate simplified model on the FLUENT code. The FLUENT model is benchmarked with the ANSYS model results for a Westinghouse 17×17 fuel assembly geometry for the case of black body radiation (emissivities = 1). The FLUENT model is found to yield conservative results in comparison to the ANSYS model for the "black" surface case. The FLUENT model benchmarked in this manner is used to solve the gray body radiation problem to provide the necessary results for determining the effective thermal conductivity of the governing PWR fuel assembly. The same modeling approach using FLUENT is then applied to the governing BWR fuel assembly, and the effective conductivity of GE-11 9×9 fuel determined.

The combined fuel rods-helium matrix is replaced by an equivalent homogeneous material that fills the basket opening by the following two-step procedure. In the first step, the FLUENT-based fuel assembly model is solved by applying equal heat generation per unit length to the individual fuel rods and a uniform boundary temperature along the basket cell opening inside periphery. The temperature difference between the peak cladding and boundary temperatures is used to determine an effective conductivity as described in the next step. For this purpose, we consider a two-dimensional cross section of a square shaped block with an edge length of  $2L$  and a uniform volumetric heat source ( $q_g$ ), cooled at the periphery with a uniform boundary temperature. Under the assumption of constant material thermal conductivity ( $K$ ), the temperature difference ( $\Delta T$ ) from the center of the cross section to the periphery is analytically given by [4.4.5]:

$$\Delta T = 0.29468 \frac{q_g L^2}{K}$$

This analytical formula is applied to determine the effective material conductivity from a known quantity of heat generation applied in the FLUENT model (smeared as a uniform heat source,  $q_g$ ) basket opening size and  $\Delta T$  calculated in the first step.

As discussed earlier, the effective fuel space conductivity must be a function of the temperature coordinate. The above two-step analysis is carried out for a number of reference temperatures. In this manner, the effective conductivity as a function of temperature is established.

In Table 4.4.5, 10×10 array type BWR fuel assembly conductivity results from a simplified analysis are presented to determine the most resistive fuel assembly in this class. The Atrium-10 fuel type is determined to be the most resistive in this class of fuel assemblies. A detailed finite-element model of this assembly type was developed to rigorously quantify the heat dissipation characteristics. The results of this study are presented in Table 4.4.6 and compared to the BWR bounding fuel assembly conductivity depicted in Figure 4.4.5. The results of this study demonstrate that the bounding fuel assembly conductivity is conservative with respect to the 10×10 class of BWR fuel assemblies.

Table 4.4.23 summarizes plant specific fuel types' effective conductivities. From these analytical results, SPC-5 is determined to be the most resistive fuel assembly in this group of fuel. A finite element model of the SPC-5 fuel assembly was developed to confirm that its in-plane heat dissipation characteristics are bounded from below by the Design Basis BWR fuel conductivities used in the HI-STORM thermal analysis.

Temperature-dependent effective conductivities of PWR and BWR design basis fuel assemblies (most resistive SNF types) are shown in Figure 4.4.5. The finite volume results are also compared to results reported from independent technical sources. From this comparison, it is readily apparent that FLUENT-based fuel assembly conductivities are conservative. The FLUENT computed values (not the published literature data) are used in the MPC thermal analysis presented in this document.

#### 4.4.1.1.3 Effective Thermal Conductivity of Boral/Sheathing/Box Wall Sandwich

Each MPC basket cell wall (except the MPC-68 and MPC-32 outer periphery cell walls) is manufactured with a Boral neutron absorbing plate for criticality control. Each Boral plate is sandwiched in a sheathing-to-basket wall pocket. A schematic of the "Box Wall-Boral-Sheathing" sandwich geometry of an MPC basket is illustrated in Figure 4.4.6. During fabrication, a uniform normal pressure is applied to each "Box Wall-Boral-Sheathing" sandwich in the assembly fixture during welding of the sheathing periphery on the box wall. This ensures adequate surface-to-surface contact for elimination of any macroscopic air gaps. The mean coefficient of linear expansion of the Boral is higher than the thermal expansion coefficients of the basket and sheathing materials. Consequently, basket heat-up from the stored SNF will further ensure a tight fit of the Boral plate in the sheathing-to-box pocket. The presence of small microscopic gaps due to less than perfect surface finish characteristics requires consideration of an interfacial contact resistance between the Boral and box-sheathing surfaces. A conservative contact resistance resulting from a 2 mil

Boral to pocket gap is applied in the analysis. In other words, no credit is taken for the interfacial pressure between Boral and stainless plate/sheet stock produced by the fixturing and welding process.

Heat conduction properties of a composite "Box Wall-Boral-Sheathing" sandwich in the two principal basket cross sectional directions as illustrated in Figure 4.4.6 (i.e., lateral "out-of-plane" and longitudinal "in-plane") are unequal. In the lateral direction, heat is transported across layers of sheathing, air-gap, Boral (B<sub>4</sub>C and cladding layers) and box wall resistances that are essentially in series (except for the small helium filled end regions shown in Figure 4.4.7). Heat conduction in the longitudinal direction, in contrast, is through an array of essentially parallel resistances comprised of these several layers listed above. For the ANSYS based MPC basket thermal model, corresponding non-isotropic effective thermal conductivities in the two orthogonal sandwich directions are determined and applied in the analysis.

These non-isotropic conductivities are determined by constructing two-dimensional finite-element models of the composite "Box Wall-Boral-Sheathing" sandwich in ANSYS. A fixed temperature is applied to one edge of the model and a fixed heat flux is applied to the other edge, and the model is solved to obtain the average temperature of the fixed-flux edge. The equivalent thermal conductivity is the obtained using the resulting temperature difference across the sandwich as input to a one-dimensional Fourier equation as follows:

$$K_{\text{eff}} = \frac{q \times L}{T_h - T_c}$$

where:

- K<sub>eff</sub> = effective thermal conductivity
- q = heat flux applied in the ANSYS model
- L = ANSYS model heat transfer path length
- T<sub>h</sub> = ANSYS calculated average edge temperature
- T<sub>c</sub> = specified edge temperature

The heat transfer path length will vary, depending on the direction of transfer (i.e., in-plane or out-of-plane).

#### 4.4.1.1.4 Modeling of Basket Conductive Heat Transport

The total conduction heat rejection capability of a fuel basket is a combination of planar and axial contributions. These component contributions are calculated independently for each MPC basket design and then combined to obtain an equivalent isotropic thermal conductivity value.

The planar heat rejection capability of each MPC basket design (i.e., MPC-24, MPC-68, MPC-32 and MPC-24E) is evaluated by developing a thermal model of the combined fuel assemblies and composite basket walls geometry on the ANSYS finite element code. The ANSYS model includes a geometric layout of the basket structure in which the basket "Box Wall-Boral-Sheathing" sandwich is replaced by a "homogeneous wall" with an equivalent thermal conductivity. Since the thermal conductivity of the Alloy X material is a weakly varying function of temperature, the equivalent "homogeneous wall" must have a

temperature-dependent effective conductivity. Similarly, as illustrated in Figure 4.4.7, the conductivities in the “in-plane” and “out-of-plane” directions of the equivalent “homogeneous wall” are different. Finally, as discussed earlier, the fuel assemblies and the surrounding basket cell openings are modeled as homogeneous heat generating regions with an effective temperature dependent in-plane conductivity. The methodology used to reduce the heterogeneous MPC basket - fuel assemblage to an equivalent homogeneous region with effective thermal properties is discussed in the following.

Consider a cylinder of height,  $L$ , and radius,  $r_o$ , with a uniform volumetric heat source term,  $q_g$ , insulated top and bottom faces, and its cylindrical boundary maintained at a uniform temperature,  $T_c$ . The maximum centerline temperature ( $T_h$ ) to boundary temperature difference is readily obtained from classical one-dimensional conduction relationships (for the case of a conducting region with uniform heat generation and a constant thermal conductivity  $K_s$ ):

$$(T_h - T_c) = q_g r_o^2 / (4 K_s)$$

Noting that the total heat generated in the cylinder ( $Q_t$ ) is  $\pi r_o^2 L q_g$ , the above temperature rise formula can be reduced to the following simplified form in terms of total heat generation per unit length ( $Q_t/L$ ):

$$(T_h - T_c) = (Q_t / L) / (4 \pi K_s)$$

This simple analytical approach is employed to determine an effective basket cross-sectional conductivity by applying an equivalence between the ANSYS finite element model of the basket and the analytical case. The equivalence principle employed in the thermal analysis is depicted in Figure 4.4.2. The 2-dimensional ANSYS finite element model of the MPC basket is solved by applying a uniform heat generation per unit length in each basket cell region (depicted as Zone 1 in Figure 4.4.2) and a constant basket periphery boundary temperature,  $T_c$ . Noting that the basket region with uniformly distributed heat sources and a constant boundary temperature is equivalent to the analytical case of a cylinder with uniform volumetric heat source discussed earlier, an effective MPC basket conductivity ( $K_{eff}$ ) is readily derived from the analytical formula and ANSYS solution leading to the following relationship:

$$K_{eff} = N (Q_f'/L) / (4 \pi [T_h' - T_c'])$$

where:

$N$  = number of fuel assemblies

$(Q_f'/L)$  = per fuel assembly heat generation per unit length applied in ANSYS model

$T_h'$  = peak basket cross-section temperature from ANSYS model

Cross sectional views of MPC basket ANSYS models are depicted in Figures 4.4.9 and 4.4.10. Notice that many of the basket supports and all shims have been conservatively neglected in the models. This conservative geometry simplification, coupled with the conservative neglect of thermal expansion that would minimize the gaps, yields conservative gap thermal resistances. Temperature-dependent equivalent thermal conductivities of the fuel regions and composite basket walls, as determined from analysis procedures described earlier, are applied to the ANSYS model. The planar ANSYS conduction model is solved by

applying a constant basket periphery temperature with uniform heat generation in the fuel region. The equivalent planar thermal conductivity values are lower bound values because, among other elements of conservatism, the effective conductivity of the most resistive SNF types (Tables 4.4.1 and 4.4.2) is used in the MPC finite element simulations.

The basket in-plane conductivities are computed for intact fuel storage and containerized fuel stored in Damaged Fuel Containers (DFCs). The MPC-24E is provided with four enlarged cells designated for storing damaged fuel. The MPC-68 has sixteen peripheral locations for damaged fuel storage in generic DFC designs. As a substantial fraction of the basket cells are occupied by intact fuel, the overall effect of DFC fuel storage on the basket heat dissipation rate is quite small. Including the effect of reduced conductivity of the DFC cells in MPC-24E, the basket conductivity is computed to drop slightly (~0.6%). In a bounding calculation in which all cells of MPC-68 are assumed occupied by fuel in DFC, the basket conductivity drops by about 5%. Conservatively, assuming 95% of intact fuel basket heat load adequately covers damaged fuel storage in the MPC-24E and MPC-68.

The axial heat rejection capability of each MPC basket design is determined by calculating the area occupied by each material in a fuel basket cross-section, multiplying by the corresponding material thermal conductivity, summing the products and dividing by the total fuel basket cross-sectional area. In accordance with NUREG-1536 guidelines, the only portion of the fuel assemblies credited in these calculations is the fuel rod cladding.

Having obtained planar and axial effective thermal conductivity contributions as described above, an equivalent isotropic thermal conductivity that yields the same overall heat transfer can be obtained. Two-dimensional conduction heat transfer in relatively short cylinders cannot be readily evaluated analytically, so an alternate approach is used herein.

Instead of computing precise isotropic conductivities, an RMS function of the planar and axial effective thermal conductivity values is used as follows:

$$k_{iso} = \sqrt{\frac{k_{rad}^2 + k_{ax}^2}{2}}$$

where:

$k_{iso}$  = equivalent isotropic thermal conductivity

$k_{rad}$  = equivalent planar thermal conductivity

$k_{ax}$  = equivalent axial thermal conductivity

This formulation has been benchmarked for specific application to the MPC basket designs and found to yield conservative equivalent isotropic thermal conductivities and, subsequently, conservative temperature results from subsequent thermal analyses.

Table 4.4.3 summarizes the isotropic MPC basket thermal conductivity values used in the subsequent cask thermal modeling. It should be noted that the isotropic conductivities calculated as described above are

actually higher than those reported in Table 4.4.3, imparting additional conservatism to the subsequent calculations.

#### 4.4.1.1.5 Heat Transfer in MPC Basket Peripheral Region

Both of the MPC designs for storing PWR or BWR fuel are provided with relatively large regions, formed between the relatively cooler MPC shell and hot basket peripheral panels, filled with helium gas. Heat transfer in these helium-filled regions corresponds to the classical case of heat transfer in a differentially heated closed cavity. Many investigators, including Eckert and Carlson (Int. J. Heat Mass Transfer, vol. 2, p. 106, 1961) and Elder (J. Fluid Mech., vol. 23, p. 77, 1965) have performed experimental studies of this arrangement. The peripheral region between the basket and MPC inner surface is simulated as a tall fluid-filled cavity of height  $H$  formed between two differentially heated surfaces ( $\Delta T$ ) separated by a small distance  $L$ . In a closed cavity, an exchange of hot and cold fluids occurs near the top and bottom ends of the cavity, resulting in a net transport of heat across the gap. The rate of heat transfer across the cavity is characterized by a Rayleigh number,  $Ra_L$ , defined as:

$$Ra_L = \frac{C_p \bar{n}^2 g \beta \Delta T L^3}{\mu K}$$

where:

|            |   |  |
|------------|---|--|
| $C_p$      | = | fluid heat capacity  |
| $\rho$     | = | fluid density  |
| $g$        | = | acceleration due to gravity  |
| $\beta$    | = | coefficient of thermal expansion (equal to reciprocal of absolute temperature for gases) |
| $\Delta T$ | = | temperature difference between the hot and cold surfaces                                 |
| $L$        | = | spacing between the hot and cold surfaces  |
| $\mu$      | = | fluid viscosity  |
| $K$        | = | fluid conductivity   |

Hewitt et al. [4.4.6] recommends the following Nusselt number correlation for heat transport in tall cavities:

$$Nu_L = 0.42 Ra_L^{1/4} Pr^{0.012} \left(\frac{H}{L}\right)^{-0.3}$$

where  $Pr$  is the Prandtl number of the cavity fill gas.

A Nusselt number of unity implies heat transfer by fluid conduction only, while a higher than unity Nusselt number is due to the "Rayleigh" effect which monotonically increases with increasing Rayleigh number. Nusselt numbers applicable to helium-filled PWR and BWR fueled HI-STORM MPC peripheral voids used in the original licensing analysis are provided in Table 4.4.4. For conservatism, however, the contribution of the Rayleigh effect is ignored in the thermal model of the MPC.

#### 4.4.1.1.6 Effective Thermal Conductivity of MPC Basket-to-Shell Aluminum Heat Conduction Elements

As shown in HI-STORM System MPC drawings in Section 1.5, an option for insertion of full-length heat conduction elements fabricated from thin aluminum Alloy 1100 sheet metal is shown in the MPC design drawings. Due to the high thermal conductivity of aluminum Alloy 1100 (about 15 times that of Alloy X), a significant rate of net heat transfer is possible along thin plates. Figure 4.4.11 shows the mathematical idealization of a typical conduction element inserted in a basket periphery panel-to-MPC shell space. The aluminum heat conduction element is shown to cover the MPC basket Alloy X peripheral panel and MPC shell (Regions I and III depicted in Figure 4.4.11) surfaces along the full-length of the basket except for isolated locations where fitup or interference with other parts precludes complete basket coverage. Heat transport to and from the aluminum heat conduction element is conservatively postulated to occur across a thin helium gap as shown in the figure (i.e., no credit is taken for contact between the aluminum heat conduction element and the Alloy X fuel basket). Aluminum surfaces inside the hollow region are sandblasted prior to fabrication to result in a rough surface finish which has a significantly higher emissivity compared to smooth surfaces of rolled aluminum. The untreated aluminum surfaces directly facing Alloy X panels have a smooth finish to minimize contact resistance.

Net heat transfer resistance from the hot basket periphery panel to the relatively cooler MPC shell along the aluminum heat conduction element pathway is a sum of three individual resistances, in regions labeled I, II, and III in Figure 4.4.11. In Region I, heat is transported from the basket to the aluminum heat conduction element surface directly facing the basket panel across a thin helium resistance gap. Longitudinal transport of heat (in the z direction) in the aluminum plate (in Region I) will result in an axially non-uniform temperature distribution. Longitudinal one-dimensional heat transfer in the Region I aluminum plate was analytically formulated to result in the following ordinary differential equation for the non-uniform temperature distribution:

$$t K_{Al} \frac{\partial^2 T}{\partial z^2} = - \frac{K_{He}}{h} (T_h - T)$$

#### Boundary Conditions

$$\begin{aligned} \frac{\partial T}{\partial z} &= 0 \text{ at } z = 0 \\ T &= T_h' \text{ at } z = P \end{aligned}$$

where (see Figure 4.4.11):

- T(z) = non-uniform aluminum metal temperature distribution
- t = heat conduction element thickness
- K<sub>Al</sub> = heat conduction element conductivity
- K<sub>He</sub> = helium conductivity
- h = helium gap thickness
- T<sub>h</sub> = hot basket temperature
- T<sub>h</sub>' = heat conduction element Region I boundary temperature at z = P
- P = heat conduction element Region I length

Solution of this ordinary differential equation subject to the imposed boundary condition is:

$$(T_h - T) = (T_h - T_h') \left[ \frac{e^{\frac{z}{\sqrt{\alpha}}} + e^{-\frac{z}{\sqrt{\alpha}}}}{e^{\frac{P}{\sqrt{\alpha}}} + e^{-\frac{P}{\sqrt{\alpha}}}} \right]$$

where  $\alpha$  is a dimensional parameter equal to  $(h \times t \times K_{Al} / K_{He})$ . The net heat transfer ( $Q_I$ ) across the Region I helium gap can be determined by the following integrated heat flux to a heat conduction element of length  $L$  as:

$$Q_I = \int_0^P \frac{K_{He}}{h} (T_h - T) (L) dz$$

Substituting the analytical temperature distribution result obtained in Equation c, the following expression for net heat transfer is obtained:

$$Q_I = \frac{K_{He} L \sqrt{\alpha}}{h} \left( 1 - \frac{1}{e^{\frac{P}{\sqrt{\alpha}}} + e^{-\frac{P}{\sqrt{\alpha}}}} \right) (T_h - T_h')$$

Based on this result, an expression for Region I resistance is obtained as shown below:

$$R_I = \frac{T_h - T_h'}{Q_I} = \frac{h}{K_{He} L \sqrt{\alpha}} \left( 1 - \frac{1}{e^{\frac{P}{\sqrt{\alpha}}} + e^{-\frac{P}{\sqrt{\alpha}}}} \right)^{-1}$$

The Region II resistance expression can be developed from the following net heat transfer equation in the vertical leg of the conduction element as shown below:

$$Q_{II} = \frac{K_{Al} L t}{W} (T_h' - T_c')$$

where  $W$  is the conduction element Region II length.

$$R_{II} = \frac{T_h' - T_c'}{Q_{II}} = \frac{W}{K_{Al} L t}$$

Similarly, a Region III resistance expression can be analytically determined as shown below:

$$\begin{aligned} R_{III} &= \frac{(T_c' - T_c)}{Q_{III}} \\ &= \frac{h}{K_{He} L \sqrt{\alpha}} \left( 1 - \frac{1}{e^{\frac{P}{\sqrt{\alpha}}} + e^{-\frac{P}{\sqrt{\alpha}}}} \right)^{-1} \end{aligned}$$

This completes the analysis for the total thermal resistance attributable to the heat conduction elements, which is equal to the sum of the three individual resistances. The total heat conduction element resistance is smeared across the basket-to-MPC shell region as an effective uniform annular gap conductivity (see Figure 4.4.2). We note that heat transport along the conduction elements is an independent conduction path in

parallel with conduction and radiation mechanisms in the large helium gaps. Helium conduction and radiation in the MPC basket-to-MPC shell peripheral gaps is accounted for separately in the ANSYS models for the MPCs, described earlier. Therefore, the net conductivity of the MPC basket-to-MPC shell peripheral gap region is the sum of the heat conduction elements effective conductivity and the helium gap conduction-radiation effective conductivity. For conservatism, however, the contribution of the heat conduction elements is ignored in the HI-STORM thermal analyses.

#### 4.4.1.1.7 Annulus Air Flow and Heat Exchange

The HI-STORM storage overpack is provided with four inlet ducts at the bottom and four outlet ducts at the top. The ducts are provided to enable relatively cooler ambient air to flow through the annular gap between the MPC and storage overpack in the manner of a classical “chimney”. Hot air is vented from the top outlet ducts to the ambient environment. Buoyancy forces induced by density differences between the ambient air and the heated air column in the MPC-to-overpack annulus sustain airflow through the annulus.

In contrast to a classical chimney, however, the heat input to the HI-STORM annulus air does not occur at the bottom of the stack. Rather, the annulus air picks up heat from the lateral surface of the MPC shell as it flows upwards. The height dependent heat absorption by the annulus air must be properly accounted for to ensure that the buoyant term in the Bernoulli equation is not overstated making the solution unconservative. To fix ideas, consider two cases of stack heat input; Case A where the heat input to the rising air is all at the bottom (the “fireplace” scenario), and Case B, where the heat input is uniform along the entire height (more representative of the ventilated cask conditions). In both cases, we will assume that the air obeys the perfect gas law; i.e., at constant pressure,  $\rho = C/T$  where  $\rho$  and  $T$  are the density and the absolute temperature of the air and  $C$  is a constant.

##### Case A: Entire Heat Input at the Bottom

In a stack of height  $H$ , where the temperature of the air is raised from  $T_i$  to  $T_o$  at the bottom (Figure 4.4.12; Case A), the net fluid “head”  $p_1$  is given by:

$$p_1 = \bar{n}_i H - \bar{n}_o H$$

$\rho_i$  and  $\rho_o$  are the densities of air corresponding to absolute temperatures  $T_i$  and  $T_o$ , respectively.

Since  $\bar{n}_i = \frac{C}{T_i}$  and  $\bar{n}_o = \frac{C}{T_o}$ , we have:

$$p_1 = CH \left( \frac{1}{T_i} - \frac{1}{T_o} \right)$$

or

$$p_1 = \frac{CH \Delta T}{T_i T_o}$$

where:  $\Delta T = T_o - T_i$

Let  $\Delta T \ll T_i$ , then we can write:

$$\begin{aligned}\frac{1}{T_o} &= \frac{1}{T_i \left(1 + \frac{\Delta T}{T_i}\right)} \\ &= \frac{1}{T_i} \left[ 1 - \frac{\Delta T}{T_i} + \dots \right]\end{aligned}$$

Substituting in the above we have:

$$p_1 = \frac{CH}{T_i} \bar{a} (1 - \bar{a} + \dots)$$

where  $\bar{a} = \frac{\Delta T}{T_i}$  (dimensionless temperature rise)

or  $p_1 = \bar{n}_1 H \bar{a} - O(\bar{a}^2)$ .

#### Case B: Uniform Heat Input

In this case, the temperature of air rises linearly from  $T_i$  at the bottom to  $T_o$  at the top (Figure 4.4.12; Case B):

$$T_o = T_i + \alpha h \quad 0 \leq h \leq H$$

where:

$$\zeta = \frac{T_o - T_i}{H} = \frac{\alpha T_i}{H}$$

The total buoyant head, in this case, is given by:

$$\begin{aligned}p_2 &= \bar{n}_1 H - \int_0^H \bar{n} dh \\ &= \bar{n}_1 H - C \int_0^H \frac{1}{T} dh \\ &= \bar{n}_1 H - C \int_0^H \frac{dh}{(T_i + \alpha h)} \\ &= \bar{n}_1 H - \frac{C}{\alpha} \ln(1 + \bar{a})\end{aligned}$$

Using the logarithmic expansion relationship and simplifying we have:

$$p_2 = \frac{\bar{n}_1 H \bar{a}}{2} - O(\bar{A}^2)$$

Neglecting terms of higher order, we conclude that  $p_2$  is only 50% of  $p_1$ , i.e., the buoyancy driver in the case of uniformly distributed heat input to the air is half of the value if the heat were all added at the bottom.

In the case of HI-STORM, the axial heat input profile into the annulus air will depend on the temperature difference between the MPC cylindrical surface and the rising air along the height (Case C in Figure 4.4.12). The MPC surface temperature profile, of course, is a strong function of the axial decay heat generation profile in the SNF. Previous analyses show that the HI-STORM "chimney" is less than 50% as effective as a classical chimney. As we explain in Subsection 4.4.1.1.9, this fact is fully recognized in the global HI-STORM thermal model implementation of FLUENT.

#### 4.4.1.1.8 Determination of Solar Heat Input

The intensity of solar radiation incident on an exposed surface depends on a number of time varying terms. The solar heat flux strongly depends upon the time of the day as well as on latitude and day of the year. Also, the presence of clouds and other atmospheric conditions (dust, haze, etc.) can significantly attenuate solar intensity levels. Rapp [4.4.2] has discussed the influence of such factors in considerable detail.

Consistent with the guidelines in NUREG-1536 [4.4.10], solar input to the exposed surfaces of the HI-STORM overpack is determined based on 12-hour insolation levels recommended in 10CFR71 (averaged over a 24-hour period) and applied to the most adversely located cask after accounting for partial blockage of incident solar radiation on the lateral surface of the cask by surrounding casks. In reality, the lateral surfaces of the cask receive solar heat depending on the azimuthal orientation of the sun during the course of the day. In order to bound this heat input, the lateral surface of the cask is assumed to receive insolation input with the solar insolation applied horizontally into the cask array. The only reduction in the heat input to the lateral surface of the cask is due to partial blockage offered by the surrounding casks. In contrast to its lateral surface, the top surface of HI-STORM is fully exposed to insolation without any mitigation effects of blockage from other bodies. In order to calculate the view factor between the most adversely located HI-STORM system in the array and the environment, a conservative geometric simplification is used. The system is reduced to a concentric cylinder model, with the inner cylinder representing the HI-STORM unit being analyzed and the outer shell representing a reflecting boundary (no energy absorption).

Thus, the radius of the inner cylinder ( $R_i$ ) is the same as the outer radius of a HI-STORM overpack. The radius of the outer cylinder ( $R_o$ ) is set such that the rectangular space ascribed to a cask is preserved. This is further explained in the next subsection. It can be shown that the view factor from the outer cylinder to the inner cylinder ( $F_{o,i}$ ) is given by [4.4.3]:

$$F_{o-i} = \frac{1}{R} - \frac{1}{\delta R} \times \left[ \cos^{-1} \left( \frac{B}{A} \right) - \frac{1}{2L} \left\{ \sqrt{(A+2)^2 - (2R)^2} \times \cos^{-1} \left( \frac{B}{RA} \right) + B \sin^{-1} \left( \frac{1}{R} \right) - \frac{\delta A}{2} \right\} \right]$$

where:

- $F_{o-i}$  = View Factor from the outer cylinder to the inner cylinder
- $R$  = Outer Cylinder Radius to Inner Cylinder Radius Ratio ( $R_o/R_i$ )
- $L$  = Overpack Height to Radius Ratio
- $A = L^2 + R^2 - 1$
- $B = L^2 - R^2 + 1$

Applying the theorem of reciprocity, the view factor ( $F_{i-a}$ ) from outer overpack surface, represented by the inner cylinder, to the ambient can be determined as:

$$F_{i-a} = 1 - F_{o-i} \frac{R_o}{R_i}$$

Finally, to bound the quantity of heat deposited onto the HI-STORM surface by insolation, the absorptivity of the cask surfaces is assumed to be unity.

#### 4.4.1.1.9 FLUENT Model for HI-STORM

In the preceding subsections, a series of analytical and numerical models to define the thermal characteristics of the various elements of the HI-STORM System are presented. The thermal modeling begins with the replacement of the Spent Nuclear Fuel (SNF) cross section and surrounding fuel cell space with a solid region with an equivalent conductivity. Since radiation is an important constituent of the heat transfer process in the SNF/storage cell space, and the rate of radiation heat transfer is a strong function of the surface temperatures, it is necessary to treat the equivalent region conductivity as a function of temperature. Because of the relatively large range of temperatures in a loaded HI-STORM System under the design basis heat loads, the effects of variation in the thermal conductivity of the Alloy X basket wall with temperature are included in the numerical analysis model. The presence of significant radiation effects in the storage cell spaces adds to the imperative to treat the equivalent storage cell lamina conductivity as temperature-dependent.

Numerical calculations and FLUENT finite-volume simulations have been performed to establish the equivalent thermal conductivity as a function of temperature for the limiting (thermally most resistive) BWR and PWR spent fuel types. Utilizing the most limiting SNF (established through a simplified analytical process for comparing conductivities) ensures that the numerical idealization for the fuel space effective conductivity is conservative for all non-limiting fuel types.

Having replaced the fuel spaces by solid square blocks with a temperature-dependent conductivity essentially renders the basket into a non-homogeneous three-dimensional solid where the non-homogeneity is introduced by the honeycomb basket structure composed of interlocking basket panels. The basket panels themselves are a composite of Alloy X cell wall, Boral neutron absorber, and Alloy X sheathing metal. A conservative approach to replace this composite section with an equivalent "solid wall" was described earlier.

In the next step, a planar section of the MPC is considered. The MPC contains a non-symmetric basket lamina wherein the equivalent fuel spaces are separated by the "equivalent" solid metal walls. The space between the basket and the MPC, called the peripheral gap, is filled with helium gas. At this stage in the thermal analysis, the SNF/basket/MPC assemblage has been replaced with a two-zone (Figure 4.4.2) cylindrical solid whose thermal conductivity is a strong function of temperature.

The fuel assembly and MPC basket effective conductivity evaluations are performed for two distinct scenarios described earlier in this section. In the first scenario, the MPC cavity is backfilled with helium only. In the second scenario, gaseous fission products from a hypothetical rupture of 10% of the stored fuel rods dilute the backfill helium gas. As previously stated, thermal analysis results for both scenarios are obtained and reported in this section.

The thermal model for the HI-STORM overpack is prepared as a three-dimensional axisymmetric body. For this purpose, the hydraulic resistances of the inlet ducts and outlet ducts, respectively, are represented by equivalent axisymmetric porous media. Two overpack configurations are evaluated – HI-STORM 100 and a shorter variation (HI-STORM 100S) overpack. HI-STORM 100S features a smaller inlet duct-to-outlet duct separation and an optional enhanced gamma shield cross plate. Since the optional gammas shield cross plate flow resistance is bounding, the optional design was conservatively evaluated in the thermal analysis. The fuel cladding temperatures for MPC emplaced in a HI-STORM 100S overpack are confirmed to be bounded by the HI-STORM 100 System thermal model solution. Thus, separate table summaries for HI-STORM 100S overpack are not provided. The axial resistance to airflow in the MPC/overpack annulus (which includes longitudinal channels to "cushion" the stresses in the MPC structure during a postulated non-mechanistic tip-over event) is replaced by a hydraulically equivalent annulus. The surfaces of the ducts and annulus are assumed to have a relative roughness ( $\epsilon$ ) of 0.001. This value is appropriate for rough cast iron, wood stave and concrete pipes, and is bounding for smooth painted surfaces (all readily accessible internal and external HI-STORM overpack carbon steel surfaces are protected from corrosion by painting or galvanization). Finally, it is necessary to describe the external boundary conditions to the overpack situated on an ISFSI pad. An isolated HI-STORM will take suction of cool air from and reject heated air to, a semi-infinite half-space. In a rectilinear HI-STORM array, however, the unit situated in the center of the grid is evidently hydraulically most disadvantaged, because of potential interference to air intake from surrounding casks. To simulate this condition in a conservative manner, we erect a hypothetical cylindrical barrier around the centrally local HI-STORM. The radius of this hypothetical cylinder,  $R_o$ , is computed from the equivalent cask array downflow hydraulic diameter ( $D_h$ ) which is obtained as follows:

$$D_h = \frac{4 \times \text{Flow Area}}{\text{Wetted Perimeter}}$$

$$= \frac{4 \left( A_o - \frac{\delta}{4} d_o^2 \right)}{\delta d_o}$$

where:

- $A_o$  = Minimum tributary area ascribable to one HI-STORM (see Figure 4.4.24).
- $d_o$  = HI-STORM overpack outside diameter

The hypothetical cylinder radius,  $R_h$ , is obtained by adding half  $D_h$  to the radius of the HI-STORM overpack. In this manner, the hydraulic equivalence between the cask array and the HI-STORM overpack to hypothetical cylindrical annulus is established.

For purposes of the design basis analyses reported in this chapter, the tributary area  $A_o$  is assumed to be equal to 346 sq. ft. Sensitivity studies on the effect of the value of  $A_o$  on the thermal performance of the HI-STORM System shows that the system response is essentially insensitive to the assumed value of the tributary area. For example, a thermal calculation using  $A_o = 225$  sq. ft. (corresponding to 15 ft. square pitch) and design basis heat load showed that the peak cladding temperature is less than 1°C greater than that computed using  $A_o = 346$  sq. ft. Therefore, the distance between the vertically arrayed HI-STORMs in an ISFSI should be guided by the practical (rather than thermal) considerations, such as personnel access to maintain air ducts or painting the cask external surfaces.

The internal surface of the hypothetical cylinder of radius  $R_h$  surrounding the HI-STORM module is conservatively assumed to be insulated. Any thermal radiation heat transfer from the HI-STORM overpack to this insulated surface will be perfectly reflected, thereby bounding radiative blocking from neighboring casks. Then, in essence, the HI-STORM module is assumed to be confined in a large cylindrical "tank" whose wall surface boundaries are modeled as zero heat flux boundaries. The air in the "tank" is the source overpack. The air in the tank is replenished by ambient air from above the top of the HI-STORM overpacks. There are two sources of heat input to the exposed surface of the HI-STORM overpack. The most important source of heat input is the internal heat generation within the MPC. The second source of heat input is insolation, which is conservatively quantified in the manner of the preceding subsection.

The FLUENT model consisting of the axisymmetric 3-D MPC space, the overpack, and the enveloping tank is schematically illustrated in Figure 4.4.13. The HI-STORM thermosiphon-enabled solution is computed in a two-step process. In the first step, a HI-STORM overpack thermal model computes the ventilation effect from annulus heating by MPC decay heat. In this model, heat dissipation is conservatively restricted to the MPC shell (i.e., heat dissipation from MPC lid and baseplate completely neglected. This modeling assumption has the effect of overstating the MPC shell, annulus air and concrete temperatures. In

the next step, the temperature of stored fuel in a pressurized helium canister (thermosiphon model) is determined using the overpack thermal solution in the first step to fashion a bounding MPC shell temperature profile for the MPC thermal model. The modeling details are provided in the Holtec benchmarking report [4.4.12]. A summary of the essential features of this model is presented in the following:

- A conservatively lower bound canister pressure of 5 atm is postulated for the thermosiphon modeling.
- Heat input due to insolation is applied to the top surface and the cylindrical surface of the overpack with a bounding maximum solar absorptivity equal to 1.0.
- The heat generation in the MPC is assumed to be uniform in each horizontal plane, but to vary in the axial direction to correspond to the axial power distribution listed in Chapter 2.
- The most disadvantageously placed cask (i.e., the one subjected to maximum radiative blockage), is modeled.
- The bottom surface of the overpack, in contact with the ISFSI pad, rejects heat through the pad to the constant temperature (77°F) earth below. For some scenarios, the bottom surface of the overpack is conservatively assumed to be adiabatic.

The finite-volume model constructed in this manner will produce an axisymmetric temperature distribution. The peak temperature will occur at the centerline and is expected to be above the axial location of peak heat generation. As will be shown in Subsection 4.4.2, the results of the finite-volume solution bear out these observations.

The HI-STORM 100 System is evaluated for two fuel storage scenarios. In one scenario, designated as uniform loading, every basket cell is assumed to be occupied with fuel producing heat at the maximum rate. Storage of moderate burnup and high burnup fuels are analyzed for this loading scenario. In another scenario, denoted as regionalized loading, a two-region fuel loading configuration is stipulated. The two regions are defined as an inner region (for storing hot fuel) and an outer region with low decay heat fuel physically enveloping the inner region. This scenario is depicted in Figure 4.4.25. The inner region is shown populated with fuel having a heat load of  $q_1$  and post-core decay time (PCDT) or age  $\tau$ , and the outer region with fuel of heat load  $q_2$  and age  $\tau_2$ , where  $q_1 > q_2$ . For conservatism the outer region fuel permissible cladding temperature ( $T_2$ ) is assumed to be that of old fuel ( $\tau = 15$  years). By ensuring that the interface boundary temperature is less than or equal to  $T_2$  ensures that fuel in the outer region is below permissible temperatures for any fuel age. To permit hot fuel storage in the inner region, a uniform low decay heat rate is stipulated for the outer region fuel. The maximum allowable heat load for inner region fuel ( $q_1$ ), then, is a function of fuel age-dependent permissible temperature set forth in Table 4.3.7 and Appendix 4.A for moderate and high burnup fuels, respectively. For the regionalized loading scenario, the most restrictive of the two burnups dependent permissible temperature limits is used in the thermal evaluation. In the HI-STORM 100 System, four central locations in the MPC-24 and MPC-24E, twelve inner cells in MPC-32

and 32 in MPC-68 are designated as inner region locations in the regionalized fuel-loading scenario. Results of thermal evaluations for both scenarios are present in Subsection 4.4.2.

#### 4.4.1.1.10 Effect of Fuel Cladding Crud Resistance

In this subsection, a conservatively bounding estimate of temperature drop across a crud film adhering to a fuel rod during dry storage conditions is determined. The evaluation is performed for a BWR fuel assembly based on an upper bound crud thickness obtained from the PNL-4835 report ([4.3.2], Table 3). The crud present on the fuel assemblies is predominately iron oxide mixed with small quantities of other metals such as cobalt, nickel, chromium, etc. Consequently, the effective conductivity of the crud mixture is expected to be in the range of typical metal alloys. Metals have thermal conductivities several orders of magnitude larger than that of helium. In the interest of extreme conservatism, however, a film of helium with the same thickness replaces the crud layer. The calculation is performed in two steps. In the first step, a crud film resistance is determined based on a bounding maximum crud layer thickness replaced with a helium film on the fuel rod surfaces. This is followed by a peak local cladding heat flux calculation for the GE 7x7 array fuel assembly postulated to emit a conservatively bounding decay heat equal to 0.5kW. The temperature drop across the crud film obtained as a product of the heat flux and crud resistance terms is determined to be less than 0.1°F. The calculations are presented below.

Bounding Crud Thickness(s) = 130µm (4.26×10<sup>-4</sup> ft) (PNL-4835)  
 Crud Conductivity (K) = 0.1 Btu/ft-hr-°F (conservatively assumed as helium)  
 GE 7x7 Fuel Assembly:

Rod O.D. = 0.563"  
 Active Fuel Length = 150"  
 Heat Transfer Area = (7x7) × (δ×0.563) × (150/144) = 90.3 ft<sup>2</sup>  
 Axial Peaking Factor = 1.195 (Burnup distribution Table 2.1.11)  
 Decay Heat = 500W (conservative assumption)

$$\text{Crud Resistance} = \frac{\delta}{K} = \frac{4.26 \times 10^{-4}}{0.1} = 4.26 \times 10^{-3} \frac{\text{ft}^2 \cdot \text{hr} \cdot ^\circ\text{F}}{\text{Btu}}$$

$$\begin{aligned} \text{Peak Heat Flux} &= \frac{(500 \times 3.417) \text{ Btu/hr}}{90.3 \text{ ft}^2} \times 1.195 \\ &= 18.92 \times 1.195 = 22.6 \frac{\text{Btu}}{\text{ft}^2 \cdot \text{hr}} \end{aligned}$$

Temperature drop (ΔT<sub>c</sub>) across crud film

$$\begin{aligned} &= 4.26 \times 10^{-3} \frac{\text{ft}^2 \cdot \text{hr} \cdot ^\circ\text{F}}{\text{Btu}} \times 22.6 \frac{\text{Btu}}{\text{ft}^2 \cdot \text{hr}} \\ &= 0.096^\circ\text{F} \end{aligned}$$

(i.e., less than 0.1°F)

Therefore, it is concluded that deposition of crud does not materially change the SNF cladding temperature.

#### 4.4.1.1.11 Thermal Conductivity Calculations with Diluted Backfill Helium

In this subsection, the thermal conductivities of mixtures of the helium backfill gas and the gaseous fission products released from a hypothetical rupture of 10% of the stored fuel rods are evaluated. The gaseous fission products release fractions are stipulated in NUREG-1536. The released gases will mix with the helium backfill gas and reduce its thermal conductivity. These reduced thermal conductivities are applied to determine fuel assembly, and MPC fuel basket and basket periphery effective conductivities for thermal evaluation of the HI-STORM System.

Appendix C of NUREG/CR-0497 [4.4.7] describes a method for calculating the effective thermal conductivity of a mixture of gases. The same method is also described by Rohsenow and Hartnett [4.2.2]. The following expression is provided by both references:

$$k_{\text{mix}} = \sum_{i=1}^n \left( \frac{k_i x_i}{x_i + \sum_{\substack{j=1 \\ j \neq i}}^n \phi_{ij} x_j} \right)$$

where:

- $k_{\text{mix}}$  = thermal conductivity of the gas mixture (Btu/hr-ft-°F)
- $n$  = number of gases
- $k_i$  = thermal conductivity of gas component  $i$  (Btu/hr-ft-°F)
- $x_i$  = mole fraction of gas component  $i$

In the preceding equation, the term  $\phi_{ij}$  is given by the following:

$$\phi_{ij} = \bar{o}_{ij} \left[ 1 + 2.41 \frac{(M_i - M_j)(M_i - 0.142 \cdot M_j)}{(M_i + M_j)^2} \right]$$

where  $M_i$  and  $M_j$  are the molecular weights of gas components  $i$  and  $j$ , and  $\phi_{ij}$  is:

$$\bar{o}_{ij} = \frac{\left[ 1 + \left( \frac{k_i}{k_j} \right)^{\frac{1}{2}} \left( \frac{M_i}{M_j} \right)^{\frac{1}{4}} \right]^2}{2^{\frac{3}{2}} \left( 1 + \frac{M_i}{M_j} \right)^{\frac{1}{2}}}$$

Table 4.4.7 presents a summary of the gas mixture thermal conductivity calculations for the MPC-24 and MPC-68 MPC designs containing design basis fuel assemblies.

Having calculated the gas mixture thermal conductivities, the effective thermal conductivities of the design basis fuel assemblies are calculated using the finite-volume model described in Subsection 4.4.1.1.2. Only the helium gas conductivity is changed, all other modeling assumptions are the same. The fuel assembly effective thermal conductivities with diluted helium are compared to those with undiluted helium in Table 4.4.8. From this table, it is observed that a 10% rod rupture condition has a relatively minor impact on the fuel assembly effective conductivity. Because the fuel regions comprise only a portion of the overall fuel basket thermal conductivity, the 10% rod rupture condition will have an even smaller impact on the basket effective conductivity.

#### 4.4.1.1.12 Effects of Hypothetical Low Fuel Rod Emissivity

The value of emissivity ( $\epsilon$ ) utilized in this FSAR was selected as 0.8 based on:

- i. the recommendation of an EPRI report [4.1.3]
- ii. Holtec's prior licensing experience with the HI-STAR 100 System
- iii. other vendors' cask licensing experience with the NRC
- iv. authoritative literature citations

The table below provides relevant third party information to support the emissivity value utilized in this FSAR.

| Source              | Reference                          | Zircaloy Emissivity |
|---------------------|------------------------------------|---------------------|
| EPRI                | [4.1.3]                            | 0.8                 |
| TN-68 TSAR          | Docket 72-1027                     | 0.8                 |
| TN-40               | Prairie Island Site Specific ISFSI | 0.8                 |
| TN-32               | Docket 72-1021                     | 0.8                 |
| Todreas & Mantuefel | [4.4.8]                            | 0.8                 |
| DOE SNF Report      | [4.4.9]                            | 0.8                 |

The appropriateness of the selected value of  $\epsilon$  is further supported by the information provided by PNL-4835 [4.3.2] and NUREG/CR-0497 [4.4.7]. PNL-4835 reports cladding oxidation thickness in U.S. Zircaloy LWR SNF assemblies (20  $\mu\text{m}$  for PWR and 30  $\mu\text{m}$  for BWR fuel). If these oxide thickness values are applied to the mathematical formulas presented for emissivity determination in [4.4.7], then the computed values are slightly higher than our assumed value of 0.8. It should be recognized that the formulas in [4.4.7] include a conservative assumption that depresses the value of computed emissivity, namely, absence of crud. Significant crud layers develop on fuel cladding surfaces during in-core operation. Crud,

which is recognized by the above-mentioned NUREG document as having a boosting effect on  $\epsilon$ , is completely neglected.

The above discussion provides a reasonable rationale for our selection of 0.8 as the value for  $\epsilon$ . However, to determine the effect of a hypothetical low emissivity of 0.4, an additional thermal analysis adopting this value has been performed. In this analysis, each fuel rod of a fuel assembly is stipulated to have this uniformly low  $\epsilon = 0.4$  and the effective fuel thermal conductivity is recalculated. In the next step, all cells of an MPC basket are assumed to be populated with this low  $\epsilon$  fuel that is further assumed to be emitting decay heat at design basis level. The effective conductivity of this basket populated with low  $\epsilon$  fuel is recalculated. Using the recalculated fuel basket conductivity, the HI-STORM system temperature field is recomputed. This exercise is performed for the MPC-24 basket because, as explained in the next paragraph, this basket design, which accommodates a fewer number of fuel assemblies (compared to the MPC-68 and MPC-32) has a higher sensitivity to the emissivity parameter. This analysis has determined that the impact of a low  $\epsilon$  assumption on the peak cladding temperature is quite small (about  $5^{\circ}\text{C}$ ). It is noted that these sensitivity calculations were performed under the completely suppressed helium thermosiphon cooling assumption. Consequently, as the burden of heat dissipation shouldered by radiation heat transfer under this assumption is much greater, the resultant computed sensitivity is a conservative upper bound for the HI-STORM system.

The relatively insignificant increase in the computed peak clad temperature as a result of applying a large penalty in  $\epsilon$  (50%) is consistent with the findings in a German Ph.D. dissertation [4.4.11]. Dr. Anton's study consisted of analyzing a cask containing 4 fuel assemblies with a total heat load of 17 kW and helium inside the fuel cavity. For an emissivity of 0.8, the calculated peak cladding temperature was  $337^{\circ}\text{C}$ . In a sensitivity study, wherein the emissivity was varied from 0.7 to 0.9, the temperature changed only by  $5^{\circ}\text{C}$ , i.e. to  $342^{\circ}\text{C}$  and  $332^{\circ}\text{C}$ . Dr. Anton ascribed two reasons for this low impact of emissivity on computed temperatures. Although the radiative heat emission by a surface decreases with lower emissivity, the fraction of heat reflected from other surfaces increases. In other words, the through-assembly heat dissipation by this means increases thereby providing some compensation for the reduced emission. Additionally, the fourth power of temperature dependence of thermal radiation heat transfer reduces the impact of changes in the coefficients on computed temperatures. For storage containers with larger number of fuel assemblies (like the HI-STORM System), an even smaller impact would be expected, since a larger fraction of the heat is dissipated via the basket conduction heat transfer.

#### 4.4.1.1.13 HI-STORM Temperature Field with Low Heat Emitting Fuel

The HI-STORM 100 thermal evaluations for BWR fuel are grouped in two categories of fuel assemblies proposed for storage in the MPC-68. The two groups are classified as Low Heat Emitting (LHE) fuel assemblies and Design Basis (DB) fuel assemblies. The LHE group of fuel assemblies are characterized by low burnup, long cooling time, and short active fuel lengths. Consequently, their heat loads are dwarfed by the DB group of fuel assemblies. The Dresden-1 (6x6 and 8x8), Quad+, and Humboldt Bay (7x7 and 6x6) fuel assemblies are grouped as the LHE fuel. This fuel is evaluated when encased in Damaged Fuel Containers (DFC). As a result of interruption of radiation heat exchange between the fuel assembly and the fuel basket by the DFC boundary, this configuration is bounding for thermal evaluation. In Table 4.4.2, two

canister types for encasing LHE fuel are evaluated – a Holtec design and an existing canister in which some of the Dresden-1 fuel is currently stored (Transnuclear D-1 canister). The most resistive LHE fuel assembly (Dresden-1 8x8) is considered for thermal evaluation (see Table 4.4.2) in a DFC container. The MPC-68 basket effective conductivity, loaded with the most resistive fuel assembly (encased in a canister) is provided in Table 4.4.3. To this basket, LHE decay heat is applied and a HI-STORM 100 System thermal solution computed. The peak cladding temperature is computed as 513°F, which is substantially below the temperature limit for long cooled fuel (~635°F).

A thoria rod canister designed for holding a maximum of twenty fuel rods arrayed in a 5x4 configuration is currently stored at the Dresden-1 spent fuel pool. The fuel rods were originally constituted as part of an 8x8 fuel assembly and used in the second and third cycle of Dresden-1 operation. The maximum fuel burnup of these rods is quite low (~14,400 MWD/MTU). The thoria rod canister internal design is a honeycomb structure formed from 12-gage stainless steel plates. The rods are loaded in individual square cells. This long cooled, part assembly (18 fuel rods) and very low fuel burnup thoria rod canister renders it a miniscule source of decay heat. The canister all-metal internal honeycomb construction serves as an additional means of heat dissipation in the fuel cell space. In accordance with fuel loading stipulation in the Technical Specifications, long cooled fuel is loaded toward the basket periphery (i.e., away from the hot central core of the fuel basket). All these considerations provide ample assurance that these fuel rods will be stored in a benign thermal environment and, therefore, remain protected during long-term storage.

#### 4.4.1.2 Test Model

A detailed analytical model for thermal design of the HI-STORM System was developed using the FLUENT CFD code and the industry standard ANSYS modeling package, as discussed in Subsection 4.4.1.1. As discussed throughout this chapter and specifically in Section 4.4.6, the analysis incorporates significant conservatism so as to compute bounding fuel cladding temperatures. Furthermore, compliance with specified limits of operation is demonstrated with adequate margins. In view of these considerations, the HI-STORM System thermal design complies with the thermal criteria set forth in the design basis (Sections 2.1 and 2.2) for long-term storage under normal conditions. Additional experimental verification of the thermal design is therefore not required.

#### 4.4.2 Maximum Temperatures

All four MPC-basket designs developed for the HI-STORM System have been analyzed to determine temperature distributions under long-term normal storage conditions, and the results summarized in this subsection. A cross-reference of HI-STORM thermal analyses at other conditions with associated subsection of the FSAR summarizing obtained results is provided in Table 4.4.22. The MPC baskets are considered to be fully loaded with design basis PWR or BWR fuel assemblies, as appropriate. The systems are arranged in an ISFSI array and subjected to design basis normal ambient conditions with insolation.

As discussed in Subsection 4.4.1.1.1, the thermal analysis is performed using a submodeling process where the results of an analysis on an individual component are incorporated into the analysis of a larger set of components. Specifically, the submodeling process yields directly computed fuel temperatures from which

fuel basket temperatures are then calculated. This modeling process differs from previous analytical approaches wherein the basket temperatures were evaluated first and then a basket-to-cladding temperature difference calculation by Wooten-Epstein or other means provided a basis for cladding temperatures. Subsection 4.4.1.1.2 describes the calculation of an effective fuel assembly thermal conductivity for an equivalent homogenous region. It is important to note that the result of this analysis is a function of thermal conductivity versus temperature. This function for fuel thermal conductivity is then input to the fuel basket effective thermal conductivity calculation described in Subsection 4.4.1.1.4. This calculation uses a finite-element methodology, wherein each fuel cell region containing multiple finite-elements has temperature-varying thermal conductivity properties. The resultant temperature-varying fuel basket thermal conductivity computed by this basket-fuel composite model is then input to the fuel basket region of the FLUENT cask model.

Because the FLUENT cask model incorporates the results of the fuel basket submodel, which in turn incorporates the fuel assembly submodel, the peak temperature reported from the FLUENT model is the peak temperature in any component. In a dry storage cask, the hottest components are the fuel assemblies. It should be noted that, because the fuel assembly models described in Subsection 4.4.1.1.2 include the fuel pellets, the FLUENT calculated peak temperatures reported in Tables 4.4.9 and 4.4.10 are actually peak pellet centerline temperatures which bound the peak cladding temperatures, and are therefore conservatively reported as the cladding temperatures.

Applying the radiative blocking factor applicable for the worst case cask location, conservatively bounding axial temperatures at the most heated fuel cladding are shown in Figures 4.4.16 and 4.4.17 for MPC-24 and MPC-68 to depict the thermosiphon effect in PWR and BWR SNF. From these plots, the upward movement of the hot spot is quite evident. As discussed in this chapter, these calculated temperature distributions incorporate many conservatisms. The maximum fuel clad temperatures for zircaloy clad fuel assemblies are listed in Tables 4.4.9, 4.4.10, 4.4.26, and 4.4.27, which also summarize maximum calculated temperatures in different parts of the MPCs and HI-STORM overpack (Table 4.4.36)..

Figures 4.4.19 and 4.4.20, respectively, depict radial temperature distribution in the PWR (MPC-24) and the BWR (MPC-68) at the horizontal plane where maximum fuel cladding temperature occurs. Finally, axial variations of the ventilation air temperatures and that of the inner shell surface are depicted in Figure 4.4.26 for a bounding heat load.

The following additional observations can be derived by inspecting the temperature field obtained from the finite volume analysis:

- The fuel cladding temperatures are in compliance with the temperature limits determined using both the DCCG methodology [4.3.5] and the PNL CSFM methodology [4.3.1].
- The maximum temperature of the basket structural material is within the stipulated design temperature.

- The maximum temperature of the Boral neutron absorber is below the material supplier's recommended limit.
- The maximum temperatures of the MPC pressure boundary materials are well below their respective ASME Code limits.
- The maximum temperatures of concrete are within the NRC's recommended limits [4.4.10] (See Table 4.3.1.)

Noting that the permissible peak cladding temperature is a function of fuel age, parametric peak fuel cladding temperature versus total decay heat load information is computed from the FLUENT thermal model solution. The allowable fuel cladding temperature limits are presented in Section 4.3 for moderate burnup fuel and in Appendix 4.A for high-burnup fuel.

Because the peak clad temperature limits are dependent on burnup and the fuel age at the start of dry storage, the allowable decay heat load is also dependent on these parameters. Tables 4.4.20, 4.4.21, 4.4.28, and 4.4.29, for the MPC-24 and MPC-68, MPC-32 and MPC-24E, respectively, present the allowable decay heat load as a function of fuel age for moderate burnup fuel. Tables 4.4.32 through 4.4.35 present the results for high burnup fuel. Burnup and cooling-time curves, developed in source-term calculations in Chapter 5 and reported in Chapter 2, are generated from the heat load limits in those tables. It is noted that the burnup and cooling time curves are developed for the most limiting fuel assembly<sup>†</sup> of each type (PWR and BWR), but are applied to all assemblies of each type. By definition, the limiting fuel assembly emits more heat than any other assembly of its type at a given burnup and cooling time does. Thus, if the limiting fuel assembly meets the allowable clad temperature limit by a certain margin, then the other fuel assemblies of its type with equal burnup and cooling time will meet the clad temperature limit by an even greater margin. The added margin can be quite considerable. For example, the design-basis PWR assembly is the B&W 15×15, which is used to determine Technical Specification limits for burnup in the HI-STORM System. For certain Westinghouse fuel types, the decay heat loads corresponding to these burnup limits will be about 15% less than that of the design-basis assembly. This decay heat over-prediction for other than design-basis assemblies renders the predicted peak temperatures extremely conservative for those assemblies.

For the regionalized loading scenario as depicted in Figure 4.4.25, outer region decay heat limits are stipulated in Table 4.4.30. The inner region heat load limit will be governed by the peak cladding temperature limit for the hot fuel, provided that the interface cladding temperature limit for long cooled fuel is not exceeded. The MPC-32 and MPC-68 heat load limits are determined by analysis to be governed by this requirement. In the MPC-24 and MPC-24E regionalized loading scenarios, the interface cladding temperature limit is reached first for certain fuel cooling times. Thus, the peak cladding temperatures for

<sup>†</sup> The limiting fuel assembly (also referred to as the design-basis assembly) is defined as that assembly which is the most heat emissive of its type (PWR or BWR) as a given burnup and cooling time.

these MPCs are below their permissible values by a greater margin. The inner region heat load limits are provided in Table 4.4.31.

The calculated temperatures are based on a series of analyses, described previously in this chapter, that incorporate many conservatisms. A list of the significant conservatisms is provided in Subsection 4.4.6. As such, the calculated temperatures are upper bound values that would exceed actual temperatures.

The above observations lead us to conclude that the temperature field in the HI-STORM System with a fully loaded MPC containing design-basis heat emitting SNF complies with all regulatory and industry temperature limits. In other words, the thermal environment in the HI-STORM System will be conducive to long-term safe storage of spent nuclear fuel.

#### 4.4.3 Minimum Temperatures

In Table 2.2.2 of this report, the minimum ambient temperature condition for the HI-STORM storage overpack and MPC is specified to be  $-40^{\circ}\text{F}$ . If, conservatively, a zero decay heat load with no solar input is applied to the stored fuel assemblies, then every component of the system at steady state would be at a temperature of  $-40^{\circ}\text{F}$ . All HI-STORM storage overpack and MPC materials of construction will satisfactorily perform their intended function in the storage mode at this minimum temperature condition. Structural evaluations in Chapter 3 show the acceptable performance of the overpack and MPC steel and concrete materials at low service temperatures. Criticality and shielding evaluations (Chapters 5 and 6) are unaffected by temperature.

#### 4.4.4 Maximum Internal Pressure

The MPC is initially filled with dry helium after fuel loading and drying prior to installing the MPC closure ring. During normal storage, the gas temperature within the MPC rises to its maximum operating basis temperature as determined based on the thermal analysis methodology described earlier. The gas pressure inside the MPC will also increase with rising temperature. The pressure rise is determined based on the ideal gas law, which states that the absolute pressure of a fixed volume of gas is proportional to its absolute temperature. Tables 4.4.12, 4.4.13, 4.4.24, and 4.4.25 present summaries of the calculations performed to determine the net free volume in the MPC-24, MPC-68, MPC-32, and MPC-24E, respectively.

The MPC maximum gas pressure is considered for a postulated accidental release of fission product gases caused by fuel rod rupture. For these fuel rod rupture conditions, the amounts of each of the release gas constituents in the MPC cavity are summed and the resulting total pressures determined from the Ideal Gas Law. Based on fission gases release fractions (per NUREG 1536 criteria [4.4.10]), net free volume and initial fill gas pressure, the bounding maximum gas pressures with 1% (normal), 10% (off-normal) and 100% (accident condition) rod rupture are given in Table 4.4.14. The maximum gas pressures listed in Table 4.4.14 are all below the MPC internal design pressure listed in Table 2.2.1.

The inclusion of PWR non-fuel hardware (BPRA control elements and thimble plugs) to the PWR baskets influences the MPC internal pressure through two distinct effects. The presence of non-fuel hardware

increases the effective basket conductivity, thus enhancing heat dissipation and lowering fuel temperatures as well as the temperature of the gas filling the space between fuel rods. The gas volume displaced by the mass of non-fuel hardware lowers the cavity free volume. These two effects, namely, temperature lowering and free volume reduction, have opposing influence on the MPC cavity pressure. The first effect lowers gas pressure while the second effect raises it. In the HI-STORM thermal analysis, the computed temperature field (with non-fuel hardware excluded) has been determined to provide a conservatively bounding temperature field for the PWR baskets (MPC-24, MPC-24E, and MPC-32). The MPC cavity free space is computed based on volume displacement by the heaviest fuel (bounding weight) with non-fuel hardware included.

During in-core irradiation of BPRAs, neutron capture by the B-10 isotope in the neutron absorbing material produces helium. Two different forms of the neutron absorbing material are used in BPRAs: Borosilicate glass and B<sub>4</sub>C in a refractory solid matrix (Al<sub>2</sub>O<sub>3</sub>). Borosilicate glass (primarily a constituent of Westinghouse BPRAs) is used in the shape of hollow pyrex glass tubes sealed within steel rods and supported on the inside by a thin-walled steel liner. To accommodate helium diffusion from the glass rod into the rod internal space, a relatively high void volume (~40%) is engineered in this type of rod design. The rod internal pressure is thus designed to remain below reactor operation conditions (2,300 psia and approximately 600°F coolant temperature). The B<sub>4</sub>C- Al<sub>2</sub>O<sub>3</sub> neutron absorber material is principally used in B&W and CE fuel BPRAs designs. The relatively low temperature of the poison material in BPRAs rods (relative to fuel pellets) favor the entrapment of helium atoms in the solid matrix.

Several BPRAs designs are used in PWR fuel that differ in the number, diameter, and length of poison rods. The older Westinghouse fuel (W-14x14 and W-15x15) has used 6, 12, 16, and 20 rods per assembly BPRAs and the later (W-17x17) fuel uses up to 24 rods per BPRAs. The BPRAs rods in the older fuel are much larger than the later fuel and, therefore, the B-10 isotope inventory in the 20-rod BPRAs bounds the newer W-17x17 fuel. Based on bounding BPRAs rods internal pressure, a large hypothetical quantity of helium (7.2 g-moles/BPRAs) is assumed to be available for release into the MPC cavity from each fuel assembly in the PWR baskets. The MPC cavity pressures (including helium from BPRAs) are summarized in Table 4.4.14.

#### 4.4.5 Maximum Thermal Stresses

Thermal expansion induced mechanical stresses due to non-uniform temperature distributions are reported in Chapter 3 of this report. Table 4.4.15 provides a summary of HI-STORM System component temperature inputs for structural evaluation. Table 4.4.19 provides a summary of confinement boundary temperatures during normal storage conditions. Structural evaluation in Section 3.4.4 references these temperature results to demonstrate confinement boundary integrity.

#### 4.4.6 Evaluation of System Performance for Normal Conditions of Storage

The HI-STORM System thermal analysis is based on a detailed and complete heat transfer model that conservatively accounts for all modes of heat transfer in various portions of the MPC and overpack. The thermal model incorporates many conservative features that render the results for long-term storage to be extremely conservative:

1. The most severe levels of environmental factors for long-term normal storage, which are an ambient temperature of 80°F and 10CFR71 insolation levels, were coincidentally imposed on the system.
2. A hypothetical rupture of 10% of the stored fuel rods was conservatively considered for determining the thermal conductivity of the diluted helium backfill gas.
3. The most adversely located HI-STORM System in an ISFSI array was considered for analysis.
4. A conservative assessment of thermosiphon effect in the MPC, which is intrinsic to the HI-STORM fuel basket design is included in the thermal analyses.
5. Not Used
6. No credit was considered for contact between fuel assemblies and the MPC basket wall or between the MPC basket and the basket supports. The fuel assemblies and MPC basket were conservatively considered to be in concentric alignment.
7. The MPC is assumed to be loaded with the SNF type which has the maximum equivalent thermal resistance of all fuel types in its category (BWR or PWR), as applicable.
8. The design basis maximum decay heat loads are used for all thermal-hydraulic analyses. For casks loaded with fuel assemblies having decay heat generation rates less than design basis, additional thermal margins of safety will exist. This is assured by defining the burnup limits, as a function of age, for the fuel assemblies based on the bounding (i.e., most heat emissive) fuel assembly types within each class (PWR or BWR). As demonstrated in the source-term calculations described Chapter 5, the B&W 15×15 and GE 7×7 are the governing PWR and BWR fuel assemblies, respectively. For all other fuel types, the heat emission rates at the design-basis burnup levels will be below the design-basis heat emission rate.
9. Not Used
10. The enhancement of heat transfer owing to the so-called "Rayleigh effect" in the basket/MPC interface region, which was included in the analyses underlying the original CoC on the HI-STORM 100 System, is neglected in this revision of the SAR for conservatism.
11. Aluminum heat conduction elements ignored in the thermal analyses.

Temperature distribution results obtained from this highly conservative thermal model show that the maximum fuel cladding temperature limits are met with adequate margins. Expected margins during normal storage will be much greater due to the many conservative assumptions incorporated in the analysis. The long-term impact of decay heat induced temperature levels on the HI-STORM System structural and neutron shielding materials is considered to be negligible. The maximum local MPC basket temperature level is below the recommended limits for structural materials in terms of susceptibility to stress, corrosion and creep-induced degradation. Furthermore, stresses induced due to imposed temperature gradients are within Code limits. Therefore, it is concluded that the HI-STORM System thermal design is in compliance with 10CFR72 requirements.

Table 4.4.1

SUMMARY OF PWR FUEL ASSEMBLY EFFECTIVE  
THERMAL CONDUCTIVITIES

| Fuel                       | @ 200°F<br>(Btu/ft-hr-°F) | @ 450°F<br>(Btu/ft-hr-°F) | @ 700°F<br>(Btu/ft-hr-°F) |
|----------------------------|---------------------------|---------------------------|---------------------------|
| W - 17x17 OFA              | 0.182                     | 0.277                     | 0.402                     |
| W - 17x17 Standard         | 0.189                     | 0.286                     | 0.413                     |
| W - 17x17 Vantage          | 0.182                     | 0.277                     | 0.402                     |
| W - 15x15 Standard         | 0.191                     | 0.294                     | 0.430                     |
| W - 14x14 Standard         | 0.182                     | 0.284                     | 0.424                     |
| W - 14x14 OFA              | 0.175                     | 0.275                     | 0.413                     |
| B&W - 17x17                | 0.191                     | 0.289                     | 0.416                     |
| B&W - 15x15                | 0.195                     | 0.298                     | 0.436                     |
| CE - 16x16                 | 0.183                     | 0.281                     | 0.411                     |
| CE - 14x14                 | 0.189                     | 0.293                     | 0.435                     |
| HN <sup>†</sup> - 15x15 SS | 0.180                     | 0.265                     | 0.370                     |
| W - 14x14 SS               | 0.170                     | 0.254                     | 0.361                     |
| B&W-15x15<br>Mark B-11     | 0.187                     | 0.289                     | 0.424                     |
| CE-14x14 (MP2)             | 0.188                     | 0.293                     | 0.434                     |
| IP-1 (14x14) SS            | 0.125                     | 0.197                     | 0.293                     |

<sup>†</sup> Haddam Neck Plant B&W or Westinghouse stainless steel clad fuel assemblies.

Table 4.4.2

SUMMARY OF BWR FUEL ASSEMBLY EFFECTIVE  
THERMAL CONDUCTIVITIES

| Fuel   | @ 200°F<br>(Btu/ft-hr-°F) | @ 450°F<br>(Btu/ft-hr-°F) | @ 700°F<br>(Btu/ft-hr-°F) |
|--|---------------------------|---------------------------|---------------------------|
| Dresden 1 - 8x8 <sup>†</sup>   | 0.119                     | 0.201                     | 0.319                     |
| Dresden 1 - 6x6 <sup>†</sup>   | 0.126                     | 0.215                     | 0.345                     |
| GE - 7x7   | 0.171                     | 0.286                     | 0.449                     |
| GE - 7x7R  | 0.171                     | 0.286                     | 0.449                     |
| GE - 8x8   | 0.168                     | 0.278                     | 0.433                     |
| GE - 8x8R  | 0.166                     | 0.275                     | 0.430                     |
| GE10 - 8x8   | 0.168                     | 0.280                     | 0.437                     |
| GE11 - 9x9   | 0.167                     | 0.273                     | 0.422                     |
| AC <sup>††</sup> -10x10 SS   | 0.152                     | 0.222                     | 0.309                     |
| Exxon-10x10 SS   | 0.151                     | 0.221                     | 0.308                     |
| Damaged Dresden-1<br>8x8 <sup>†</sup> (in a Holtec<br>damaged fuel<br>container) | 0.107                     | 0.169                     | 0.254                     |
| Humboldt Bay-7x7 <sup>†</sup>  | 0.127                     | 0.215                     | 0.343                     |
| Dresden-1 Thin Clad<br>6x6 <sup>†</sup>  | 0.124                     | 0.212                     | 0.343                     |
| Damaged Dresden-1<br>8x8 (in TN D-1<br>canister) <sup>†</sup>                    | 0.107                     | 0.168                     | 0.252                     |
| 8x8 Quad <sup>†</sup><br>Westinghouse <sup>†</sup>                               | 0.164                     | 0.276                     | 0.435                     |

† Cladding temperatures of low heat emitting Dresden (intact and damaged) SNF in the HI-STORM System will be bounded by design basis fuel cladding temperatures. Therefore, these fuel assembly types are excluded from the list of fuel assemblies (zircaloy clad) evaluated to determine the most resistive SNF type.

†† Allis-Chalmers stainless steel clad fuel assemblies.

Table 4.4.3

MPC BASKET EQUIVALENT ISOTROPIC THERMAL CONDUCTIVITY VALUES<sup>††</sup>

| Basket                                   | @200°F<br>(Btu/ft-hr-°F) | @450°F<br>(Btu/ft-hr-°F) | @700°F<br>(Btu/ft-hr-°F) |
|--|--------------------------|--------------------------|--------------------------|
| MPC-24 (Zircaloy<br>Clad Fuel)           | 1.109                    | 1.495                    | 1.955                    |
| MPC-68 (Zircaloy<br>Clad Fuel)           | 1.111                    | 1.347                    | 1.591                    |
| MPC-24 (Stainless<br>Steel Clad Fuel) †  | 0.897                    | 1.213                    | 1.577(a)                 |
| MPC-68 (Stainless<br>Steel Clad Fuel) †  | 1.070                    | 1.270                    | 1.451(b)                 |
| MPC-32 (Zircaloy<br>Clad Fuel)           | 1.015                    | 1.271                    | 1.546                    |
| MPC-32 (Stainless<br>Steel Clad Fuel) †  | 0.806                    | 0.987                    | 1.161 (c)                |
| MPC-24E (Zircaloy<br>Clad Fuel)          | 1.216                    | 1.637                    | 2.133                    |
| MPC-24E (Stainless<br>Steel Clad fuel) † | 0.991                    | 1.351                    | 1.766 (d)                |

- (a) Conductivity is 19% less than corresponding zircaloy fueled basket.
- (b) Conductivity is 9% less than corresponding zircaloy fueled basket.
- (c) Conductivity is 25% less than corresponding zircaloy fueled basket.
- (d) Conductivity is 17% less than corresponding zircaloy fueled basket.

<sup>††</sup> The values reported in this table are conservatively understated.

<sup>†</sup> Evaluated in a damaged fuel canister (conservatively bounding)

Table 4.4.4

CLOSED CAVITY NUSSOLT NUMBER RESULTS  
FOR HELIUM-FILLED MPC PERIPHERAL VOIDS†

| Temperature (°F) | Nusselt Number<br>(PWR Baskets) | Nusselt Number<br>(BWR Basket) |
|------------------|---------------------------------|--------------------------------|
| 200              | 3.17                            | 2.41                           |
| 450              | 2.56                            | 1.95                           |
| 700              | 2.21                            | 1.68                           |

† For conservatism the Rayleigh effect is ignored in the MPC thermal analyses.

Table 4.4.5

SUMMARY OF 10x10 ARRAY TYPE BWR FUEL ASSEMBLY  
EFFECTIVE THERMAL CONDUCTIVITIES<sup>†</sup>

| Fuel Assembly | @ 200°F<br>(Btu/ft-hr-°F) | @ 450°F<br>(Btu/ft-hr-°F) | @ 700°F<br>(Btu/ft-hr-°F) |
|---------------|---------------------------|---------------------------|---------------------------|
| GE-12/14      | 0.166                     | 0.269                     | 0.412                     |
| Atrium-10     | 0.164                     | 0.266                     | 0.409                     |
| SVEA-96       | 0.164                     | 0.269                     | 0.416                     |

<sup>†</sup> The conductivities reported in this table are obtained by the simplified method described in the beginning of Subsection 4.4.1.1.2.

Table 4.4.6

COMPARISON OF ARTIUM-10 BWR FUEL ASSEMBLY CONDUCTIVITY<sup>†</sup> WITH  
THE BOUNDING<sup>††</sup> BWR FUEL ASSEMBLY CONDUCTIVITY

| Temperature (°F) | Atrium-10 BWR Assembly |         | Bounding BWR Assembly |         |
|------------------|------------------------|---------|-----------------------|---------|
|                  | (Btu/ft-hr-°F)         | (W/m-K) | (Btu/ft-hr-°F)        | (W/m-K) |
| 200              | 0.225                  | 0.389   | 0.171                 | 0.296   |
| 450              | 0.345                  | 0.597   | 0.271                 | 0.469   |
| 700              | 0.504                  | 0.872   | 0.410                 | 0.710   |

<sup>†</sup> The reported effective conductivity has been obtained from a rigorous finite-element model.

<sup>††</sup> The bounding BWR fuel assembly conductivity applied in the MPC-68 basket thermal analysis.

Table 4.4.7

SUMMARY OF THERMAL CONDUCTIVITY CALCULATIONS  
FOR MPC HELIUM DILUTED BY RELEASED ROD GASES

| Component Gas                        | Molecular Weight<br>(g/mole) | Component Gas Mole Fractions and<br>Mixture Conductivity (Btu/hr-ft-°F) |  |
|--------------------------------------|------------------------------|---|--|
|                                      |                              | MPC-24  | MPC-68   |
| MPC Backfill Helium                  | 4                            | 0.951   | 0.962  |
| Fuel Rod Backfill Helium             | 4                            | 0.023   | $5.750 \times 10^{-3}$                             |
| Rod Tritium                          | 3                            | $1.154 \times 10^{-5}$  | $4.483 \times 10^{-5}$                             |
| Rod Krypton                          | 85                           | $2.372 \times 10^{-3}$  | $2.905 \times 10^{-3}$                             |
| Rod Xenon                            | 131                          | 0.024   | 0.030  |
| Rod Iodine                           | 129                          | $1.019 \times 10^{-3}$  | $1.273 \times 10^{-3}$                             |
| Mixture of Gases (diluted<br>helium) | N/A                          | 0.088 at 200°F<br>0.116 at 450°F<br>0.142 at 700°F                      | 0.086 at 200°F<br>0.113 at 450°F<br>0.139 at 700°F |

Table 4.4.8

COMPARISON OF COMPONENT THERMAL CONDUCTIVITIES  
WITH AND WITHOUT BACKFILL HELIUM DILUTION

|   | @ 200°F<br>(Btu/hr-ft-°F) | @ 450°F<br>(Btu/hr-ft-°F) | @ 700°F<br>(Btu/hr-ft-°F) |
|---|---------------------------|---------------------------|---------------------------|
| GE-11 9×9 Fuel Assembly with Undiluted Helium   | 0.171                     | 0.271                     | 0.410                     |
| GE-11 9×9 Fuel Assembly with Diluted Helium     | 0.158                     | 0.254                     | 0.385                     |
| W 17×17 OFA Fuel Assembly with Undiluted Helium | 0.257                     | 0.406                     | 0.604                     |
| W 17×17 OFA Fuel Assembly with Diluted Helium   | 0.213                     | 0.347                     | 0.537                     |

Table 4.4.9

HI-STORM<sup>†</sup> SYSTEM LONG-TERM NORMAL  
STORAGE MAXIMUM TEMPERATURES  
(MPC-24 BASKET)

| Component        | Normal Condition Temp. (°F) | Long-Term Temperature Limit (°F) |
|------------------|-----------------------------|----------------------------------|
| Fuel Cladding    | 691                         | 787 <sup>††</sup>                |
| MPC Basket       | 650                         | 725 <sup>†††</sup>               |
| Basket Periphery | 486                         | 725 <sup>†††</sup>               |
| MPC Outer Shell  | 344                         | 450                              |

<sup>†</sup> Bounding overpack temperatures are provided in Table 4.4.36.

<sup>††</sup> The temperature limit is in accordance with DCCG (gross rupture) criteria. Permissible peak cladding temperature is 691°F (PNL Criteria).

<sup>†††</sup> The ASME Code allowable temperature of the fuel basket Alloy X materials is 800°F. This lower temperature limit is imposed to add additional conservatism to the analysis of the HI-STORM System.

Table 4.4.10

HI-STORM<sup>†</sup> SYSTEM LONG-TERM NORMAL  
STORAGE MAXIMUM TEMPERATURES  
(MPC-68 BASKET)

| Component        | Normal Condition Temp. (°F) | Long-Term Temperature Limit (°F) |
|------------------|-----------------------------|----------------------------------|
| Fuel Cladding    | 740                         | 824 <sup>††</sup>                |
| MPC Basket       | 720                         | 725 <sup>†††</sup>               |
| Basket Periphery | 501                         | 725 <sup>†††</sup>               |
| MPC Outer Shell  | 347                         | 450                              |

<sup>†</sup> Bounding overpack temperatures are provided in Table 4.4.36.

<sup>††</sup> The temperature limit is in accordance with DCCG (gross rupture) criteria. Permissible cladding temperature is 742°F (PNL criteria).

<sup>†††</sup> The ASME Code allowable temperature of the fuel basket Alloy X materials is 800°F. This lower temperature limit is imposed to add additional conservatism to the analysis of the HI-STORM System.

Table 4.4.11

INTENTIONALLY DELETED

Table 4.4.12

SUMMARY OF MPC-24 FREE VOLUME CALCULATIONS

| Item                                    | Volume (ft <sup>3</sup> ) |
|---|---------------------------|
| Cavity Volume                           | 367.9                     |
| Basket Metal Volume                     | 39.7                      |
| Bounding Fuel Assemblies Volume         | 78.8                      |
| Basket Supports and Fuel Spacers Volume | 6.1                       |
| Aluminum Conduction Elements            | 5.9 <sup>†</sup>          |
| Net Free Volume                         | 237.5 (6,724 liters)      |

<sup>†</sup> Bounding 1,000 lbs weight assumed.

Table 4.4.13

SUMMARY OF MPC-68 FREE VOLUME CALCULATIONS

| Item                                    | Volume (ft <sup>3</sup> ) |
|---|---------------------------|
| Cavity Volume                           | 367.3                     |
| Basket Metal Volume                     | 34.8                      |
| Bounding Fuel Assemblies Volume         | 93.0                      |
| Basket Supports and Fuel Spacers Volume | 11.3                      |
| Aluminum Conduction Elements            | 5.9 <sup>†</sup>          |
| Net Free Volume                         | 222.3 (6,294 liters)      |

<sup>†</sup> Bounding 1,000 lbs weight assumed

Table 4.4.14  
SUMMARY OF MPC CONFINEMENT BOUNDARY PRESSURES<sup>†</sup>  
FOR LONG-TERM STORAGE

| Condition                  | Pressure (psig) |
|----------------------------|-----------------|
| <b>MPC-24:</b>             |                 |
| Initial backfill (at 70°F) | 31.3            |
| Normal condition           | 66.4            |
| With 1% rods rupture       | 66.1            |
| With 10% rods rupture      | 72.2            |
| With 100% rods rupture     | 132.5           |
| <b>MPC-68:</b>             |                 |
| Initial backfill (at 70°F) | 31.3            |
| Normal condition           | 67.1            |
| With 1% rods rupture       | 67.5            |
| With 10% rods rupture      | 71.1            |
| With 100% rods rupture     | 107.6           |
| <b>MPC-32:</b>             |                 |
| Initial backfill (at 70°F) | 31.3            |
| Normal Condition           | 65.6            |
| With 1% rods rupture       | 66.5            |
| With 10% rods rupture      | 75.0            |
| With 100% rods rupture     | 160.1           |
| <b>MPC-24E:</b>            |                 |
| Initial backfill (at 70°F) | 31.3            |
| Normal Condition           | 65.8            |
| With 1% rods rupture       | 66.4            |
| With 10% rods rupture      | 72.5            |
| With 100% rods rupture     | 133.5           |

<sup>†</sup> Per NUREG-1536, pressure analyses with ruptured fuel rods (including BPRA rods for PWR fuel) is performed with release of 100% of the ruptured fuel rod fill gas and 30% of the significant radioactive gaseous fission products.

Table 4.4.15

SUMMARY OF HI-STORM SYSTEM COMPONENT TEMPERATURES  
FOR LONG-TERM STORAGE (°F)

| Location             | MPC-24 | MPC-68 | MPC-32 | MPC-24E |
|----------------------|--------|--------|--------|---------|
| MPC Basket Top:      |        |        |        |         |
| Basket periphery     | 485    | 501    | 496    | 488     |
| MPC shell            | 344    | 348    | 351    | 346     |
| Overpack Inner Shell | 199    | 199    | 199    | 199     |
| Overpack Outer Shell | 124    | 124    | 124    | 124     |
| MPC Basket Bottom:   |        |        |        |         |
| Basket periphery     | 281    | 280    | 290    | 284     |
| MPC shell            | 256    | 258    | 261    | 258     |
| Overpack Inner Shell | 106    | 106    | 106    | 106     |
| Overpack Outer Shell | 107    | 107    | 107    | 107     |

Table 4.4.16

INTENTIONALLY DELETED

Table 4.4.17

INTENTIONALLY DELETED

Table 4.4.18

INTENTIONALLY DELETED

Table 4.4.19

SUMMARY OF MPC CONFINEMENT BOUNDARY  
TEMPERATURE DISTRIBUTIONS

| Location                                    | MPC-24<br>(°F) | MPC-68<br>(°F) | MPC-32<br>(°F) | MPC-24E<br>(°F) |
|---|----------------|----------------|----------------|-----------------|
| MPC Lid Inside Surface at Centerline        | 463            | 502            | 487            | 462             |
| MPC Lid Outside Surface at Centerline       | 427            | 454            | 447            | 425             |
| MPC Lid Inside Surface at Periphery         | 371            | 381            | 383            | 372             |
| MPC Lid Outside Surface at Periphery        | 360            | 375            | 372            | 358             |
| MPC Baseplate Inside Surface at Centerline  | 207            | 209            | 214            | 209             |
| MPC Baseplate Outside Surface at Centerline | 200            | 203            | 208            | 202             |
| MPC Baseplate Inside Surface at Periphery   | 243            | 246            | 249            | 245             |
| MPC Baseplate Outside Surface at Periphery  | 194            | 196            | 199            | 195             |

Table 4.4.20

MPC-24 DESIGN-BASIS MAXIMUM HEAT LOAD†  
 VERSUS FUEL AGE AT LOADING (MODERATE BURNUP)

| Fuel Age At Loading (years) | Permissible Heat Load (kW) |
|-----------------------------|----------------------------|
| 5                           | 27.77                      |
| 6                           | 26.96                      |
| 7                           | 24.74                      |
| 10                          | 24.23                      |
| 15                          | 23.66                      |

† The cask heat load limits ( $Q_r$ ) presented in this table pertain to loading the MPC with uniformly aged fuel assemblies emitting heat at the design basis maximum rate ( $q_r$ ), where “ $\tau$ ” is the age of the fuel at the start of dry storage. For a cask loaded with a mix of fuel ages, the cask heat load limit shall be the sum of the individual assembly decay heat limits (as a function of  $\tau$ ) as specified in the Appendix B to COC 1014.

Table 4.4.21

MPC-68 DESIGN-BASIS MAXIMUM HEAT LOAD†  
 VERSUS FUEL AGE AT LOADING (MODERATE BURNUP)

| Fuel Age At Loading (years) | Permissible Heat Load (kW) |
|-----------------------------|----------------------------|
| 5                           | 28.19                      |
| 6                           | 26.81                      |
| 7                           | 24.71                      |
| 10                          | 24.18                      |
| 15                          | 23.60                      |

† The cask heat load limits ( $Q_t$ ) presented in this table pertain to loading the MPC with uniformly aged fuel assemblies emitting heat at the design basis maximum rate ( $q_t$ ), where "t" is the age of fuel at the start of dry storage. For a cask loaded with a mix of fuel ages, the cask heat load limit shall be the sum of the individual assembly decay heat limits (as a function of fuel age) as specified in the Appendix B to COC 1014.

Table 4.4.22  
MATRIX OF HI-STORM SYSTEM THERMAL EVALUATIONS

| Scenario | Description             | Ultimate Heat Sink | Analysis Type | Principal Input Parameters  | Results in FSAR Subsection |
|----------|-------------------------|--------------------|---------------|-----------------------------|----------------------------|
| 1        | Long Term Normal        | Ambient            | SS            | $N_T, Q_D, ST, SC, I_O$     | 4.4.2                      |
| 2        | Off-Normal Environment  | Ambient            | SS(B)         | $O_T, Q_D, ST, SC, I_O$     | 11.1.2                     |
| 3        | Extreme Environment     | Ambient            | SS(B)         | $E_T, Q_D, ST, SC, I_O$     | 11.2.15                    |
| 4        | Partial Ducts Blockage  | Ambient            | SS(B)         | $N_T, Q_D, ST, SC, I_{1/4}$ | 11.1.4                     |
| 5        | Ducts Blockage Accident | Overpack           | TA            | $N_T, Q_D, ST, SC, I_C$     | 11.2.13                    |
| 6        | Fire Accident           | Overpack           | TA            | $Q_D, F$                    | 11.2.4                     |
| 7        | Tip Over Accident       | Overpack           | AH            | $Q_D$                       | 11.2.3                     |
| 8        | Debris Burial Accident  | Overpack           | AH            | $Q_D$                       | 11.2.14                    |

Legend:

|   |  |
|---|--|
| <p><math>N_T</math> - Maximum Annual Average (Normal) Temperature (80°F)<br/> <math>O_T</math> - Off-Normal Temperature (100°F)<br/> <math>E_T</math> - Extreme Hot Temperature (125°F)<br/> <math>Q_D</math> - Design Basis Maximum Heat Load<br/> SS - Steady State<br/> SS(B) - Bounding Steady State<br/> TA - Transient Analysis<br/> AH - Adiabatic Heating</p> | <p><math>I_O</math> - All Inlet Ducts Open<br/> <math>I_{1/2}</math> - Half of Inlet Ducts Open<br/> <math>I_{1/4}</math> - Quarter of Inlet Ducts Open<br/> <math>I_C</math> - All Inlet Ducts Closed<br/> ST - Insolation Heating (Top)<br/> SC - Insolation Heating (Curved)<br/> F - Fire Heating (1475°F)</p> |
|---|--|

Table 4.4.23

## PLANT SPECIFIC BWR FUEL TYPES EFFECTIVE CONDUCTIVITY†

| Fuel                   | @200°C<br>[Btu/ft-hr-°F] | @450°F<br>[Btu/ft-hr-°F] | @700°F<br>[Btu/ft-hr-°F] |
|------------------------|--------------------------|--------------------------|--------------------------|
| Oyster Creek (7x7)     | 0.161                    | 0.269                    | 0.422                    |
| Oyster Creek (8x8)     | 0.162                    | 0.266                    | 0.413                    |
| TVA Browns Ferry (8x8) | 0.160                    | 0.264                    | 0.411                    |
| SPC-5 (9x9)            | 0.149                    | 0.245                    | 0.380                    |
| ANF 8x8                | 0.167                    | 0.277                    | 0.433                    |
| ANF-9X (9x9)           | 0.165                    | 0.272                    | 0.423                    |

† The conductivities reported in this table are obtained by a simplified analytical method in Subsection 4.4.1.1.2.

Table 4.4.24

SUMMARY OF MPC-32 FREE VOLUME CALCULATIONS

| Item                                    | Volume (ft <sup>3</sup> ) |
|---|---------------------------|
| Cavity Volume                           | 367.9                     |
| Basket Metal Volume                     | 27.4                      |
| Bounding Free Assemblies Volume         | 105.0                     |
| Basket Supports and Fuel Spacers Volume | 9.0                       |
| Optional Aluminum Conduction Elements   | 5.9                       |
| Net Free Volume                         | 220.6 (6,247 liters)      |

Table 4.4.25

SUMMARY OF MPC-24E FREE VOLUME CALCULATIONS

| Item                                    | Volume (ft <sup>3</sup> ) |
|---|---------------------------|
| Cavity Volume                           | 367.9                     |
| Basket Metal Volume                     | 51.2                      |
| Bounding Fuel Assemblies Volume         | 78.8                      |
| Basket Supports and Fuel Spacers Volume | 6.1                       |
| Optional Aluminum Conduction Elements   | 5.9                       |
| Net Free Volume                         | 225.9 (6,398 liters)      |

Table 4.4.26

HI-STORM<sup>†</sup> SYSTEM LONG-TERM NORMAL STORAGE MAXIMUM TEMPERATURES  
(MPC-32 BASKET)

| Component        | Normal Condition Temp. (°F) | Long-Term Temperature Limit (°F) |
|------------------|-----------------------------|----------------------------------|
| Fuel Cladding    | 691                         | 787 <sup>††</sup>                |
| MPC Basket       | 660                         | 725 <sup>†††</sup>               |
| Basket Periphery | 496                         | 725 <sup>†††</sup>               |
| MPC Outer Shell  | 351                         | 450                              |

<sup>†</sup> Bounding overpack temperatures are provided in Table 4.4.36.

<sup>††</sup> The temperature limit is in accordance with DCCG (gross rupture) criteria. Permissible peak cladding temperature is 691°F PNL Criteria).

<sup>†††</sup> The ASME Code allowable temperature of the fuel basket Alloy X materials is 800°F. This lower temperature limit is imposed to add additional conservatism in the analysis of the HI-STORM Systems.

Table 4.4.27

HI-STORM† SYSTEM LONG-TERM NORMAL STORAGE MAXIMUM TEMPERATURES  
(MPC-24E BASKET)

| Component        | Normal Condition Temp. (°F) | Long-Term Temperature Limit (°F) |
|------------------|-----------------------------|----------------------------------|
| Fuel Cladding    | 691                         | 787 <sup>††</sup>                |
| MPC Basket       | 650                         | 725 <sup>†††</sup>               |
| Basket Periphery | 492                         | 725 <sup>†††</sup>               |
| MPC Outer Shell  | 347                         | 450                              |

† Bounding overpack temperatures are provided in Table 4.4.36.

†† The temperature limit is in accordance with DCCG (gross rupture) criteria. Permissible peak cladding temperature is 691°F (PNL Criteria).

††† The ASME Code allowable temperature of the fuel basket Alloy X materials is 800°F. This lower temperature limit is imposed to add additional conservatism to the analysis of the HI-STORM System

Table 4.4.28

MPC-32 DESIGN BASIS MAXIMUM HEAT LOAD<sup>†</sup> VERSUS FUEL AGE AT LOADING  
(MODERATE BURNUP)

| Fuel Age at Loading (years) | Permissible Heat Load (kW) |
|-----------------------------|----------------------------|
| 5                           | 28.74                      |
| 6                           | 27.95                      |
| 7                           | 25.79                      |
| 10                          | 25.26                      |
| 15                          | 24.68                      |

<sup>†</sup> The cask heat load limits ( $Q_c$ ) presented in this table pertain to loading the MPC with uniformly aged fuel assemblies emitting heat at the design basis maximum rate ( $q_c$ ) where " $\tau$ " is the age of fuel at the start of dry storage. For a cask loaded with a mix of fuel ages, the cask heat load limit shall be the sum of the individual assembly decay heat limits (as a function of fuel age) as specified in the Appendix B to CoC 1014.

Table 4.4.29

MPC-24E DESIGN BASIS MAXIMUM HEAT LOAD<sup>†</sup> VERSUS FUEL AGE AT LOADING  
(MODERATE BURNUP)

| Fuel Age at Loading (years) | Permissible Heat Load (kW) |
|-----------------------------|----------------------------|
| 5                           | 28.17                      |
| 6                           | 27.33                      |
| 7                           | 25.05                      |
| 10                          | 24.53                      |
| 15                          | 23.95                      |

<sup>†</sup> The cask heat load limits ( $Q_c$ ) presented in this table pertain to loading the MPC with uniformly aged fuel assemblies emitting heat at the design basis maximum rate ( $q_c$ ), where “ $\tau$ ” is the age of fuel at the start of dry storage. For a cask loaded with a mix of fuel ages, the cask heat load limit shall be the sum of the individual assembly decay heat limits (as a function of fuel age) as specified in the Appendix B to COC 1014.

Table 4.4.30

REGIONALIZED LOADING OUTER REGION HEAT LOAD LIMITS

| <b>MPC Type</b> | <b>Inner Region Assemblies</b> | <b>Outer Region Assemblies</b> | <b>Outer Region Heat Load (kW)</b> |
|-----------------|--------------------------------|--------------------------------|------------------------------------|
| MPC-24          | 4                              | 20                             | 18                                 |
| MPC-24E         | 4                              | 20                             | 18                                 |
| MPC-32          | 12                             | 20                             | 12                                 |
| MPC-68          | 32                             | 36                             | 9.9                                |

Table 4.4.31

REGIONALIZED LOADING INNER REGION HEAT LOAD LIMITS (kW)

| Fuel Age (years) | MPC-24            | MPC-24E           | MPC-32 | MPC-68 |
|------------------|-------------------|-------------------|--------|--------|
| 5                | 5.88 <sup>†</sup> | 6.16 <sup>†</sup> | 13.58  | 16.02  |
| 6                | 5.88 <sup>†</sup> | 6.16 <sup>†</sup> | 12.87  | 14.99  |
| 7                | 5.34              | 5.58              | 11.92  | 13.40  |
| 10               | 4.94              | 5.16              | 11.40  | 12.99  |
| 15               | 4.66              | 4.86              | 11.02  | 12.54  |

<sup>†</sup> Inner region heat load governed by interface cladding temperature limit.

Table 4.4.32

MPC-24 DESIGN BASIS MAXIMUM HEAT LOAD<sup>†</sup> VERSUS FUEL AGE  
AT LOADING (HIGH BURNUP)

| Fuel Age at Loading (yrs) | Permissible Heat Load (kW) |
|---------------------------|----------------------------|
| 5                         | 27.12                      |
| 6                         | 26.09                      |
| 7                         | 24.74                      |
| 10                        | 24.02                      |
| 15                        | 23.50                      |

<sup>†</sup> The cask heat load limits ( $Q_{\tau}$ ) presented in this table pertain to loading the MPC with uniformly aged fuel assemblies emitting heat at the design basis maximum rate ( $q_{\tau}$ ), where " $\tau$ " is the age of fuel at the start of dry storage. For a cask loaded with a mix of fuel ages, the cask heat load limit shall be the sum of the individual assembly decay heat limits (as a function of fuel age) as specified in the Appendix B to COC 1014.

Table 4.4.33

MPC-24E DESIGN BASIS MAXIMUM HEAT LOAD†  
 VERSUS FUEL AGE AT LOADING (HIGH BURNUP)

| Fuel Age at Loading (yrs) | Permissible Heat Load (kW) |
|---------------------------|----------------------------|
| 5                         | 27.50                      |
| 6                         | 26.44                      |
| 7                         | 25.05                      |
| 10                        | 24.31                      |
| 15                        | 23.79                      |

† The cask heat load limits ( $Q_{\tau}$ ) presented in this table pertain to loading the MPC with uniformly aged fuel assemblies emitting heat at the design basis maximum rate ( $q_{\tau}$ ), where “ $\tau$ ” is the age of fuel at the start of dry storage. For a cask loaded with a mix of fuel ages, the cask heat load limit shall be the sum of the individual assembly decay heat limits (as a function of fuel age) as specified in the Appendix B to COC 1014.

Table 4.4.34

MPC-32 DESIGN BASIS MAXIMUM HEAT LOAD†  
 VERSUS FUEL AGE AT LOADING (HIGH BURNUP)

| Fuel Age at Loading (yrs) | Permissible Heat Load (kW) |
|---------------------------|----------------------------|
| 5                         | 28.10                      |
| 6                         | 27.10                      |
| 7                         | 25.79                      |
| 10                        | 25.05                      |
| 15                        | 24.53                      |

† The cask heat load limits ( $Q_c$ ) presented in this table pertain to loading the MPC with uniformly aged fuel assemblies emitting heat at the design basis maximum rate ( $q_c$ ), where “ $\tau$ ” is the age of fuel at the start of dry storage. For a cask loaded with a mix of fuel ages, the cask heat load limit shall be the sum of the individual assembly decay heat limits (as a function of fuel age) as specified in the Appendix B to COC 1014.

Table 4.4.35

MPC-68 DESIGN BASIS MAXIMUM HEAT LOAD†  
 VERSUS FUEL AGE AT LOADING (HIGH BURNUP)

| Fuel Age at Loading (yrs) | Permissible Heat Load (kW) |
|---------------------------|----------------------------|
| 5                         | 28.19                      |
| 6                         | 26.81                      |
| 7                         | 24.71                      |
| 10                        | 24.18                      |
| 15                        | 23.60                      |

† The cask heat load limits ( $Q_c$ ) presented in this table pertain to loading the MPC with uniformly aged fuel assemblies emitting heat at the design basis maximum rate ( $q_c$ ), where "τ" is the age of fuel at the start of dry storage. For a cask loaded with a mix of fuel ages, the cask heat load limit shall be the sum of the individual assembly decay heat limits (as a function of fuel age) as specified in the Appendix B to COC 1014.

Table 4.4.36

BOUNDING LONG-TERM NORMAL STORAGE  
HI-STORM OVERPACK TEMPERATURES

| Component†         | Local Section Temperature††<br>(°F) | Long-Term Temperature Limit<br>(°F) |
|--------------------|-------------------------------------|-------------------------------------|
| Inner shell        | 199                                 | 350                                 |
| Outer shell        | 145                                 | 350                                 |
| Lid bottom plate   | 339                                 | 350                                 |
| Lid top plate      | 196                                 | 350                                 |
| MPC pedestal plate | 208                                 | 350                                 |
| Baseplate          | 111                                 | 350                                 |
| Radial shield      | 172                                 | 200                                 |
| Air outlet†††      | 206                                 |                                     |

† See Figure 1.2 8 for a description of HI-STORM components.

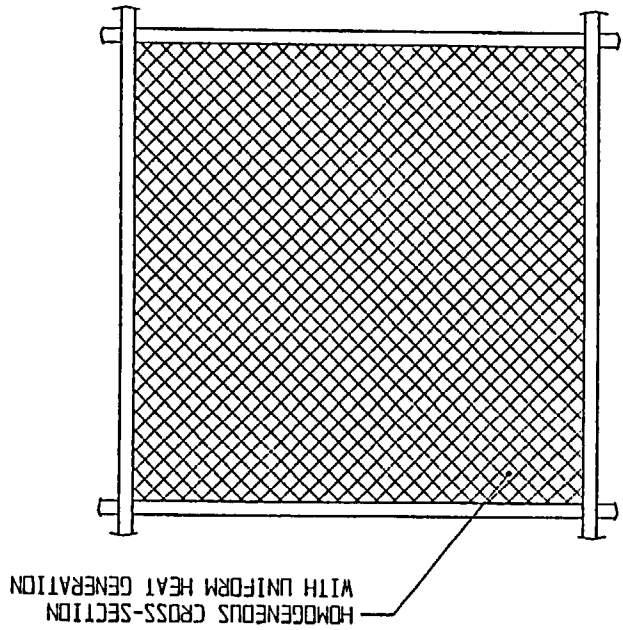
†† Section temperature is defined as the through-thickness average temperature.

††† Reported herein for the option of temperature measurement surveillance of outlet ducts air temperature as set forth in the Technical Specifications.

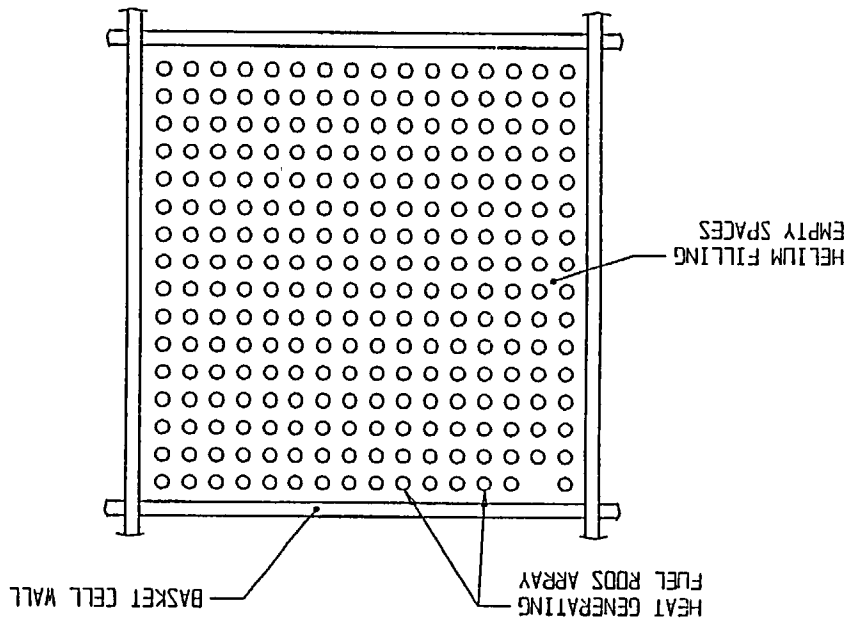
+

FIGURE 4.4.1: HOMOGENIZATION OF THE STORAGE CELL CROSS-SECTION

(b) SOLID REGION OF EFFECTIVE CONDUCTIVITY



(a) TYPICAL FUEL CELL



+

(

(

(

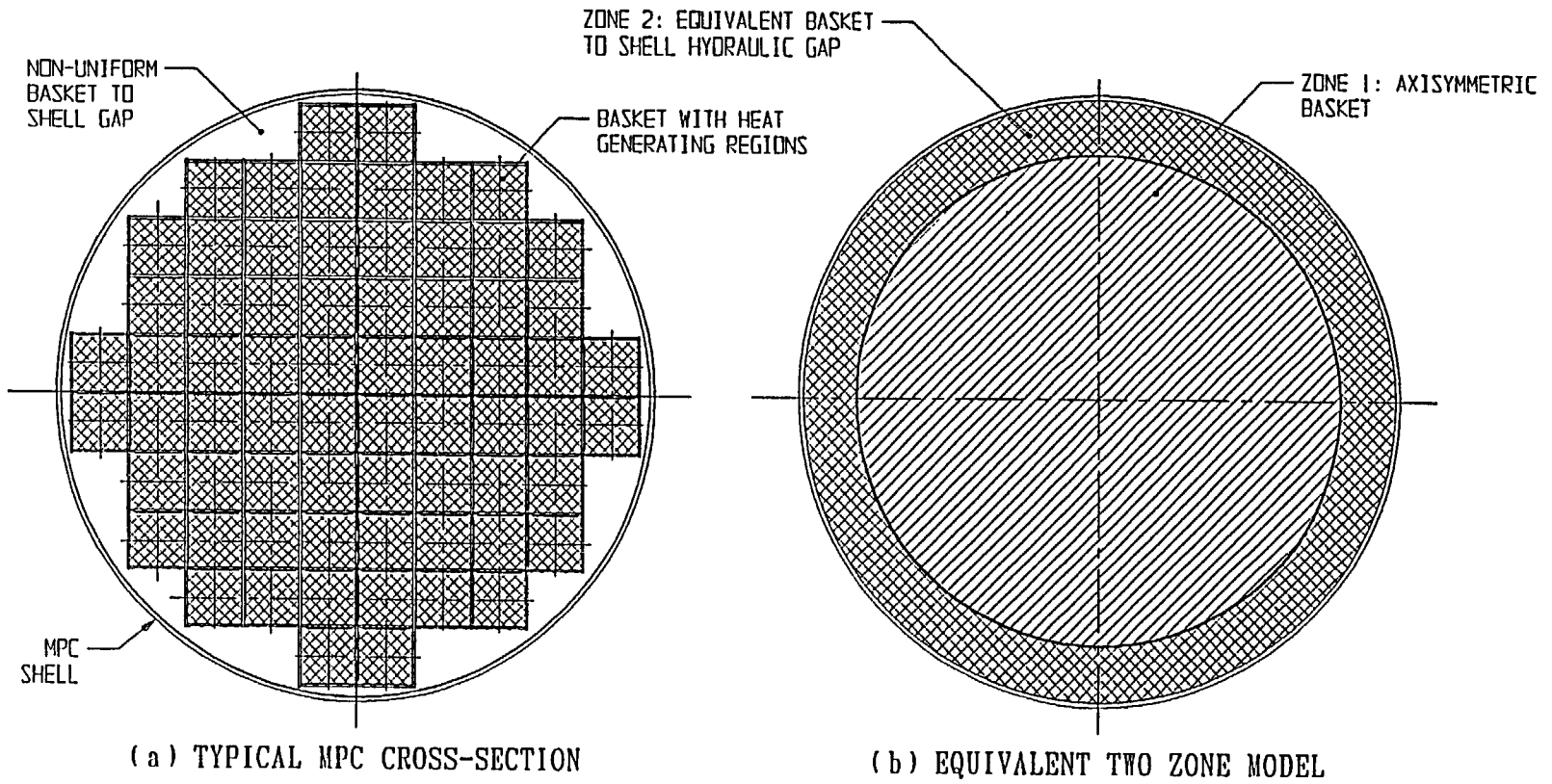
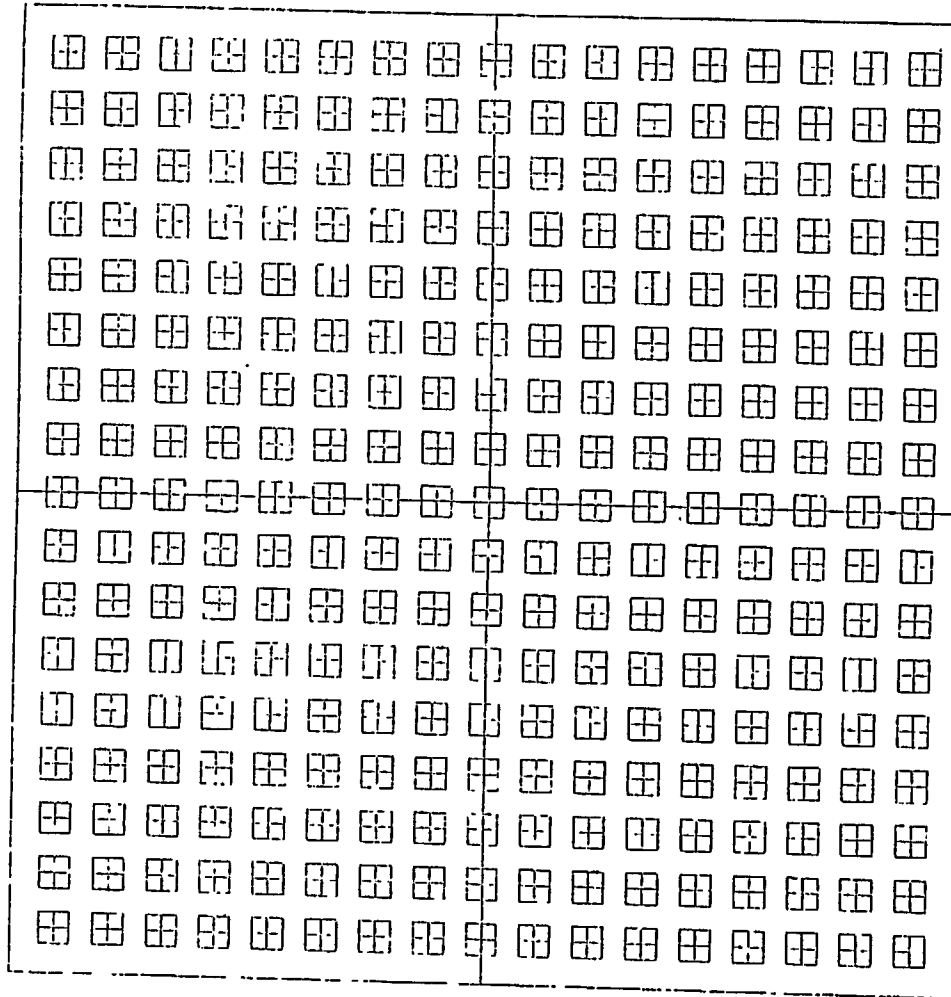


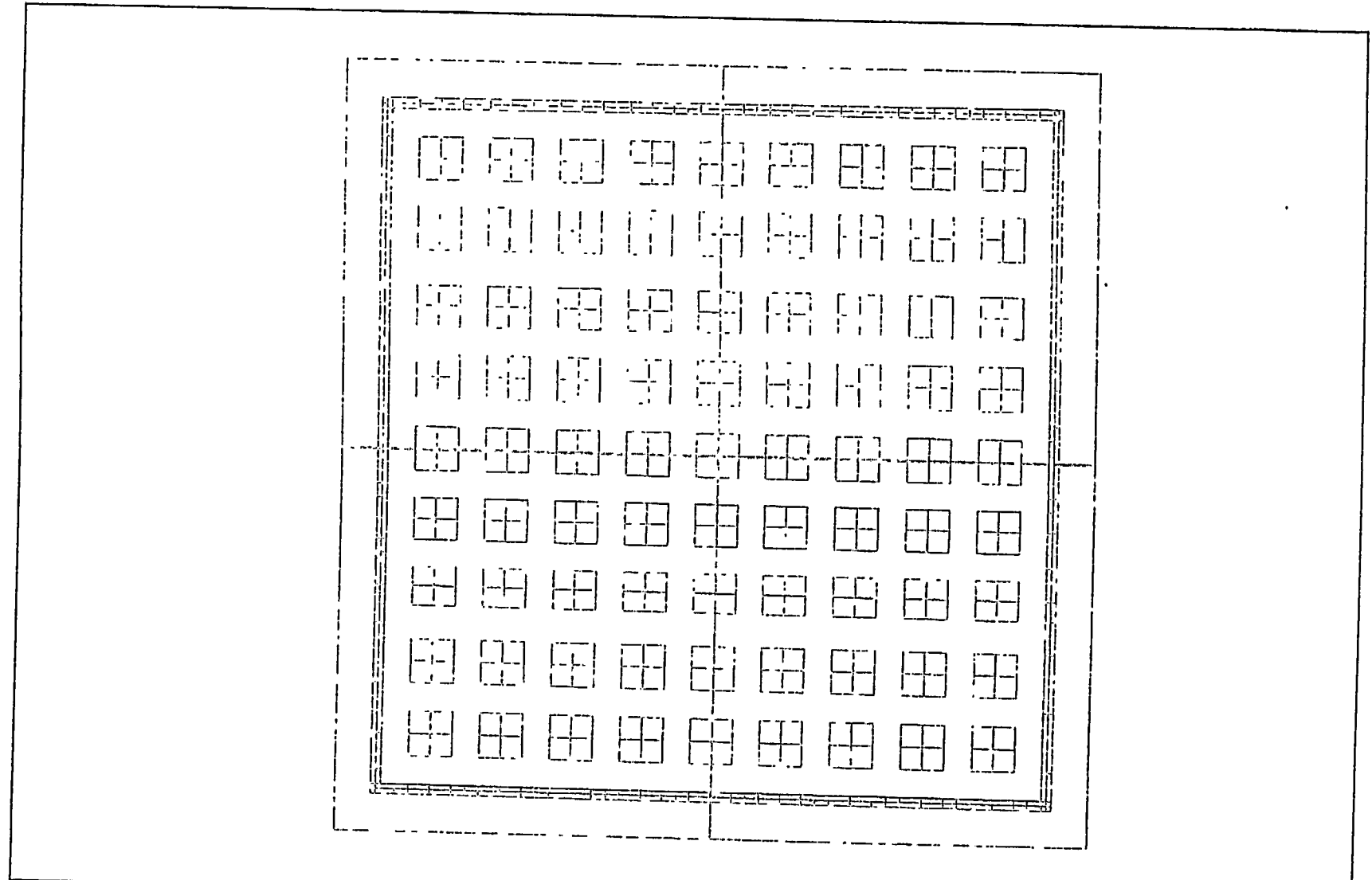
FIGURE 4.4.2; MPC CROSS-SECTION REPLACED WITH AN EQUIVALENT TWO ZONE AXISYMMETRIC BODY



W17X17 OFA FUEL ASSEMBLY MODEL

Nov 11 1997  
Fluent 4.32  
Fluent Inc.

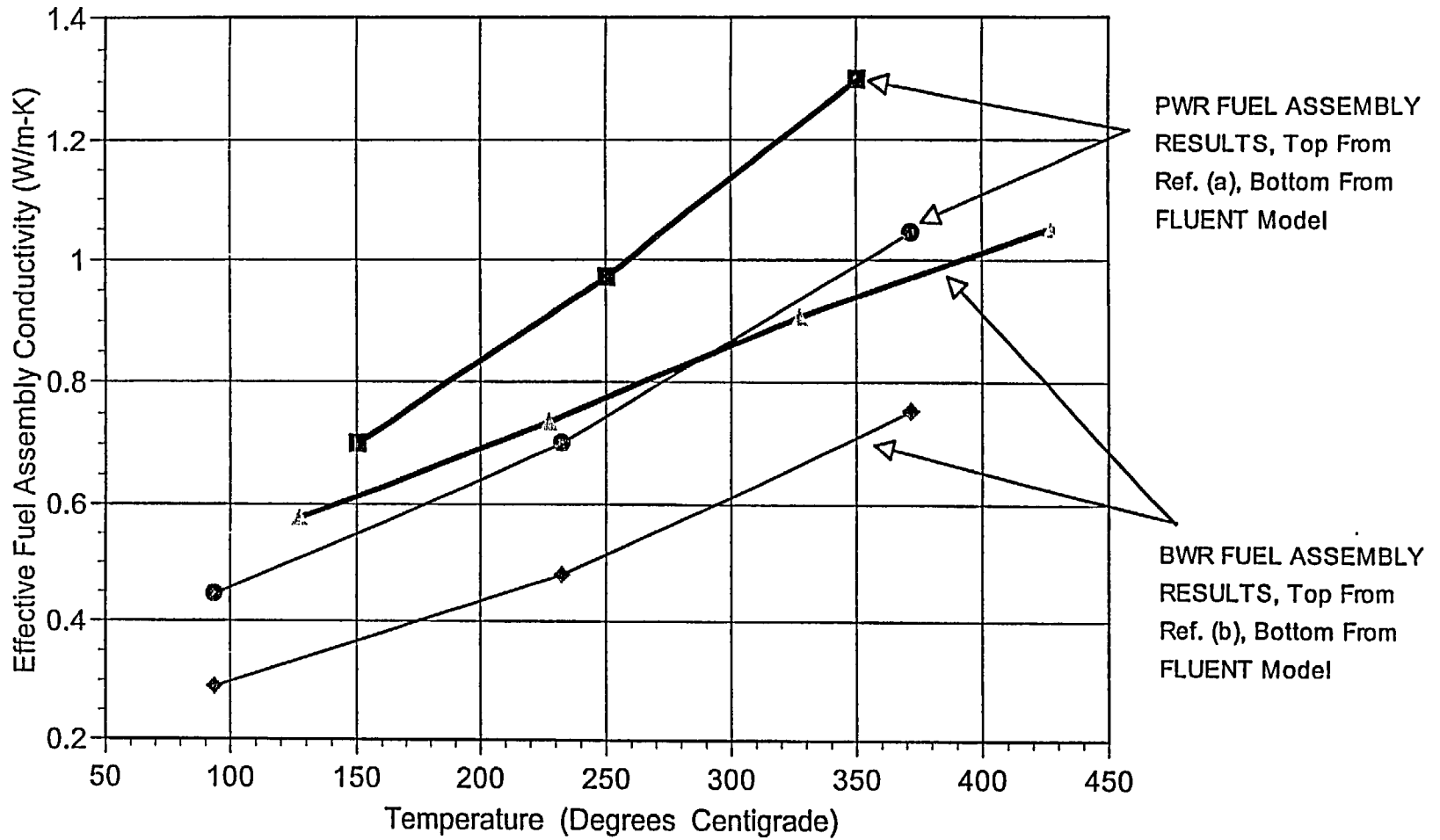
FIGURE 4.4.3: WESTINGHOUSE 17x17 OFA PWR FUEL ASSEMBLY MODEL



GE11-9X9 CHANNELED FUEL ASSEMBLY MODEL

Nov 11 1997  
Fluent 4.32  
Fluent Inc.

FIGURE 4.4.4: GENERAL ELECTRIC 9x9 BWR FUEL ASSEMBLY MODEL



(a) "Determination of SNF Peak Temperatures in the Waste Package", Bahney & Doering, HLRWM Sixth Annual Conf., Pages 671-673, (April 30 - May 5, 1995).

(b) "A Method for Determining the Spent-Fuel Contribution to Transport Cask Containment Requirements", Sandia Report SAND90-2406, page II-132, (1992).

FIGURE 4.4.5; COMPARISON OF FLUENT CALCULATED FUEL ASSEMBLY CONDUCTIVITY RESULTS WITH PUBLISHED TECHNICAL DATA

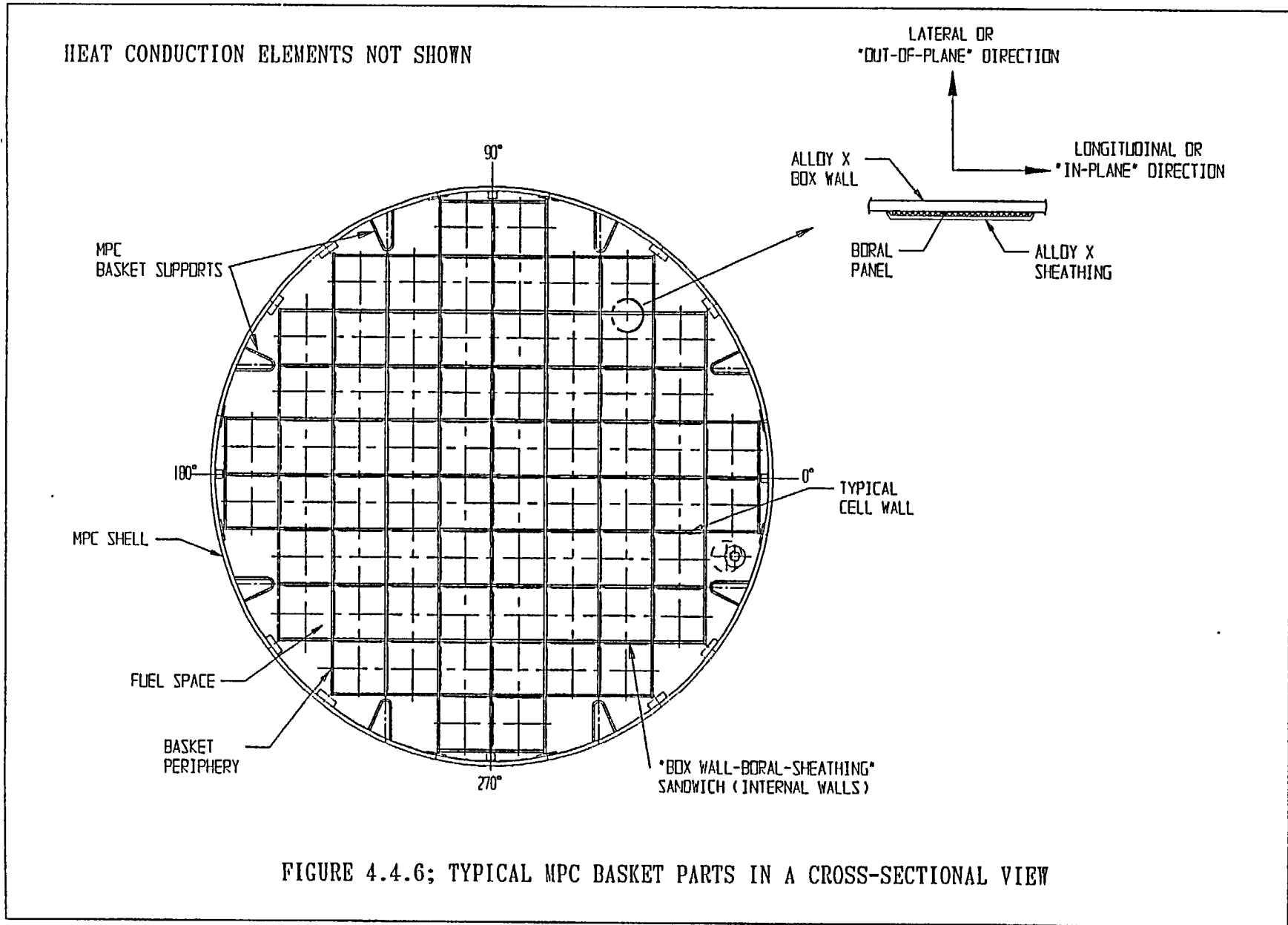


FIGURE 4.4.6; TYPICAL MPC BASKET PARTS IN A CROSS-SECTIONAL VIEW

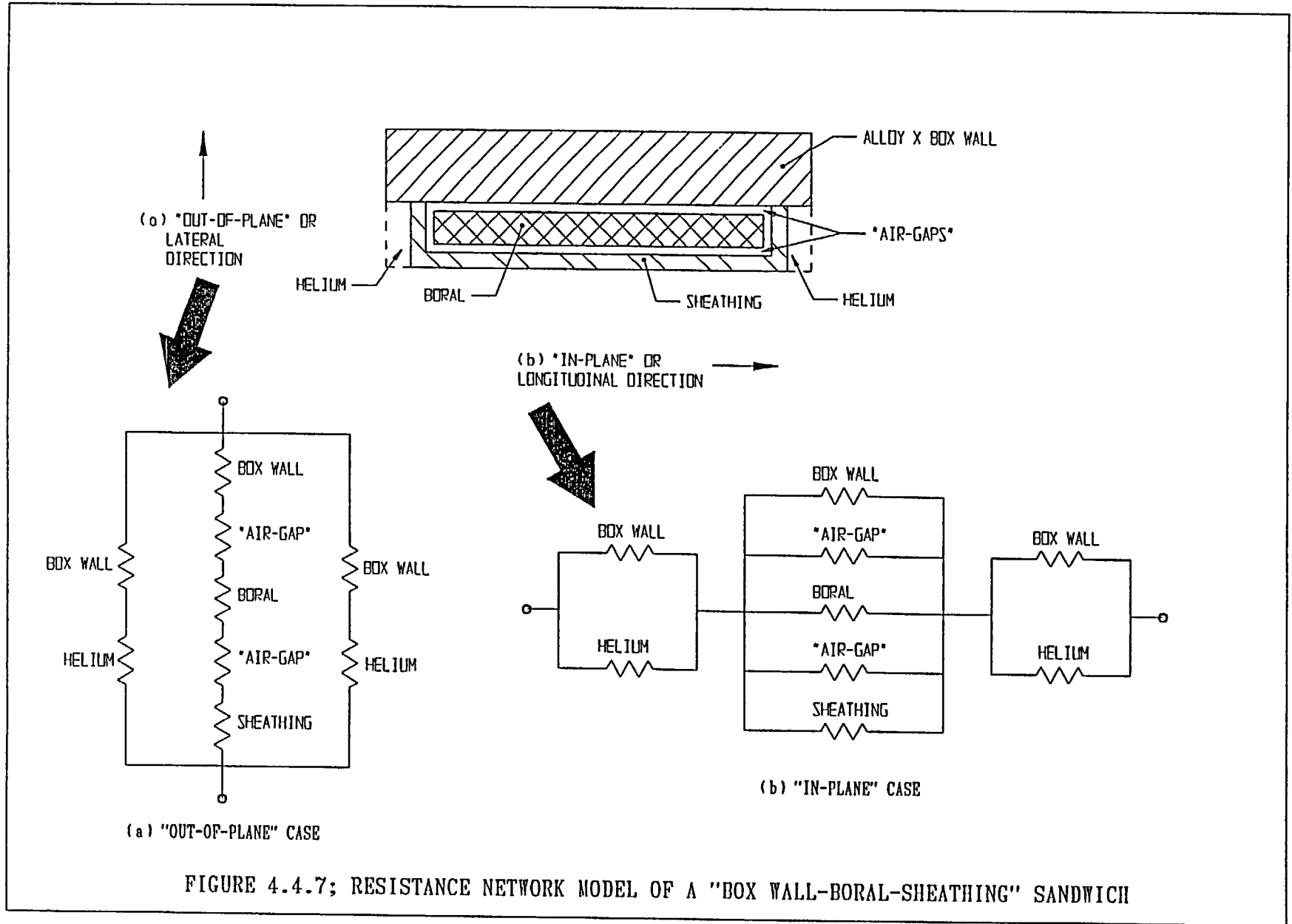
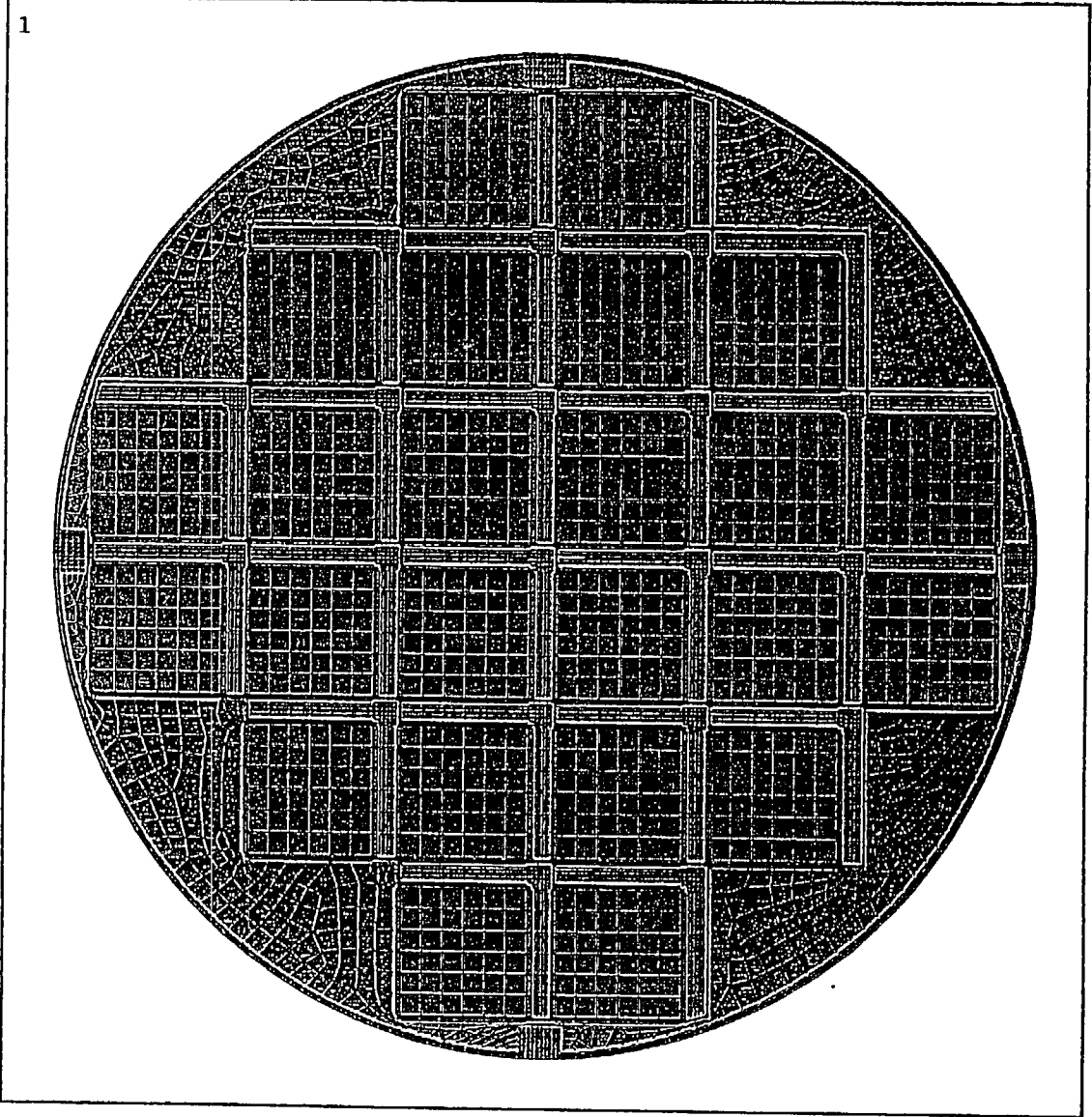


FIGURE 4.4.7; RESISTANCE NETWORK MODEL OF A "BOX WALL-BORAL-SHEATHING" SANDWICH

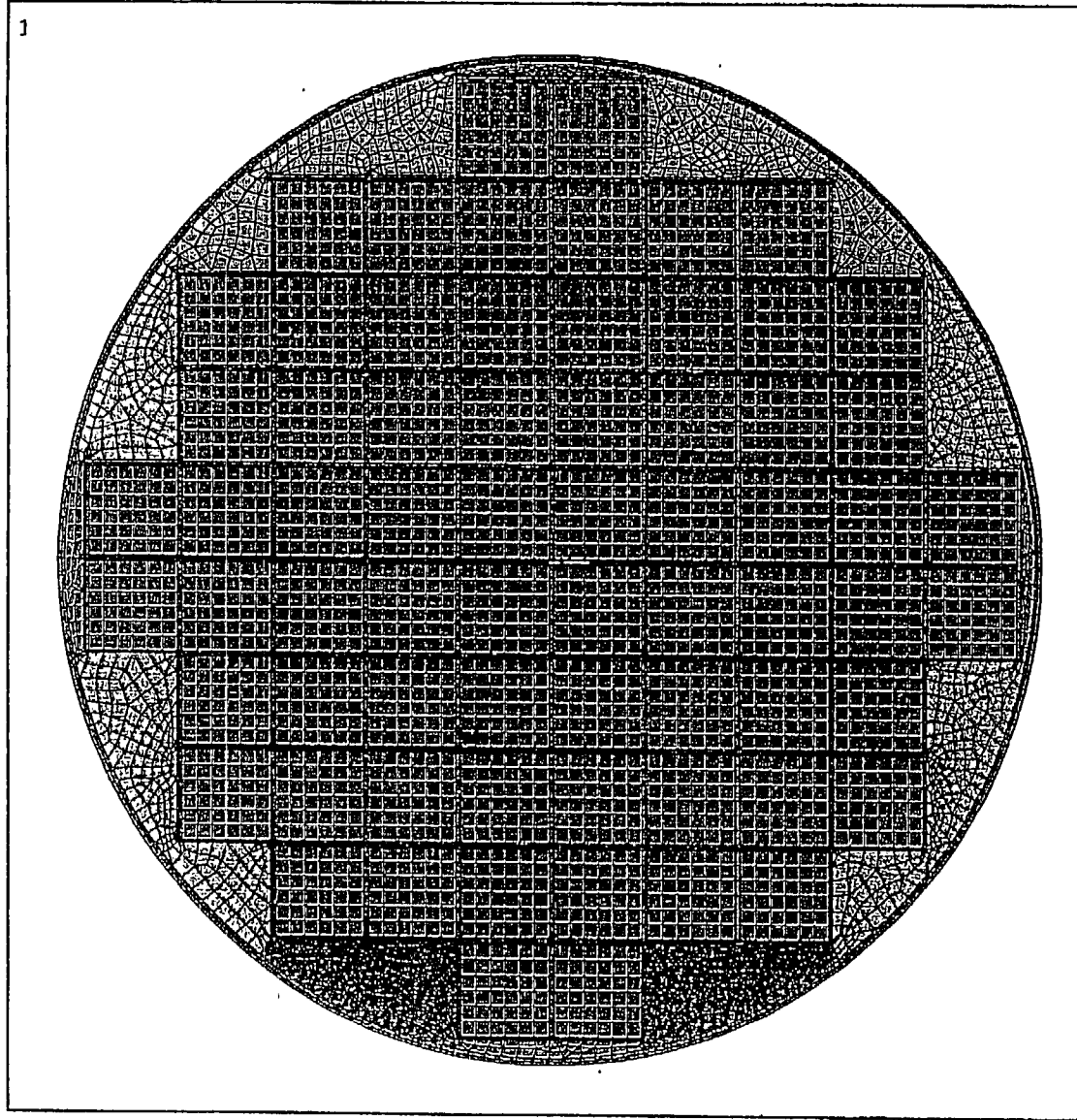
FIGURE 4.4.8

THIS FIGURE INTENTIONALLY DELETED.



ANSYS 5.3  
NOV 13 1997  
11:26:52  
PLOT NO. 1  
ELEMENTS  
MAT NUM  
  
ZV =1  
\*DIST=37.606  
Z-BUFFER

FIGURE 4.4.9; MPC-24 BASKET CROSS-SECTION ANSYS FINITE ELEMENT MODEL



ANSYS 5.3  
NOV 13 1997  
11:28:39  
PLOT NO. 1  
ELEMENTS  
MAT NUM  
  
ZV =1  
\*DIST=37.606  
Z-BUFFER

FIGURE 4.4.10; MPC-68 BASKET CROSS-SECTION ANSYS FINITE ELEMENT MODEL

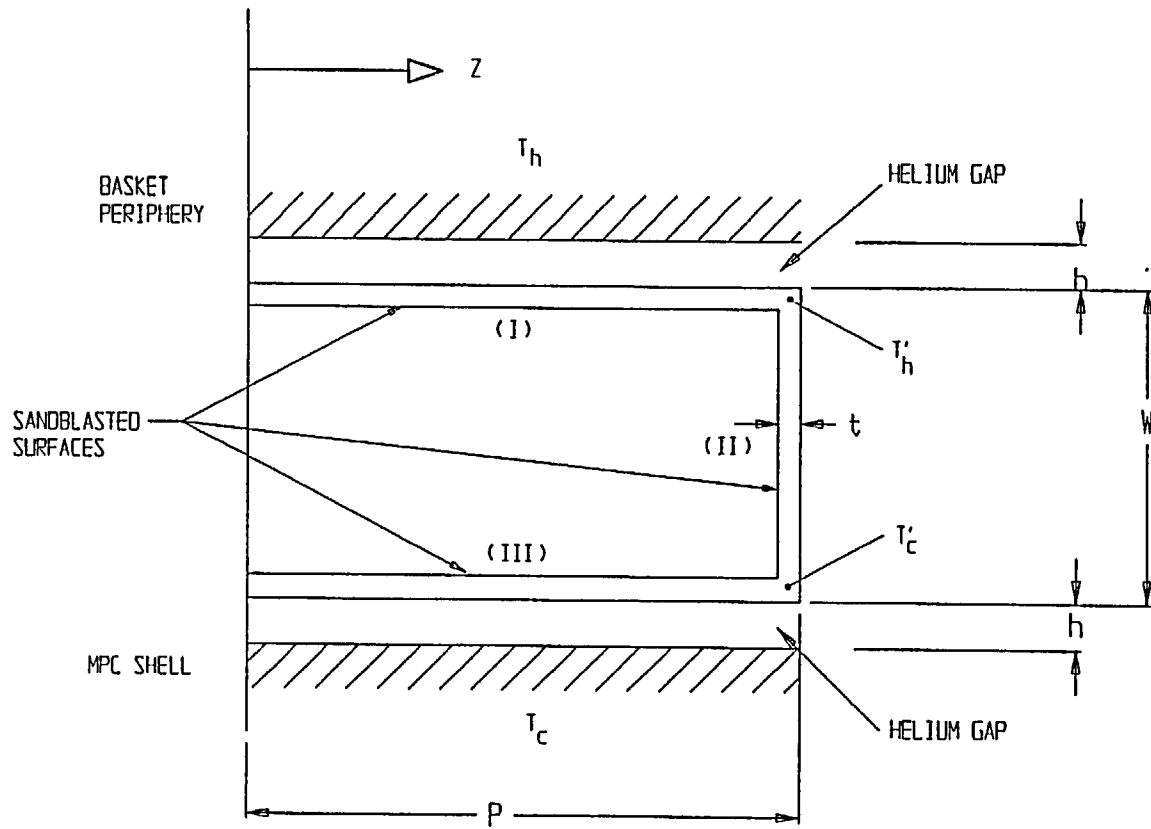


FIGURE 4.4.11; ILLUSTRATION OF AN MPC BASKET TO SHELL ALUMINUM HEAT CONDUCTION ELEMENT

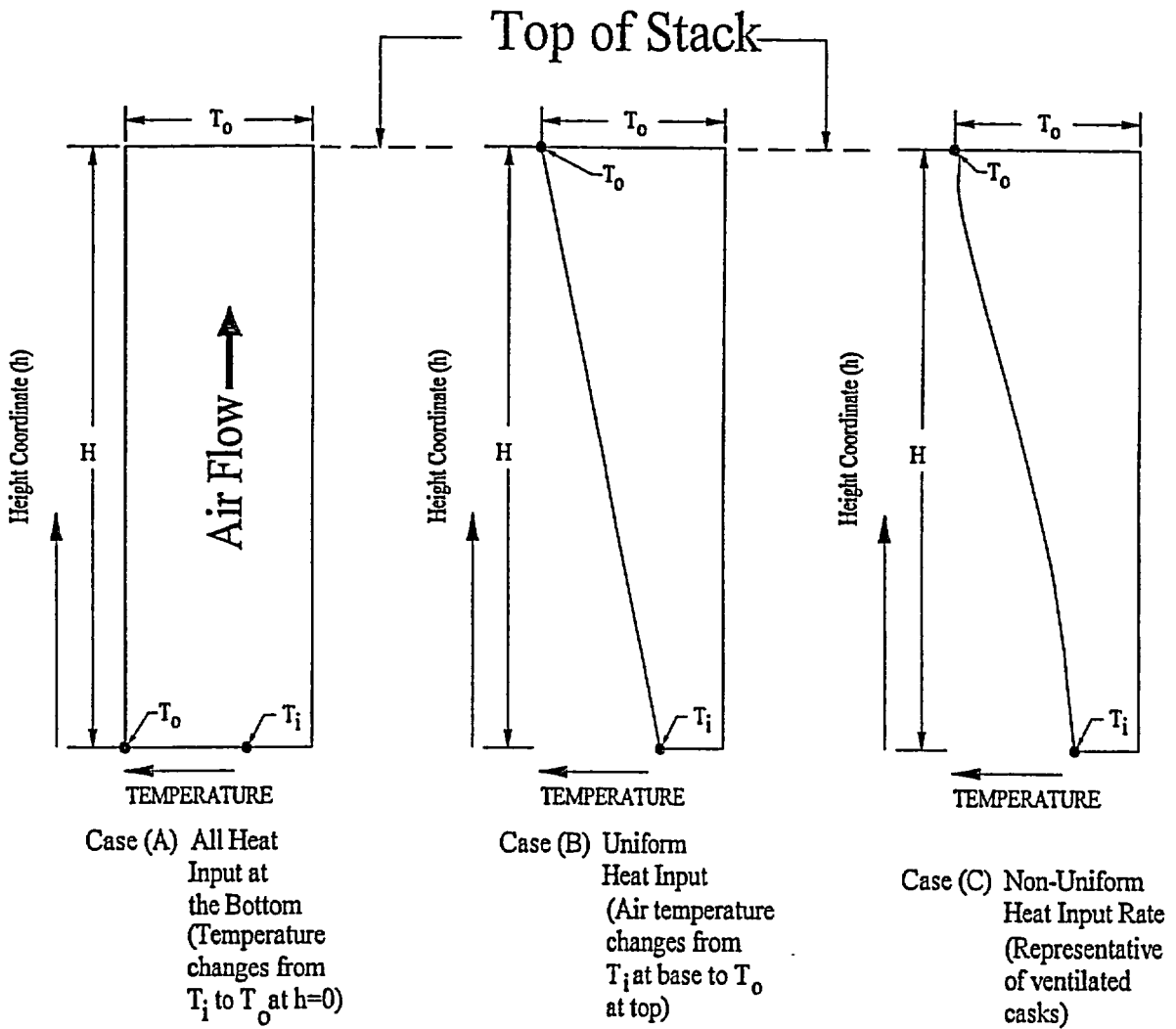


Figure 4.4.12; Stack Air Temperature as a Function of Height

LEGEND:    ↓ ↓ ↓ ↓    INSULATION  
               ××××××    INSULATED BOUNDARY

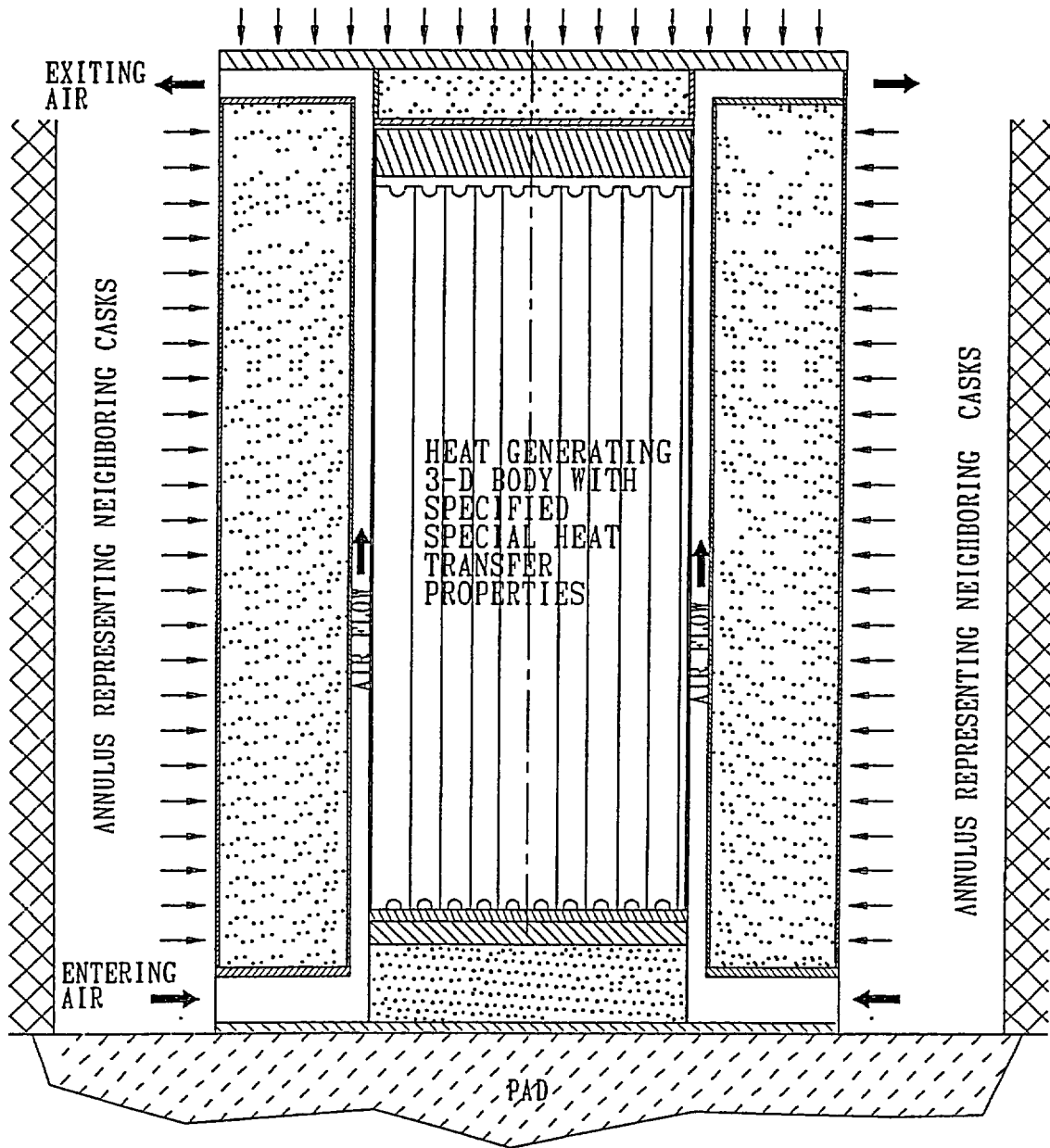


FIGURE 4.4.13; SCHEMATIC DEPICTION OF THE HI-STORM THERMAL ANALYSIS

FIGURE 4.4.14

THIS FIGURE INTENTIONALLY DELETED